International Journal of Informatics Society

11/20 Vol. 12 No.2 ISSN 1883-4566

Informatics Society

Aims and Scope

The purpose of this journal is to provide an open forum to publish high quality research papers in the areas of informatics and related fields to promote the exchange of research ideas, experiences and results.

Informatics is the systematic study of Information and the application of research methods to study Information systems and services. It deals primarily with human aspects of information, such as its qu ality and value as a resource. Informatics also referred to as Information science, studies t he structure, algorithms, behavior, and interactions of natural and a rtificial systems that store, process, access and communicate information. It also develops its own conceptual and theoretical foundations and utilizes foundations developed in other fields. The advent of computers, its ubiquity and ease to use has led to th e study of info rmatics that has computational, cognitive and social aspects, including study of the social impact of information technologies.

The characteristic of informatics' context is amalgamation of technologies. For creating an informatics product, it is necessary to integrate many technologies, such as mathematics, linguistics, engineering and other emerging new fields.

Guest Editor's Message

Yoshinobu Kawabe

Guest Editor of Thirty-fourth Issue of International Journal of Informatics Society

We are delighted to have the Thirty-fifth issue of the International Journal of Informatics Soci-ety (IJIS) published. This issue includes selected papers from the Twelfth International Workshop on Informatics (IWIN2019), which was held at Hamburg, Germany, Sept. 8-11, 2019. The workshop was the thirteenth event for the Infor-matics Society, and was intended to bring to-gether researchers and practitioners to share and exchange their experiences, discuss challenges and present original ideas in all aspects of infor-matics and computer networks. In the workshop 25 papers were presented in seven technical ses-sions. The workshop was successfully finished with precious experiences provided to the partic-ipants. It highlighted the latest research results in the area of informatics and its applications that include networking, mobile ubiquitous systems, data analytics, business systems, education sys-tems, design methodology, intelligent systems, groupware and social systems.

Each paper submitted IWIN2019 was re-viewed in terms of technical content, scientific rigor, novelty, originality and quality of presen-tation by at least two reviewers. Through those reviews 20 papers were selected for publication candidates of IJIS Journal, and they were further reviewed as a Journal paper. We have three cat-egories of IJIS papers, Regular papers, Indus-trial papers, and Invited papers, each of which were reviewed from the different points of view. This volume includes seven papers among those accepted papers, which have been improved through the workshop discussion and the re-viewers' comments.

We publish the journal in print as well as in an electronic form over the Internet. We hope that the issue would be of interest to many research-ers as well as engineers and practitioners over the world.

Yoshinobu Kawabe received his B.E., M.E., and D.E. degrees in information engineering from Nagoya Institute of Technology in 1995, 1997, and 2003. He joined NTT Communication Science Laboratories, Nippon Telegraph and Telephone Corporation in 1997. In 2002, he was a visiting research scientist at MIT Laboratory for Computer Science. Since 2008, he has been at Aichi Institute of Technology, a professor at the Department of Information Science. His re-search interests include term rewriting systems, process algebras, network programming lan-guages, formal methods, security/privacy verifi-cation, and computational trust. He is a member of ACM, JSSST, IPSJ, and IEICE.

Invited Paper

Spectrally-Shaping Viscoelastic Finite-Difference Time Domain Model of a Membrane

Rolf Bader†
†Institute of Systematic Musicology
University of Hamburg
Neue Rabenstr. 13, 20354 Hamburg, Germany
R_Bader@t-online.de

Abstract - The damping of musical instruments is spectrally-shaped, showing beatings and non-exponential decay. Such behaviour can be explained by viscoelastic damping, which also shows spectral sidebands and mode coupling. Previous physical models of musical instruments do only roughly implement viscoelastic damping. The present Finite-Difference Time Domain spectrally-shaping viscoelastic model on the other hand models complex damping spectra as physically reasoned viscoelasticity discussing a membrane. The model assumes a memory, delaying the strains of previous time points, while convolving these strains with a damping function, only to add it to the present stress. It therefore uses a complex Young's modulus and a complex tension, where the real part represents damping. The damping function is calculated as the inverse Laplace transform of the complex Young's modulus spectrum. Contrary to modal analysis, the resulting amplitude decay of a damped target frequency is not exponential. This is in accordance with the physics of viscoelasticity acting with a memory. Amplitude and frequency modulations are found, leading to sidebands in the spectrum. The damping frequency width Q of neighboring frequencies damped by a target frequency is discussed. A sharper Q with longer memory and smaller inverse Laplace transform real kernel constant γ is found as expected.

Keywords: Physical Modeling, Musical Instrument Acoustics, Viscoelastic Damping, Finite-Difference Time Domain Method, Percussion instrument

1 INTRODUCTION

A vibrational system has basically two types of damping, an external damping caused by energy loss due to radiation, and an internal damping caused by energy loss within the structure. The reasons for the internal energy loss are not perfectly clear [17]. There are thermodynamic losses [15] of several kinds, viscoelastic losses due to shearing, atomistic and quantum mechanical considerations of molecular restructuring [9] [21] next to other explanations. Thermal losses expect materials with a higher thermal conductivity to be damped stronger. But although e.g. a metal plate has higher thermal conductivity than a wooden plate, the wooden plate is damped stronger. Therefore thermal losses are expected not to be the major contribution to internal losses. The present paper discusses internal losses due to viscoelasticity only.

Physical models of the drum have been performed for Indian drum heads [19], the snare drum [7], or the bass drum [3] using Finite-Difference methods. Fractal derivatives have been suggested to replace complex models by single, but fractal derivatives. These lead to a power law of damping [13]. Chaigne uses a Maxwell time-dependent model for damped plates [8] with still considerable differences between model and experiment.

All these models do not allow for a spectrally-shaping viscoelastic damping in the physical model. They only assume an exponential damping curve depending on frequency. Basically two damping terms are used as part of the differential equation, a first-order time derivative of the dependent variable multiplied by a damping constant, and a first-order time and second-order spatial derivative of the dependent variable with plates or membranes. In the first case a perfect exponential damping depending of frequency results. In the second case higher frequencies are damped stronger, compared to the perfect exponential decay case [8]. The second case becomes necessary in cases with strong viscoelasticity.

Nevertheless, the damping behaviour of material used for musical instruments like wood or leather has a complex frequency-dependency. Although exponential in general, some frequency bands might be damped stronger, some weaker, compared to the perfect exponential damping. This is assumed to contribute strongly to the 'liveliness' of wood or leather as material for musical instruments. Guitars built of plastic, like e.g. the Maccaferri plastic guitar, are often perceived to sound plastic, and are therefore rejected [12]. The material property of a spectrally-shaping viscoelastic damping is therefore crucial when replacing traditional material with polymer or hybrid material.

This also holds for physical models of musical instruments, which need to sound as realistic as possible. Using a spectrally-shaping viscoelastic damping method in the models allows for a realistic reproduction of musical instrument sounds. The role of internal damping has not been in the focus of musical acoustics over the last decades. Still as models improve in quality, the differences between real and modeled instruments still existing seem to be caused to a great extent by the lack of a spectrally-shaping viscoelastic damping model.

Experimental data of viscoelastic losses in leather show an increase of damping with higher temperatures above its glass transition temperature [11] which are additionally frequency dependent. Higher water content of leather also leads to higher internal damping. The reasons for such a damping behavior are mainly thought to be a reconfiguration of collagen fibers, within them and between the fibers, where water

molecules become part of the collagen structure [11]. Collagen is a very stiff protein and therefore leather is basically considered a crystal. Still the layering of leather fibers allows gaps which are filled by water, as well as by molecules which are introduced by the process of tanning. Here water molecules enter in two ways, either as larger portions between collagen fibers or as single molecules between or even within collagen molecules. The former is responsible for leather to freeze to a hard plate around zero degree Celsius. The other water molecules lead to a slow melting process around a certain temperature, adding most to the strong viscoelastic properties of leather. Additional components of this viscoelastic internal damping are sudden changes in the molecular geometries when stress is applied. All these processes lead to a phase shift between stress and strain which again leads to an internal energy loss of the vibration. Internal damping can be very strong and therefore contributes considerably to the timbre of a drum built of leather.

Basic models of viscoelastic damping have mainly been discussed with Finite-Element Methods [24]. Here the Maxwell and the Kelvin-Voigt model for relaxation and creep respectively are normally used as time integration models, where combinations of both are able to build arbitrarily complex damping behavior. Both creep and relaxation may have very short but also very long time constants. Guitar builders speak of the 'flowing' of wood when the tension the strings apply to the soundboard leads to a plastic strong deformation of the soundboard over years. Relaxation appears with musical instruments which have plates under tension, like top and back plates of guitars or a crowned piano soundboard. Instrument builders often estimate that the internal tension relaxes over about one year and the deformation due to tension becomes again a plastic deformation with no internal tension left.

Sound absorbing material research uses mainly bitumen-, liquid- and nanotube-based materials [25]. The modeling in this field is nearly exclusively done using the Maxwell or the Kelvin-Voigt model. Again damping is strongest when the operation temperature of the material meets the glass-transition temperature. Complex frequency- and temperature-dependent damping curves appear with sandwich plates [26]. Using a center-finite-difference method [27] shows the appearance of frequency band-gaps in periodically stiffened plates, still here caused by the periodicity of the material and not mainly by viscoelastic effects. The methods used are modal analysis and do not consider the development of the damped amplitudes.

The complex nature of internal damping also appears with wood. In a review paper [5] finds a close correlation between Young's modulus and the damping parameter $\tan\ \delta$ for 450 wood species, the relation between imaginary and real parts of a complex Young's modulus, an index often used when measuring viscoelasticity. This index is not taking frequency-dependence of damping into consideration. Damping correlates with Young's modulus, but not with wood density [6]. Comparing normal and compression wood, where the amount of cellulose is higher, it appears the the micro fiber angle (MFA), the angle the cellulose fibers lay inside the second cell wall correlate with both, Young's modulus and damping [4]. Obataya et al. investigate the influence of viscoelasticity to the vibration of reeds [16].

Viscoelasticity may also vary over musical instrument geometries. Adding additional paste to a drum head is a common practice for drums in Southeast Asia. Indian drums, especially *tablas* are studied in terms of the additional mass added to their drum head [19] [18] called *sihai* which is placed concentric for the *dayan* and off-centric for the *bayan* drum. Varying the width, position, smoothness and strength of the *sihai* it was found that the harmonic overtone relations of the drum modes change and can meet values very close to harmonic ratios.

Tablas have a clear pitch, still they are not played as melody instruments. The Myanmar drum circle *pat wain* on the other hand needs to be tuned to pitches over about three octaves [1]. The paste adds considerable viscoelasticity to the drum, next to the leather the drum head is built of. Experimentally it was found that a double-headed drum, like the *pat wain* shows a coupling of the drum heads for lower modes, while the higher modes are more or less decoupled [22] [18]. Normally the upper drum head is keeping its frequency at the lower modes while the lower drum head is forced into the motion and frequency of the upper one.

Several other studies deal with drums. The vibration of the Karen bronze or 'frog' drum has been studied experimentally [14], finding complex modes up to 3 kHz. The influence of non-uniform tension of a drum head was studied using laser-interferometry measurements, where degenerated modes have been found [23] mostly leading to musical beats. The eigenmodes of the drum vessel were analyzed using Finite-Element methods [10]. The coupling between the drum head and the wooden shell was investigated using Finite-Elements for a bass drum [3].

The model presented allows for a very precise computer simulation of vibrational systems in general, using a drum as an example. As internal damping shapes the overall spectral amplitude shape of sounding objects considerably, the suggested model in future can also be used in sound design, sonification, auralization, room acoustics, or in urban environmental noise problems. These topics have become an intense focus of modern engineering over the last years, where simple estimations of overall energy, roughness, sharpness, or brightness of a sound are way not enough to satisfy modern auditory demands. As musical instruments have always been subject to very precise tuning of timbre they are an excellent benchmark.

The method of using Finite-Difference Time Domain (FDTD) sound synthesis belongs to the analysis-by-synthesis approach. It is an alternative to the analyzing branch of information processing, taking existing sounds and deriving their properties using spectral analysis or related techniques. The model approach on the other side gives detailed insight into the material and geometrical properties of the objects, and therefore allows the formulation of a state-space of all possible sounds. Such a state-space can then be used to understand existing sounds with respect to their physical sources, and therefore help to classify and identify sounds with analytical information processing tools much easier. This makes an interplay

between the two analysis ways possible, the forward synthesis and the backward analysis techniques. Such model tools will be subject to machine learning based on physical modeling in the near future. Still this interplay can only reasonably work when using physical models, taking all crucial parameters into consideration. As internal damping strongly shapes the sound of musical instruments, as well as all sounding objects in a frequency-dependent way, without such a model as presented here a precise relation between physics and analysis can only be rough. Due to the complex nature of internal viscoelastic damping such a model is complex too. Additionally, the literature in this field is scarce. The present model is a suggestion to fill this gap to some extend.

First the paper considers viscoelasticity as a frequency-dependent spectrum of a Young's modulus, as known from literature, and later the stiffness of a membrane. Transferring the equations into the time-domain is done via an inverse Laplace transform. Results for a reduced system, a 0-dimensional mass-spring system are discussed, showing complex decay behavior, as well as sidebands with strong damping. Then results for the membrane are shown, estimating the damping strength in correlation with the input parameters of the model as well as the damping frequency width, the impact of a damped target frequency onto its neighboring frequencies.

2 METHOD

2.1 Viscoelastic Finite-Difference Model

The drum membrane is modeled as a Finite-Difference Time Domain (FDTD) model, used before in models of whole geometries of a guitar, a violin and several other musical instruments [2]. It is implementing the equation of a membrane with tension T(x,y), area density ν(x,y) = m(x,y) / B, damping constant D, and displacement u, like

$$\frac{\mathrm{T(x,y)}}{\nu(\mathrm{x,y})}\left(\frac{\partial^2 \mathrm{u}}{\partial \mathrm{x}^2}+\frac{\partial^2 \mathrm{u}}{\partial \mathrm{y}^2}\right)=\frac{\partial^2 \mathrm{u}}{\partial \mathrm{t}^2}+\mathrm{D}\,\frac{\partial \mathrm{u}}{\partial \mathrm{t}}\,. \tag{1}$$

The tension is often called T in the literature, and E is denoting the Young's modulus. Both are closely related, as E is measured in Pascal [Pa], or force per area, and T is measured in Newton [N]. In viscoelastic literature mainly the Young's modulus E is used, defined as the proportionality constant between stress and strain. As the differential equation of the membrane can also be interpreted as a stress-strain relation, we discuss the viscoelastic model using Young's modulus E at first, and later use tension T or Young's modulus E, to be close to literature conventions.

The area density ν(x,y) depends on the mass m divided by the area B of the membrane. As is the case with membranes which are nonuniform in thickness, its mass varies along x and y. Therefore ν(x,y) depends on space. Also the tension T(x,y) has a spatial distribution. If a drum is tuned by adjusting tuning pegs at its rim, most often it is not possible to adjust the tuning pegs such, that the drum has a perfectly uniform tension distribution over its whole area. Therefore also the tension T(x,y) depend on x and y. The implemented model therefore allows any density and tension distribution. Still as the focus of this paper is on the viscoelastic damping, density and tension are kept constant, although the model itself easily allows for complex distributions.

This differential equation of the membrane includes a damping term, which leads to an exponential decay of the drum eigenfrequencies, both in time and in frequency. Each partial is therefore exponentially decaying, and the spectrum of the sound will have an exponential decay towards higher frequencies. All this damping depends on a single variable alone. Still experiments nearly never show such a simple behavior. Although damping roughly behaves exponentially, strong deviations appear from such a simple exponential decay, showing amplitude fluctuations, sudden drops, especially right after tone onset or a decay much longer than expected. Indeed literature shows viscoelastic damping to result in a spectral band-gap, and multiple damped bands end up in a complex amplitude spectrum, as discussed in the introduction.

To account for this, internal damping can be expressed as a complex and frequency dependent Young's modulus E(s) with the complex frequency

$$\mathrm{s}=\alpha+\imath\omega\,. \tag{2}$$

Then the stress-strain relation in the frequency domain becomes

$$\sigma(\mathrm{s})=\mathrm{E(s)}\,\epsilon(\mathrm{s})\,, \tag{3}$$

with stress σ and strain ϵ. To implement this in a model, the multiplication in the frequency domain can be transformed into the time-domain as a time convolution like

$$\sigma(\mathrm{t})=\int_0^\infty \epsilon(\mathrm{t}-\tau)\,\mathrm{h}(\tau)\,d\tau\,. \tag{4}$$

Here $\mathrm{h}(\tau)$ is a function representing the time domain of the complex Young's modulus E(s). The present stress is the result of all previous strains weighted by $\mathrm{h}(\tau)$. An inverse Laplace transform is used to transfer E(s) into $\mathrm{h}(\tau)$ like

$$\mathrm{h}(\tau)=\frac{1}{2\pi\imath}\int_{\mathrm{s}=\gamma-\imath\infty}^{\mathrm{s}=\gamma+\imath\infty}\mathrm{E(s)}e^{\mathrm{s}\tau}d\mathrm{s}\,. \tag{5}$$

Here γ is a constant for all ω and need to be chosen such that the solution converges. The choice of γ, together with E(s), determines the damping strength, and therefore is chosen to meet a desired damping. Still for all E(s), γ is a constant.

This solution converges to the non-viscoelastic case when E(s) does not have any real part. In this trivial case with constant Young's modulus E_0 the inverse Laplace transform is

$$\mathrm{h}(\tau)=\mathrm{E}_0\,\delta(\tau)\,, \tag{6}$$

where δ(t) is the Kroneker delta function with $\delta(0)=1$ and $\delta(\tau\neq 0)=0$. An unusual material with internal damping only at frequency ω_0 has

$$\mathrm{h}(\tau)=\mathrm{E}_0\,\delta(\tau)+\mathrm{Re}\{\mathrm{E(s)}\}\,e^{\mathrm{s}\tau}\,, \tag{7}$$

with damping amplitude $\mathrm{Re}\{\mathrm{E(s)}\}$.

Therefore a frequency-dependent internal damping spectrum can be written like

$$\mathrm{h}(\tau) = \int_{\mathrm{s}} \mathrm{Re}\{\mathrm{E(s)}\}\; e^{s\tau} d\mathrm{s}\;. \tag{8}$$

Each spectral component of a sound is damped with its own damping parameter μ(s) and therefore has a time series like

$$\mathrm{u(s,\,t)} = \mathrm{A(s)}\; e^{-\mu\,\mathrm{t}}\; e^{\imath\;\omega\;\mathrm{t}}\;. \tag{9}$$

Note that it is necessary to clearly distinguish between the real part of the Young's modulus Re{E(s)}, the real part of the inverse Laplace integrations γ, and the decay μ. Re{E(s)} is a material property, the viscoelasticity of the vibrating material. Re{E(s)} can be measured experimentally by examining the phase relation between stress and strain of a material under vibration of frequency s. γ is a signal processing tool which defines the frequency range, or the filter Q of damping. Indeed real viscoelasticity appearing at a certain frequency has also a Q-value. Therefore also this parameter can be measured. Still as additional sound properties appear with viscoelasticity, like amplitude modulation, side bands or mode coupling, defining a simple filter Q is only a rough approximation of the viscoelastic behaviour. Therefore the relation between γ and Q is not straightforward. Finally, μ is only an analysis parameter, the damping exponent of the resulting time series, as best fit to the decay of the respective frequency. Again as the real damped time series shows beatings and non-exponential decay behaviour, μ is a rough estimate. Eq. 9 is therefore an oversimplification of the real process, and therefore γ will only be a rough estimation of the general decay of single frequencies. Only the whole viscoelastic equation is suitable to model real behaviour, which is caused by the combination of Re{E(s)} and γ.

2.2 Complex Young's Modulus and Complex Tension

There is a temporal delay between stress and strain which can be expressed as an angle δ, the phase relation between stress and strain for a single frequency. δ is often measured as this phase relation, and in the literature often written as

$$\tan\delta = \mathrm{E_I}/\mathrm{E_R}\;, \tag{10}$$

the relation between the imaginary and real parts of the complex Young's modulus.

The stress-strain relation is also the definition of the Young's modulus. In the case of a membrane we do not have a Young's modulus, so we need to transfer the idea.

Strain is dimensionless and refers to the potential energy of the system caused by displacement differences. The stress is weighted force applied to the structure in order to obtain the strain. In the dynamical case this force can have different parts, the acceleration of the system, damping, or external forces. The unit of the Young's modulus is that of stress, force over area, as strain is dimensionless.

The stress-strain relation is therefore a force balance, according to Newton's idea of mechanical systems in which all interactions can be written as a sum of forces (actio-reactio). Therefore it is straightforward to replace the strain with the spatial differentiation of the membrane, another force term, and the Young's modulus by force over area density. As the area density is hardly complex, clearly the tension is the parameter we can refer to as complex and frequency dependent. Then the viscoelastic membrane equation reads

$$\int_{\tau=0}^{\infty} \mathrm{h}(\tau)\frac{\mathrm{T(x,y)}}{\nu}\left(\frac{\partial^2\mathrm{u(x,y,t-\tau)}}{\partial\mathrm{x}^2}+\frac{\partial^2\mathrm{u(x,y,t-\tau)}}{\partial\mathrm{y}^2}\right)d\tau\;=\frac{\partial^2\mathrm{u(x,y,t)}}{\partial\mathrm{t}^2}. \tag{11}$$

Note that in this equation the damping term with damping constant D and first derivative of displacement with respect to time was omitted, as it is no longer necessary. All damping can be modeled using the viscoelastic term. Still viscoelasticity is not the only cause for damping. Another major damping is that of radiation loss. This again is complex and beyond the scope of this paper. Due to complex mode shapes, the radiation loss of complex geometries can be calculated analytically only for very simple geometries. There is no general analytical solution. Still roughly this damping is exponential with respect to frequency. Therefore one might still keep the first-order differential term with respect to time as a damping term of external damping.

2.3 Analytical Proof of Non-Exponential Time Decay of Viscoelastic Damping

Now we can analytically decide, if the viscoelastic decay is exponential in time or not. Solving this equation is not trivial, both for the spatial part v(x,y) as well as for the temporal w(t) with

$$\mathrm{u(x,y,t)} = \mathrm{v(x,y)}\;\;\mathrm{w(t)}\;. \tag{12}$$

As we are interested in the temporal development of single frequencies, we can leave the exact solution of v(x,y) for a later stage, and assume that when finding this solution, which is subject to some boundary condition, it can be differentiated with

$$\frac{\partial^2\mathrm{w(x,y)}}{\partial\mathrm{x}^2}+\frac{\partial^2\mathrm{w(x,y)}}{\partial\mathrm{y}^2}=\mathrm{b(s)}\;\mathrm{w(x,y)}\;, \tag{13}$$

where b(s) is a constant depending on s. Then Eq. 11 simplifies to

$$\frac{\mathrm{T(x,y)}\;\mathrm{b(s)}}{\mu}\int_{\tau=0}^{\infty}\mathrm{h}(\tau)\mathrm{w(t-\tau)}\;d\tau=\frac{\partial^2\mathrm{w(t)}}{\partial\mathrm{t}^2}. \tag{14}$$

Basically, b(s) w(x,y) could be the solution of any set of linear differential equations, and we will use this later, studying the model with a 0-dimensional mass-spring system. The viscoelastic model for such a system would be

$$\mathrm{K}\int_{\tau=0}^{\infty}\mathrm{h}(\tau)\mathrm{w(t-\tau)}\;d\tau=\frac{\partial^2\mathrm{w(t)}}{\partial\mathrm{t}^2}\;, \tag{15}$$

where K is the spring stiffness.

It is interesting to see that inserting the expected exponential damping solution into Eq. 14 or Eq. 15, similar to Eq. 9,

$$\mathrm{w(t)} = \mathrm{A}\;e^{-\alpha\mathrm{t}}e^{\imath\omega\mathrm{t}} \tag{16}$$

is obviously not solving it. This means that the model of a frequency-dependent viscoelasticity, as time delay of previous strains entering the present stress, does not necessarily lead to the straight solution of an exponential decaying wave.

2.4 Memory Effect of Viscoelasticity

This is reasonable when remembering the physical reasoning of viscoelasticity as a delay of previous strains acting to a present stress. Such a system has a memory, and previous vibrations will act on the present one. In most cases this leads to a damping, as the additional acceleration produced by the previous strains counteracts the present acceleration, therefore reducing it and therefore damping the system.

Still the previous strains might also act as an additional acceleration, which then is driving the system. Considering a strong viscoelastic damping, where most of the energy is gone after 10 ms. If the $h(\tau)$ is longer than 10 ms and still acts until 15 ms, the acceleration supplied by $h(\tau)$ after 10 ms does not find a vibration on the geometry which it could counteract anymore and will drive the system again. This means that the strain stored in system has a kind of a memory and will act as an energy supply.

This additional energy will again be subject to viscoelastic damping later on again, and so the system will decay on the long run. But in such a situation we would expect an amplitude beating on top of a generally exponential decay. Such amplitude beatings are indeed found experimentally quite often. Of course they may have many reasons, like degenerated or close modes interacting and beating, or like complex couplings in complex geometries which musical instruments most often are. Still viscoelastic damping can also be a source of such amplitude beatings.

To go one step further in this discussion, when increasing the memory time, which in our model is decreasing γ, the amount of stored strain acts will increase the damping but will also increase the driving. Then the total damping behavior will be a combination of damping and driving, and we will expect a peak for strongest damping at a certain value of γ, which we will indeed find in the model results later on. Therefore the relation between the strength of viscoelasticity γ and the resulting decay exponent μ is highly nonlinear. Again there is no analytical solution to this relation and therefore one task below is to calculate the relation for a parameter space of both parameters, together with the third parameter changing μ, which is the viscoelasticity $\mathrm{Re}\{\mathrm{E(s)}\}$.

To push this even further, with extreme values of γ we will even expect the driving to be larger than the damping, and the system will not decay but increase in energy. This is no physical case anymore in terms of normal viscoelastic damped systems. Still it is a feature which we might use to model energy supply to a system. Of course this need to be done carefully, as a real energy supply by a string or another coupled part of a musical instrument might follow different rules.

Still the beating found is perfectly physical and known from strongly viscoelastic damped systems, e.g. when rotating an egg. When suddenly rotating an egg with a hand, the hard wall of the egg will follow the acceleration without delay, still the proteins inside the egg are driven only by the eggs wall and follow the movement only with a visible delay. This takes energy from the wall rotation, and it will slow down considerably. But then one can visually experience the wall to again accelerate, as the energy in the proteins are again acting on the walls with a considerable delay. Then the walls indeed have been accelerated again after some time. Therefore in principle such energy supply due to memory is a physically expected behavior, and might play a role with musical instruments with higher frequencies as we will see in the results section.

2.5 Discretization

When implementing the equations on a GPU, the integral cannot be performed over an infinite time span. It is memory expensive to store previous strains for all nodal points of the membrane geometry and perform convolutions for all node points at each calculated time point. Therefore the equation restricts the integration time to T. Additionally the calculation is time discrete. This transforms Eq. 3 into

$$\sigma_{\mathrm{t}} = \sum_{\tau=0}^{\mathrm{N}-1} \epsilon_{\mathrm{t}-\tau} \mathrm{h}_{\tau} \ , \tag{17}$$

with strain σ_{t} at discrete time point t and N samples to use. Also the integral of the discrete viscoelastic function h_τ becomes a sum, where only integer multiples of the periodicity T = N / r at sampling rate r can be used like

$$\mathrm{h}_{\tau} = \frac{1}{2\pi 1} \sum_{\mathrm{k}=1}^{\mathrm{N}} \mathrm{E_k}\, e^{\gamma\ \tau/\mathrm{r}} e^{\imath\ \omega_{\mathrm{k}}\ \tau/\mathrm{r}}, \text{ with } \tau = 0, 1, 2, 3, ...\mathrm{N}-1 \tag{18}$$

where $\mathrm{E_k}$ are now the discrete complex values for frequencies

$$\omega_{\mathrm{k}} = 2\pi \text{ k / r with k = 1,2,3,...N} \ . \tag{19}$$

As the calculation itself is kept in the time domain, $h(\tau)$ need to be real and therefore is rewritten like

$$\mathrm{h}_{\tau} = \mathrm{E}_0\ \delta(\tau)\ + \frac{1}{2\pi} \sum_{\mathrm{k}=1}^{\mathrm{N}} \mathrm{Re}\{\mathrm{E_k}\}\ e^{\gamma\ \tau/\mathrm{r}} \sin(\omega_{\mathrm{k}}\ \tau/\mathrm{r} + \phi_{\mathrm{k}}),$$

$$\text{with } \tau = 0, 1, 2, 3, ...\mathrm{N}-1 \tag{20}$$

The Kroneker delta function sums up all imaginary parts of the $\mathrm{E_k}$ and for itself behaves like the non-viscoelastic case, as shown above. The following sum can be performed only for those ω_{k} where $\mathrm{Re}\{\mathrm{E_k}\} \neq 0$ and is zero for all others. The sine functions need to be used for the transient case, where a drum is hit by a stick, or a guitar string by a finger, etc. There, starting from t = 0, the strains only build up, starting from $\epsilon(0) = 0$. Then the phase $\phi_{\mathrm{k}} = 0$. When using a cosine term, the convolution would be out of phase with the strains and therefore no viscoelastic damping can occur. Depending on the musical instrument investigated, ϕ_k can be any function, in the present study $\phi_{\mathrm{k}} = 0$ for all k.

Note that the Young's modulus in the case of no viscoelastic damping is now purely imaginary instead of real and only

get a real part when viscoelastic damping takes place. The reason is the use of s= $\alpha + \imath\omega$, where ω is the frequency and α the damping. This is no loss of generality, as also stress and strain are defined as functions of s like $\sigma(s)$ and $\omega(s)$, and therefore in terms of no viscoelastic damping their relative phases are zero as physically true.

Now as total damping consists of internal plus radiation damping, a term for modeling radiation damping is missing. The omitted temporal derivate term would not serve here well, as radiation damping is only roughly related to a simple exponential decay, the derivative term leads to, as discussed above. Radiation loss depends on the eigenmode shape of the radiating body and therefore also need to be modeled frequency-dependent, just like internal damping. Radiation damping could therefore be modeled geometrically by adding the air volume around the drum to the model. Still this would make computational time very much higher.

Still radiation loss can be calculated in alternative ways. If the geometry is simple, like with a circular drum, radiation loss can be calculated analytically. Alternatively, radiation loss can be calculated for more complex geometries when the vibration modes are known. Then radiation can be calculated as forward propagation by integrating the mode vibration into the air surrounding the drum. The amount of cancellation of energy due to phase differences in the modes determines the energy loss of this mode due to sound radiation. As the Finite-Difference model suggested here calculates the mode shapes anyway, this approach can be used to determine the energy loss due to radiation.

In this paper we are interested in viscoelastic damping alone. Addition other dampings would make the solution a combination of them and it would be hard to distinguish the strength of each damping one from another.

2.6 Membrane Model Properties

A circular drum was modelled with a radius of 10 cm a membrane tension $T = 1.7 \times 10^6\ N$ and an area density of $\mu = 10^{-3}$kg / m^2 which results in a fundamental frequency $f_0 = 306$ Hz for the undamped membrane. A regular rectangular grid of 104×104 nodal points was used laying over the circular membrane, where only grid points in the membrane area were used. The boundary conditions were fixed, so the displacement at the rim was $u_{rim} = 0$, but all possible slopes $\frac{\partial u_{rim}}{\partial x}$ and $\frac{\partial u_{rim}}{\partial x}$ were allowed.

Three frequencies were tested, the fundamental frequency $f_0 = 306$ Hz, $f_0 = 1092$ Hz and a high frequency $f_1 = 4174$ Hz. These frequencies are peaks in the undamped membrane and the influence of viscoelastic damping on them was tested.

The calculations were performed on a Graphics Processing Unit (GPU) with massive parallel computation. Still the model is not real-time and - depending on the GPU used - calculating one second of sound with a sample rate of 96 kHz takes between five to ten seconds.

The spatial grid was implemented on the GPU using three vectors of length $104 \times 104 = 10816$ vector entries, one for displacement, one for velocity, and one for displacement storage. The acceleration memory was implemented as a vector of $104 \times 104 \times 1000 = 10816000$ entries. The CUDA language was used, implementing the model on an NVIDIA GTX 1070 GPU on a laptop. The calculations for acceleration at a present time point, for velocity at a present time point, and for viscoelastic damping using the acceleration memory vector were implemented for all 10816 nodal points in parallel. The new accelerations on the grid were added to the end of the circular acceleration memory vector, and the pointer of this vector was shifted by one vector entry. After performing one time step the new calculated displacements were transferred to the displacement storage vector. From this displacement storage vector, in the next time step, the new accelerations etc. were calculated.

2.7 Post-Processing

To calculate the exponential decay parameter μ from the resulting time series of the model, a Wavelet transform at f_0 was performed using a complex Morlet wavelet. For adjacent time points the amplitude of the peak frequency was taken, resulting in a time series of this peak. An exponential decay of this amplitude leads to a steady slope when taking the logarithm of the amplitude time series, a method well known from room acoustics. This slope was calculated using a linear fit model with the data. With very fast decays only the part of the series was used which lies before the amplitude starts fluctuating strongly (see example below).

As viscoelastic damping applied to a single frequency is partly like a filter, for now simplifying by neglecting the amplitude modulation or the sideband effect, the frequency width of this filter is calculated from the time series too. As we deal with a musical signal having discrete eigenvalues this is not a straightforward process, like it would be when we would consider a continuous spectrum. The only way to estimate the influence of damping of a target frequency f_0 onto a neighbouring frequency f_1 is to calculate both damping coefficients μ_0 and μ_1. In analogy to the filter quality definition of Q = f / Δf, with Δ f the frequency width of half the amplitude as the center frequency of the band gap, we define the filter quality Q like

$$Q = \frac{\mu_0}{\mu_1} / \Delta f \,, \tag{21}$$

where $\Delta f = |f_0 - f_1|$. Q therefore gets higher with a narrower band gap, as one might be used to from filter Q values. In cases the neighbouring frequency f_1 is not affected by the damping, $\mu_1 = 0$. In these cases calculating Q from it does not make sense anymore, as this frequency no longer tells about the width of the band gap. In these cases no Q is displayed anymore. We will have this case below, and as there f_1 is the closest peak next to f_0 we cannot tell about the bandwidth anymore. Still this is not a problem, as defining a band gap only makes sense if there is an effect on neighboring frequencies, which no longer is the case there. These values are therefore of particular interest, in these cases one frequency can be damped without any effect to the rest of the spectrum.

3 RESULTS

To test the decay behavior, at first the model is applied to a 0-dimensional mass-spring system. Then results for the membrane are presented, discussing frequency dependency, Q-values, as well as stability.

3.1 Viscoelastic Damping of a Mass-Spring System

The most simple case of viscoelastic damping is that of a mass-spring system of Eq. 15, which is modeled here with D= 10^9 and mass m=1. The initial values are for the velocity $v(0) = 0$ and the displacement u(0) = 1, which were chosen to easily fit an exponential decay curve to the resulting time series u, starting at u(0) = 1.

The calculation was performed for four values of γ = 1, 1/10, 1/40 and 1/140, as shown in Fig. 1. The respective functions h are plotted within each case at the right lower corner. To each plot an exponential function was fitted by hand, starting at u(0) = 1 and meeting the next peak. The gray curve is the integral of the viscoelastic force acting back on the respective time point. In the general model $\sigma = \mathrm{E}\,\epsilon$ the displacement u would be the stress σ, and the stored acceleration corresponds to strain ϵ, which acts on the stress with a memory, the integral of the strains at the previous time points with h(τ). A sample rate of 96 kHz was used in the simulation to be the same as with the following example of a membrane.

Theory expects with no damping ($\gamma = 1$) a phase alignment between stress and strain, which is the case, and can be seen in the top plot of Fig. 1. The small time gap between the two curves comes from the time integration algorithm, delaying the acting integrated strain to the next sample point of the stress.

Also according to theory, with viscoelastic damping, strain and stress are out of phase with the strain leading, as shown with γ = 1/10 in the second plot from top. The function $h(\tau)$ is very short in this case and acts on the strain less than 1 ms. Still the damping is already strong with a fast decay over 5 ms.

Still when fitting an exponential curve to u(t), as e.g. with γ = 1/10, the curve does not fit the model results perfectly. The exponent μ of this fit was chosen by hand, starting at unity with t=0 and meeting the first peak of u(t). With following peaks the error increases. This becomes worse with higher damping case of γ = 1/40 (third plot from top).

This deviation of the decay of u(t) from an exponential decay is even worse for γ = 1/140. Here an amplitude and frequency modulation appears and u(t) is far from having a simple decay behavior. The deviations of decay in the first two examples γ = 1/10 and γ = 1/40 are therefore no artifacts of the calculation, but a basic behavior of viscoelastic damping.

The reason for this behavior appears when examining the integrated strain curve in gray e.g. with γ = 1/140. It only increases over two periods, as integration time is relatively long here, and previous u(t) enter over up to 6 ms. Still damping acts on u(t) right from the start, decaying u(t) fast.

Now the damping appears as the stored acceleration over time and is counteracting the acceleration at the present mo-

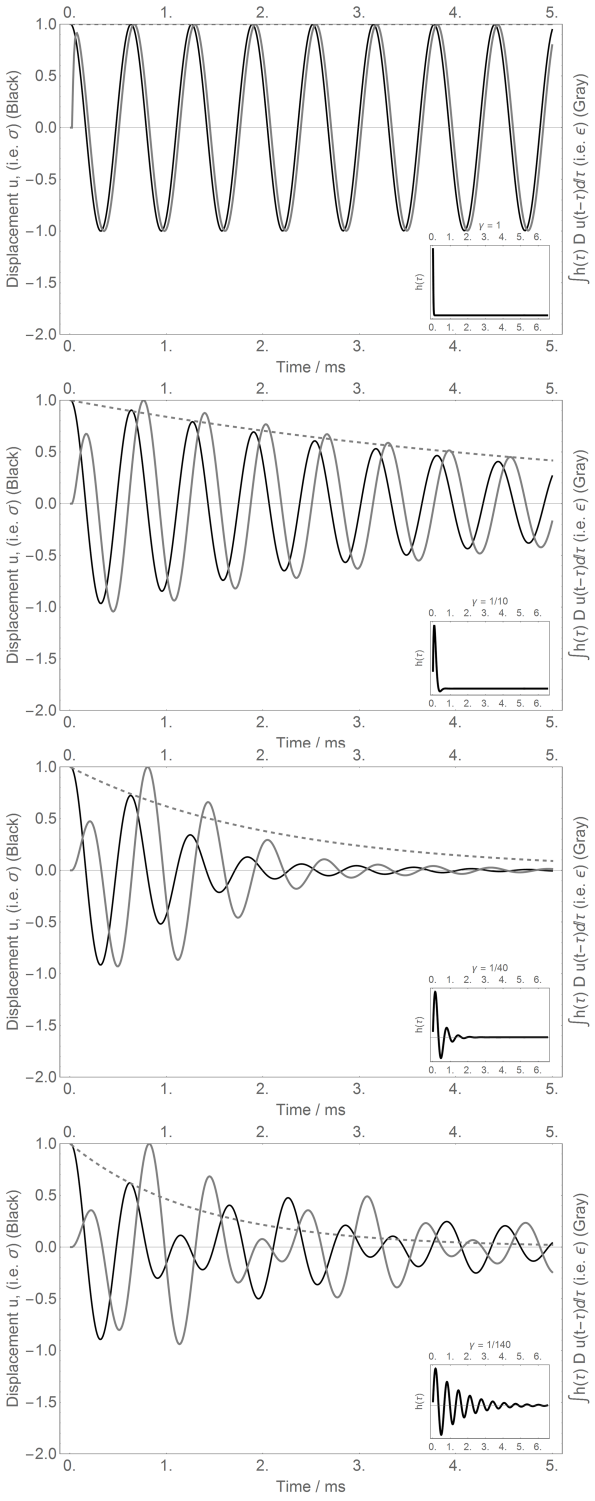

Figure 1: For viscoelastic damped time series u(t) of a mass-spring system with spring constant $D = 10^9$ vibrating at 1536 Hz, viscoelastic function h with a length of 10 periods of f, and for four inverse Laplace transform real kernel values γ = 1, 1/10, 1/40 and 1/140 (top to bottom). In each case h is inserted as a side plot within each case. An exponential fit is applied in all cases by hand to meet the first peak of u(t). In all cases such an exponential fit does not meet the results. For smaller γ an amplitude and frequency modulation appears.

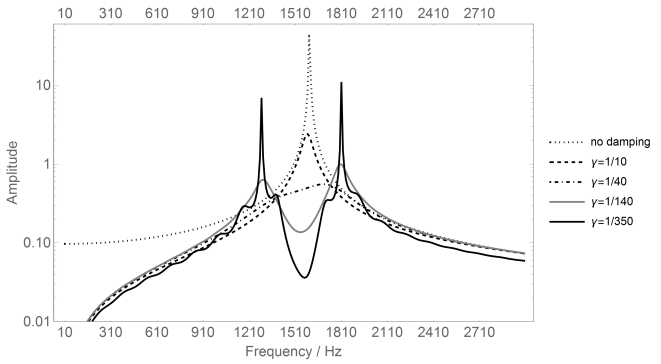

Figure 2: Spectra of the viscoelastic damped mass-spring system shown in Fig. 1 for no damping, γ = 1/10, 1/40, 1/140 and the additional case of 1/350. The original frequency at f = 1536 Hz is decaying with lower γ. At the same time sidebands appear, which become considerably strong with $\gamma = 1/350$. These sidebands are the result of the amplitude and frequency modulation of the decaying time series u(t) for small γ.

ment damping the system. Still if the system is already damped quite strongly and the stored acceleration is strong too, the counteraction overshoots, and part of the stored acceleration is now no longer acting as damping but as an energy supply. This is a fundamental physical behavior of viscoelastic damping, which was tried to illustrate with the example of the rotating egg above.

The back and forth of damping and enhancing of u(t) by the integrate d strain in the system leads to an amplitude, but also to a frequency modulation.

Fig. 2 shows the spectra of the time series of Fig. 1 for γ = 1/10, 1/40, 1/140 and additionally γ = 1/350. The case of γ = 1 is plotted too.

The decay at f clearly becomes stronger with decreasing γ, and the peak is gone with γ = 1/40. Still with γ = 1/140 two sidebands appear above and below f. With γ = 1/350 a series of these sidebands appear above and below f. These are the results of the amplitude and frequency modulation of the mass-spring system by the viscoelastic damping.

Therefore, as a first result of the method we find that a viscoelastic damped system does not have a simple exponential decay, as expected analytically, as shown above. This implies that Eq. 9 is not a solution of the system, which is expected, as it is no solution of the viscoelastic differential equation 11. We therefore find that the naive replacement of a real Young's modulus by a complex one, often assumed in modal analysis, leading to a simple exponential decay of the respective partial may be a good approximation with very slowly decaying modes, but is not sufficient for fast decays. Still most structures of musical instruments, like wooden plates or membranes, especially at high frequencies often have a very fast decay, and therefore can show a very complicated decay behavior and a decay time not meeting that of an exponential decay.

The example is only 0-dimensional. Therefore the appearing side bands clearly come from the modulation of the vibrating point mass. Still with higher-dimensional geometries,

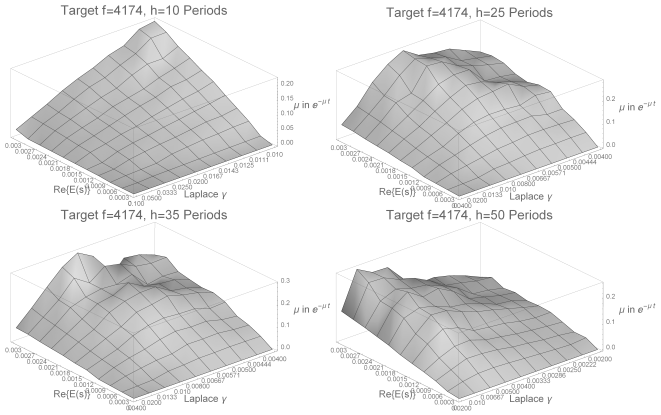

Figure 3: Damping exponent μ calculated as interpolation from the time series of the model at f = 4174 Hz for four different amounts of periods of f: 10, 25, 35 and 50 periods. In each case Re$\{$E(s)$\}$ was increased from 0 to 0.0003 in ten equal steps, and the inverse Laplace real part of integration γ was used from 1/10 to 1/100 (10 periods), 1/25 to 1/250 (25 and 35 periods) and 1/50 to 1/500 (50 periods). These values were used to stay within a stable region of the model. The resulting μ have a peak around $\gamma = 1/150$, independent from the amount of periods used. μ decreases after this peak, indicating a growing influence of driving energy caused by longer delays.

like with the membrane discussed next, the energy of the side bands might meet other vibrating frequencies present at the side band frequencies. Then we have an energy transfer between two modes, a mode coupling. Such a mode coupling is hard to distinguish from other effects in a higher-dimensional geometry. Still as the 0-dimensional case is clearly showing a mode coupling, we do expect such an energy transfer between modes also for all higher-dimensional cases.

3.2 Viscoelastic Membrane

To test the membrane model it is damped at one single frequency only, here at $f_1 = 4174$ Hz, later also at $f_0 = 1092$ Hz and $f_0 = 306$ Hz. The model has three tunable parameters for one frequency, the real part of the Young's modulus Re$\{$E(s)$\}$, the inverse Laplace transform integration real constant γ, and the length of h(τ), the time series corresponding to E(s).

As shown with the mass-spring model, the damping is not an exponential decay. Still to arrive at an estimate about the damping strength, such an exponent μ is still calculated, using a complex Morlet wavelet transform with a very long wavelet number of 60 wave periods, as discussed above. Other methods could be used, like detecting the last amplitude of the damped frequency in time above a certain threshold. Still with amplitude modulated sounds, easily present in musical instruments, this might lead to artifacts as well. The problem of defining such a parameter is also one of measuring damping from a recorded sound, which is not at all trivial, and beyond the scope of this paper.

Fig. 3 shows all three parameters discussed above changed within a parameter space. Four cases of the length of $h(\tau)$

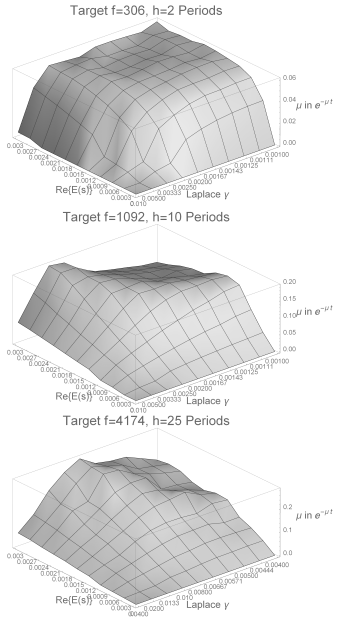

Figure 4: Damping exponent μ for three target frequencies damped by the model: 306 Hz, 1092 Hz, 4174 Hz over their stable parameter range for γ and Re{E(s)}. The basic property of a maximum damping at a certain γ is present in all cases.

are shown in the amount of periods of f_1, 10, 25, 35 and 50 periods. The up axis is the resulting damping exponent μ as calculated from the resulting time series by exponential fit of the amplitudes from the wavelet transform. The other axis are Re{E(s)}, which in all cases has been varied in ten equal steps from 0 to 0.0003, and the Laplace transform real parameter γ. This has different variations, depending on the amount of periods used, it was varied from 1/10 to 1/100 (10 periods), 1/25 to 1/250 (25 and 35 periods) and 1/50 to 1/500 (50 periods). The parameters were set this way to ensure a stable algorithm. When increasing the parameters beyond the shown region, the resulting time series will constantly and exponentially increase in amplitude, which is unphysical as there is no additional energy supply to the system. In other words, for values beyond the shown parameter spaces the algorithm blows up. Therefore we have a trade-off between stability and computational cost, as longer $h(\tau)$ means more computation time and memory.

In three cases, 25, 35 and 50 periods, there is a peak of maximum damping μ. Damping increases with increasing Re{E(s)} as expected, but also when lowering γ from high values to lower ones. The peak in all three cases is around $\gamma = 1/150$. The 10 period case does not reach this γ and therefore the peak is not present there.

After $\gamma = 1/150$ the damping exponent μ decreases again. This is expected remembering the results of the mass-spring system, as with smaller γ the viscoelasticity also acts as a delayed energy supply. The fact that the peaks of maximum decay μ are independent of the length of h(τ) is according to theory.

As a consequence one might find that 10 periods are enough for such a frequency, as here the maximum possible damping

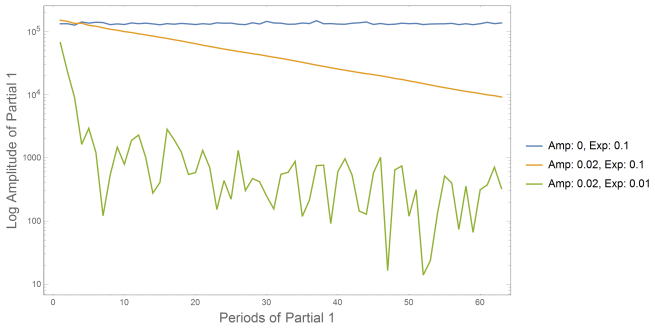

Figure 5: Three examples of the decay of frequency $f_0 = 306$ Hz for three different cases, a) Re{E(x)} = 0, $\gamma = 1/10$, b) Re{E(x)} = 0.02, $\gamma = 1/10$, c) Re{E(x)} = 0.02, $\gamma = 1/100$. The decays are steady transformed into a decay parameter μ by a linear model fit. The case c) has a fast decay and continuous fluctuations afterwards. Here only the beginning has been used to fit the linear decay model.

can be reached, next to all other damping strengths. Still this is not perfectly the case because of two reasons. First, when discussing the filter depth, or filter quality Q of the model, the length h(τ) does play a crucial role, as we will see below. Secondly, the damping curve changes with smaller γ making larger h(τ) necessary. Therefore when reproducing a complex damping amplitude decay curve, this might only be possible using small γ for which large h(τ) are needed.

A maximum μ at a certain γ found with 4174 Hz is also true for other frequencies. In Fig. 4 three cases are shown, for 306 Hz (γ from 0.001 to 0.01), 1092 Hz (γ from 0.004 to 0.04) and again for 4174 Hz (γ from 0.004 to 0.04) with $Re\{E(s)\}$ from 0 to 0.0003 in ten steps in all cases. The maximum damping μ in the resulting time series at a certain γ is present in all cases. This feature holds over the whole frequency range as expected, although γ becomes larger with lower frequencies.

The decay of three examples for the case of $f_0 = 306$ Hz are shown in Fig. 5. The plot displays the peak amplitudes over time for adjacent periods of f_0. The amplitude axis is logarithmic, therefore with an exponential decay a straight line with a constant slope is expected. In the first case of no damping the slope is zero. For the second case of a slightly damped f_0 the slope is very constant and the decay does not deviate from a simple exponential one considerably. Titting a μ to this decay is therefore straightforward. Still the third example shows a very fast decay, followed by an amplitude fluctuation which is overall decaying but much slower than its beginning. The fluctuations are no noise, as the amplitude is not small enough to end in discretization noise. Also the periodicity is quite regular and starts at the fast decay part already. This is an example of a complex damping and closely aligns with the results from the mass-spring model.

3.3 Damping Frequency Width Q

When damping a spectrum at a certain frequency, neighboring frequencies will be effected too. This corresponds to filter theory, where the width of the filter might be defined as Q= Δ f / f, where f is the frequency and Δf is the frequency

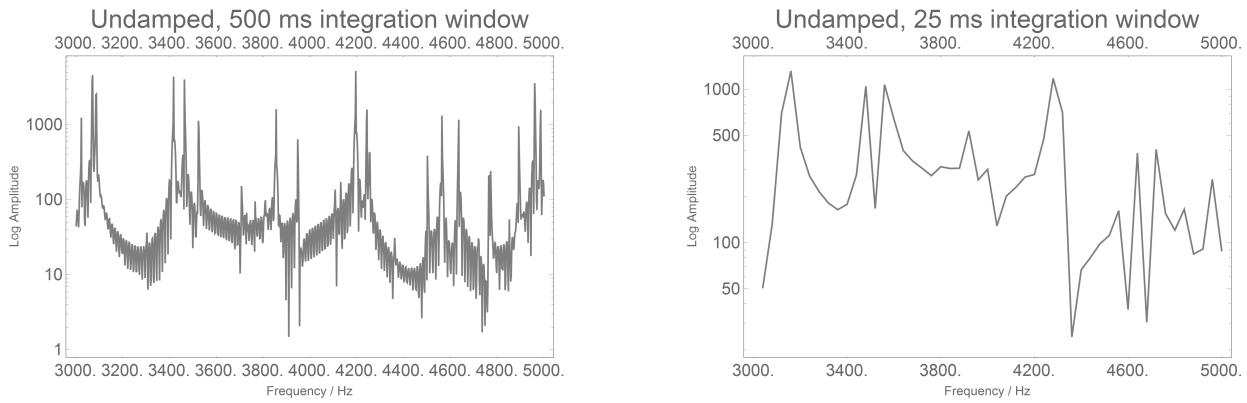

Figure 6: Spectra of the frequency region around f = 4174 Hz over an FFT length of 500 ms (left) and 50 ms (right). The peaks resolved for 500 ms are blurred for 50 ms. As the length of $h(\tau)$ is between 1 and 6 ms, the damping algorithm deals with the blurred case. Therefore the neighbouring frequencies f_1 = 3860 Hz and f_2 = 4587 Hz were used for calculating the damping frequency width Q.

width over half the amplitude of neighboring damping. As discussed in the methods section, this definition cannot trivially be transferred to the present case, as we do not have a continuous spectrum, but one consisting of discrete mode frequencies. Therefore the damping of the neighboring frequencies f_1 and f_2 below and above the damping target frequency f are taken as a reference for the damping frequency width Q.

In the present case, again looking at 4174 Hz as the target frequency, a bundle of single frequencies are present. Still only when using a large Fourier transform window of about 500 ms these single frequencies are resolved. As the length of the function $h(\tau)$ has a maximum of about 6 ms and often is less than 1 ms, these single frequencies are not resolved during the damping process. Therefore in the analysis the broader peak around f = 4174 Hz, f_1 = 3860 Hz and f_2 = 4587 Hz are taken. The frequencies were calculated using again the Wavelet transform using a wavelet number of 5, and detecting the frequencies at amplitude maxima of the blurred spectral peaks.

In Fig. 7 and Fig. 8 the Q for the case of f = 4174 Hz and the two neighbouring frequencies f_1 and f_2 are shown. Both compare f once with f_1 (left plot each) and f with f_2 (right plot each). Each line represents changing $\mathrm{Re}\{E(s)\}$ for one γ.

Overall with decreasing γ, Q increases. This means that when the function $h(\tau)$ decays slower, the sharpness of damping improves. This is expected and is analog to filter theory. The dependency of Q on $\mathrm{Re}\{E(s)\}$ may be neglected, like with the 10 period case for f_1 (first figure, left plot). Still in the case of f_2 there clearly is a dependency on the real part of the complex Young's modulus, still not a trivial one.

The reason for this behavior could be found in the fact that the target frequency damping effects all peaks present in the peak bundle around f_2, which results in a complex amplitude modulation of f_2, caused by the beating of frequencies. As these single frequencies in the bundle are damping with a different amount, depending on their distance from f, the amplitude modulation is not constant and might become very complex. Then fitting a simple exponential decay to such a complex decay could lead to such a behavior.

When examining the 50 period cases, although the basic pattern of increased Q with decreased γ continues, the plot looks more complex than for the 10 period case. The reason is that with longer $h(\tau)$ the amplitude beating, as discussed with the mass-spring system, is getting more and more prominent. Combined with the very fast decay of the partial and the problem discussed above with the beating within the frequency bundle, the fit of the decay to a simple exponential fit will again cause such a complex pattern.

In the 50 period plots we also find some curves not complete and ending at some $\mathrm{Re}\{E(s)\}$ with no values on the left anymore. This are the cases where there is no damping of f_1 or f_2 anymore when damping f, and therefore Q becomes infinity (not displayed). These cases are particularly interesting, as they mean a very sharp Q with no influence of the target frequency on neighbouring frequencies.

Similar results appear for the 25 period and 35 period case at this frequency, therefore displaying the results is omitted here. A gradual transition from 10 period with fairly ordered curves to 50 period with more complex behavior can be observed with the 25 and 35 period cases.

4 CONCLUSION

When implementing viscoelastic damping as a memory effect in the time-domain, the resulting amplitude drop of the damped frequencies is not a simple exponential decay. With small viscoelastic effects and long decay times the difference between the real and the exponential decay might be small. Still with strong damping present in wood or leather, an exponential decay rate is no longer a good approximation.

Furthermore, due to the memory effect beatings appear in the decay due to energy supply from the memory to the present vibration, leading to an amplitude increase. This leads to an amplitude and frequency oscillation and therefore to sidebands in the spectrum. These sidebands mean an energy transfer from the target frequency of damping to neighboring frequencies which causes a mode coupling.

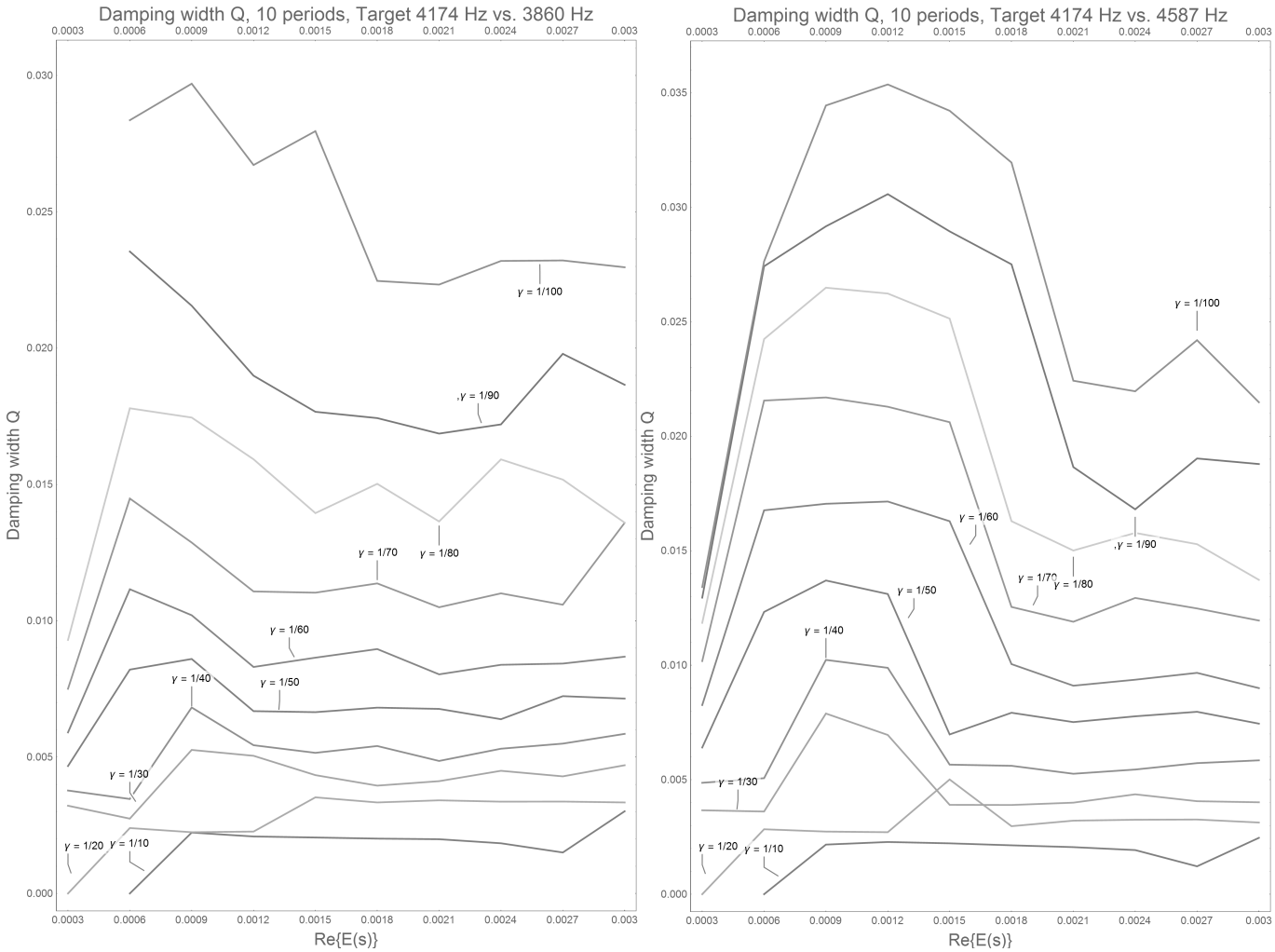

Figure 7: Damping width Q for the 10 period case comparing the target frequency f with f_1 (left plot) and f_2 (right plot). In both cases Q increases with decreasing γ, therefore lowering the damping of the neighboring frequencies when damping the target. For f_2 a dependency of Q on $\mathrm{Re}\{E(s)\}$ appears which is not so prominent with f_1.

Also the length of the memory in most viscoelastic cases is very short, it might be below 1 ms, maybe up to 6 ms (although the time constant of viscoelastic damping might be up to weeks or years as discussed in the introduction). But within very short time scales the frequency range of damping has a certain width, and therefore a damping width Q can be defined as the relation of damping strength of the target frequency to neighboring frequencies. This damping width is larger with smaller damping functions $h(\tau)$ and smaller exponents γ as expected. Still this damping width also means that many peaks in this regions are damped simultaneously, but with different strength, depending on their distance to the target frequency. This leads to very complex amplitude beatings in these regions during the decay.

Many of these damping behavior found, like a very sharp decay right after the beginning of the sound followed by a slower decay with amplitude beating, are present in real musical instrument recordings. Such sounds are found with percussion instruments like the xylophone, bass and snare drums of a modern drum kit, or with wood blocks. They are also found with harps, flamenco guitars, or upright pianos. All such instruments have a complex initial transient, followed by a pitched decaying sound. Still there are many other reasons for amplitude decay, like radiation damping, energy conversion between modes, or related things. Still viscoelastic damping is one of the components leading to such behavior.

After understanding the behavior of viscoelastic damping in terms of the amplitude decay, the next step is to model the recorded damping of a real guitar top plate or piano soundboard with the viscoelastic damping model. This is work for future projects.

ACKNOWLEDGEMENTS

The work was funded by Deutsche Forschungsgemeinschaft (DFG).

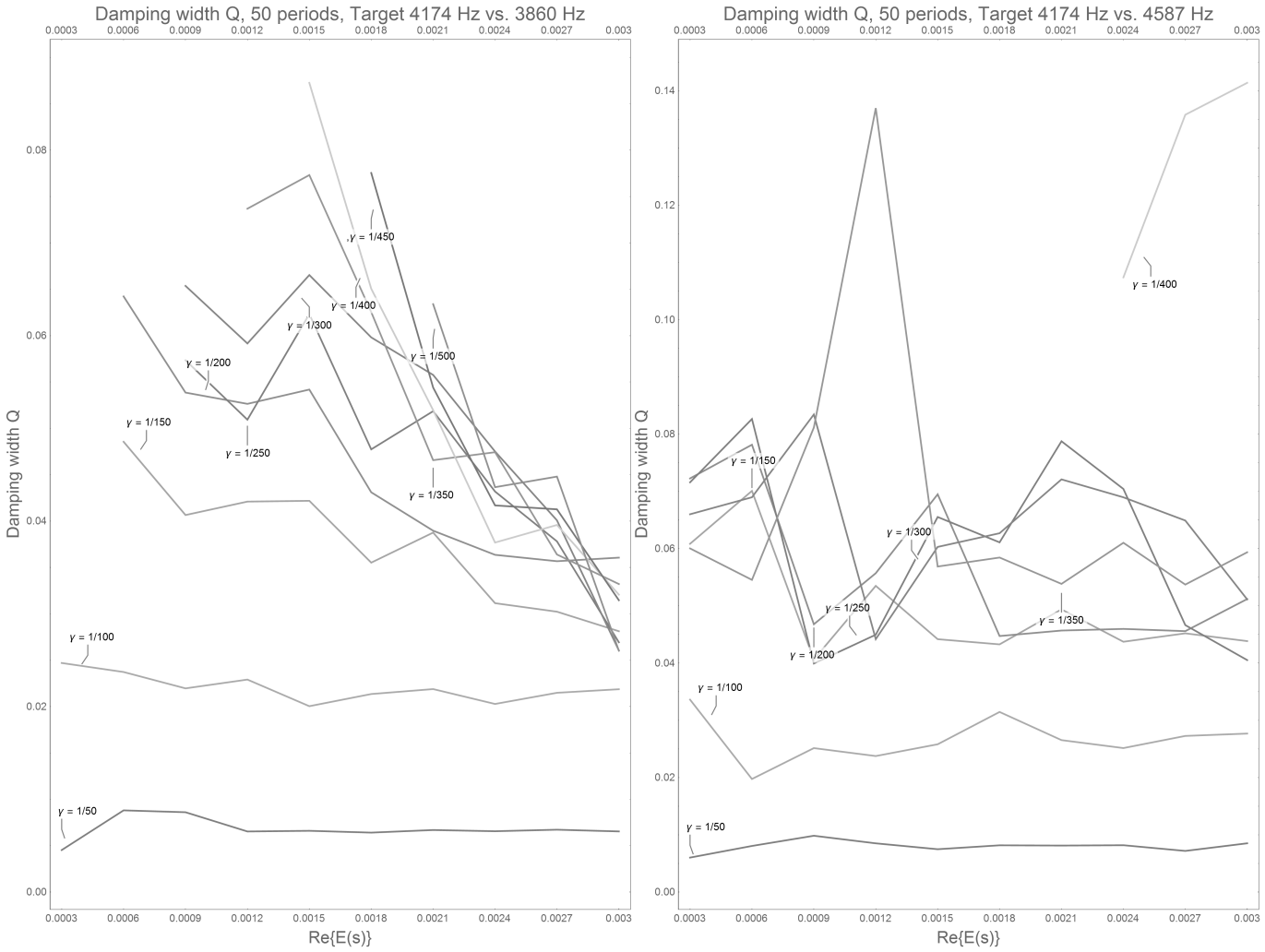

Figure 8: Same as Fig. 7, here for the 50 period case with lower γ. The basic pattern of larger Q with lower γ repeats, still in a more chaotic manner. This is due to very fast decay and the fact that the fitting of the damping curve to an exponential fit used to estimate μ, from witch Q is calculated becomes more problematic. The cases where the lines end (left plot high Q, low γ mean that there is no damping found anymore of the neighboring frequencies. Therefore here the damping Q is so sharp that it does no longer affect neighboring modes.

REFERENCES

[1] R. Bader, "Finite-Difference model of mode shape changes of the Myanmar *pat wain* drum circle using tuning paste", *Proc. Mtgt. Acoust*, vol. 29, 035004, pp. 1-14 (2016).

[2] R. Bader, "Nonlinearities and Synchronization in Musical Acoustics and Music Psychology," Springer-Verlag, Berlin, Heidelberg, Current Research in Systematic Musicology, vol. 2, pp. 157–284 (2013)

[3] R. Bader, "Finite-element calculation of a bass drum," *J. Acoust. Soc. Am.*, vol. 119, pp. 3290 (2006).

[4] I. Brémaud, J. Ruelle, A. Thibaut, and B. Thibaut, "Changes in viscoelastic vibrational properties between compression and normal wood : roles of microbril angle and of lignin," *Holzforschung*, vol. 67(1), pp. 75-85 (2013).

[5] I. Brémaud, "What do we know on " resonance wood " properties? Selective review and ongoing research," *Proceedings of the Acoustics 2012 Nantes Conference* (2012).

[6] I. Brémaud, J. Gril, and B. Thibaut, "Anisotropy of wood vibrational properties: dependence on grain angle and review of literature data," *Wood Sci. Technol.*, vol. 45, pp. 735–754 (2011).

[7] S. Bilbao, "Time-domain simulation and sound synthesis for the snare drum," *J. Acoust. Soc. Am.*, vol. 131 (1), pp. 914-925 (2012).

[8] A. Chaigne, and Ch. Lambourg, "Time-domain simulation of damped impacted plates. I. Theory and experiments," *J. Acoust. Soc. Am.*, vol. 109 (4), pp. 1422-1432 (2001).

[9] A.D. French, and G.P. Johnson, "Advanced conformational energy surfaces for cellobiose," *Cellulose* vol. 11 pp. 449–462 (2004).

[10] Y.-F. Hwang, and H. Suzuki, "A finite-element analysis on the free vibration of Japanese drum wood barrels under material property uncertainty," *Acoust. Sci. & Tech.*, vol. 37 (3), pp. 115-122 (2016).
[11] S. Jeyapalina, "Studies of the hydro-thermal and viscoelastic properties of leather," PhD, Univ. of Leichester (2004).
[12] Maccaferri plastic guitar in the Museum of Arts and Applied Science, Sydney. Seen 13.5.2019: https://maas.museum/inside-the-collection/2009/06/17/maccaferri-plastic-guitar/
[13] W. Müller, M. Kästner, J. Brummund, and J. Ulbricht, "On the numerical handling of fractional viscoelastic material models in a FE analysis," *Comput. Mech.*, vol. 51, pp. 999-1012 (2013).
[14] L.M. Nickerson, and Th.D. Rossing, "Acoustics of the Karen bronze drums," *J. Acoust. Soc. Am.*, vol. 106, pp. 2254 (1999).
[15] A.N. Norris, and D.M. Photiadis, "Thermoelastic Relaxation in Elastic Structures, with Applications to Thin Plates," *arXiv*, arXiv:cond-mat/0405323v2 [cond-mat.mtrl-sci] (2004).
[16] E. Obataya, T. Umezawa, F. Nakatsubo, and M. Norimoto, "The effects of water soluble extractives on the acoustics properties of reed (*Arundo donax L.*)", *Holzforschung*, vol. 53, pp. 63-67 (1999).
[17] A. Pierce, "Intrinsic damping, relaxation processes, and internal friction in vibrating systems," *POMA*, vol. 9, pp. 1-16, (2010).
[18] Th.D. Rossing, "Science of Percussion instruments." World Scientific, Singapore (2008).
[19] G. Sathej and R. Adhikari, "The eigenspectra of Indian musical drums," *J. Acoust. Soc. Am.*, vol. 126 (2), pp. 831-838 (2009).
[20] H. Suzuki and Y. Miamoto, "Resonance frequency changes of Japanese drum (nagado daiko) diaphragms due to temperature, humidity, and aging," *Acoust. Sci. & Tech.*, vol. 33 (4), pp. 277-278 (2012).
[21] A. Tramer, Ch. Jungen, and F. Lahmani, "Energy Dissipation in Molecular Systems." Springer (2005).
[22] R. Worland, "Demonstration of coupled membrane modes on a musical drum," *J. Acoust. Soc. Am.*, vol. 130, pp. 2397 (2011).
[23] R. Worland, "Normal modes of a musical drum head under non-uniform tension," *J. Acoust. Soc. Am.*, vol. 127 (1), pp. 525-533 (2010).
[24] P. Wriggers, "Nichtlineare Finite-Element Methoden. [Nonlinear Finite-Element Methods]", Springer (2001).
[25] X.Q. Zhou, D.Y. Yu, X.Y. Shao, S.Q. Zhang, and S. Wang: "Research and applications of viscoelastic vibration damping materials: A review," *Composite Structures*, vol. 135, pp. 460-480 (2016).
[26] X.Y. Zhou, D.Y. Yu, X.Y. Shao, S. Wang, and Y.H. Tian: "Asymptotic analysis on flexural dynamic characteristics for a sandwich plate with periodically perforated viscoelastic damping material core," *Composite Structures*, vol. 119, pp. 487-504 (2015).
[27] X.Q. Zhou, D.Y. Yu, X. Shao, S. Wang, and Y.H. Tian: "Band gap characteristics of periodically stiffened-thin-plate based on center-finite-difference-method," *Thin-Walled Structures*, vol. 82, pp. 115-123 (2014).

(Received May 1, 2020)

Rolf Bader Rolf Bader is professor for Systematic Musicology at the University of Hamburg. He also studied Physics, Ethnology, and Historical Musicology. After teaching at Stanford University as a Visiting Scholar is a lecturer for Systematic Musicology in Hamburg since 2007. His main research interests are Physical Modeling of Musical Instruments, Timbre and Rhythm Perception, Musical Signal Processing, Room Acoustics, or Music Ethnology. He also worked on Self-organization and Synergetics of Musical Instruments and Music Perception. He is the editor of the Springer Handbook of Systematic Musicology, and wrote monographs like Computational Mechanics of the Classical Guitar (Springer 2005) or Nonlinearities and Synchronization in Musical Acoustics and Music Psychology. He is editor-in-chief of the Springer Series Current Research in Systematic Musicology where he also published a monograph, as well as the volume Sound-Perception-Performance and Computational Phonogram Archiving as an editor. He also works as an Ethnomusicologist mainly in Myanmar, Cambodia, China, India or Sri Lanka and is about to build up a Computational Ethnomusicological Sound Archive ESRA at his Institute. He is also a musician and composer in the fields of free improvised and electronic music, as well as Fusion and Rock, and published several CDs.

Invited Paper

Digital to Natural - Innovation for Smart World

Susumu Yamamoto*, Akira Nakayama*, and Katsuhiko Kawazoe*

*NIPPON TELEGRAPH AND TELEPHONE CORPORATION, Japan
{susumu.yamamoto.vk, akira.nakayama.vr, k.kawazoe}@hco.ntt.co.jp

Abstract - With the development of information and communication technologies, it is hoped that a world in which all people can live bountiful and happy lives can be achieved using innovative technologies. In other words, a Smart World. "Digital to Natural" is a transformation that is crucial to turning the concept of a Smart World into a reality. It means not only pursuing the ultimate digital vision of high-speed, high-capacity, high-definition performance, but also creating new value that can be achieved by naturally capturing and making the best use of a variety of information that previously could not be captured by humans. This will allow people to naturally and unconsciously benefit from technology. This paper describes what should be considered in order for technology to evolve into a more natural form, and shows technologies that support it such as AI, visual media, and ICT infrastructures – IOWN. This paper also presents concepts for several services that this technology can enable.

Keywords: natural, generous AI, Kirari, IOWN, Point of Atmosphere

1 INTRODUCTION

With the development of information and communication technologies (ICT), the society of the future will be the fifth society to evolve, following on from the previous four stages of human social evolution. Society 5.0 can be regarded as a super smart society that takes the fullest advantage of digital innovation[1]. The world that will be created through society 5.0 is a Smart World, in which everyone's lives and society itself will be totally changed for the better in every way.

How can we create this new Smart World? In creating new value for society, it is of course important to consider "technology innovation" that seeks to improve performance, such as communication capacity, but it is also important to consider "value innovation" that creates new social values at the same time.

ICT has evolved as the frontier of "digital." But should we continue along this path? In other words, what should we aim for next at this time when "digital" has reached its peak? We believe that what we should aim for is embodied by the keyword "natural." That is "Digital to Natural." The next step in digital's evolution is towards natural.

This paper describes what should be considered so that technology can evolve into a more natural form, and shows the technology that supports it and the concepts of the services that it enables. The rest of this paper is organized as follows; Section 2 presents some examples of what we think of as natural. Section 3 shows the direction in which the technologies supporting natural should go, particularly for AI, visual media, and ICT infrastructures. Section 4 presents the concepts of services that blend naturally into people's lives, and Section 5 concludes this paper.

2 DIGITAL TO NATURAL

"Digital to Natural" is the next paradigm change for technologies. This section describes two viewpoints: why and what we think of as natural for the evolution of technologies.

2.1 "Natural" for Diverse Value Judgement

In a diverse world, inhabited by people of all nationalities, ages and backgrounds, it is full of different value judgements. In such a world, "natural" is important if individuals and businesses, regardless of their characteristics, are to benefit from technology. Sometimes it keeps a caring eye on the lives of people without them being aware of it; sometimes it helps people do things more efficiently; and sometimes it appeals to their emotions. It also helps to provide a comfortable environment that is friendly to people and the global environment. We think the future of ICT should be seen in this way.

For technology to make this vision a reality, it is not enough to develop high-definition and high-sensitivity sensors and obtain more information. We will need innovative information processing that understands the senses of others and the subjectivity of each individual, and to look beyond conventional wisdom toward the diversity of life and systems. Where the result of such technology can be enjoyed by humans without feeling any stress or discomfort, we call this congenial state "natural" and this state is the objective which we pursue.

2.2 Creating Innovation through Learning from Living Things

The diversity of values is not limited to the human world. For example, imagine beautiful yellow flowers. Human beings perceive colors in a certain way that allows them to appreciate and enjoy the beauty of flowers (Figure 1(a)). The way in which honeybees perceive flowers, on the other hand, is very different as they can see ultraviolet rays, and the center of the flower is emphasized (Figure 1(b)). For honeybees, a beautiful-looking flower has no intrinsic value. However, it is important for them to know where the nectar

and pollen of flowers is in order to live, and that is the "value" for honeybees.

Let's take another example; imagine mantis shrimps in the sea. They have receptors that can discriminate as many as 12 different colors [2]. Humans discriminate intermediate colors based on three primary color (red, blue, and green) receptors and information processing in the brain. In contrast, mantis shrimps sense things extremely rapidly with their 12-color receptors and minimal information-processing (Figure 2). What's of value to them is a high-speed response in order to capture their prey moving through the water. In the case of honeybees, what's remarkable is that they can see what humans cannot. What is notable about mantis shrimps is that they have a mechanism for directly processing information.

For a long time, humans have created innovations through learning from other living things, especially by mimicking them. The designs of jet planes and trains are examples of using such a mimicry approach. We want to take it a step further. Every animal species has a unique sensory world in which it lives. Jakob von Uexküll, a German biologist, called this phenomenon "umwelt" to signify a self-centered world, using the German term for "environment." [3] It means that how things look varies depending on the viewer. Accordingly, the type of information a species transmits and the way it processes information vary depending on what is of value to that species. We believe that if we regard the world as a field that holds diverse values, and if we can use "natural" information as it exists in the world, hitherto unused due to the digitization of current sensors being limited, such as digital sampling and quantization, we will be able to create new values that we could have never previously imagined.

(a) (b)

Photo by Bjørn Rørslett / Science Photo Library (Aflo)

Figure 1: Flower as viewed by humans and honeybees.

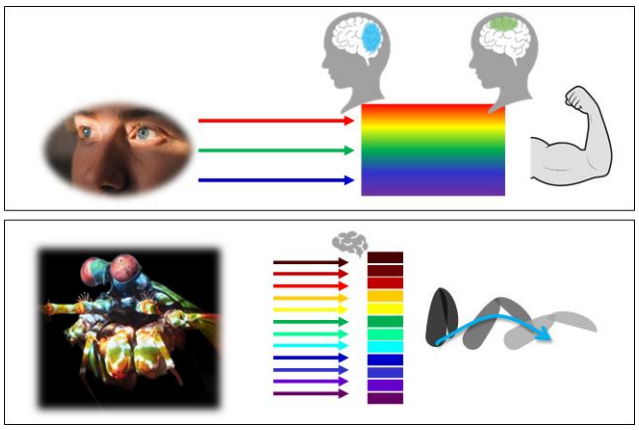

Figure 2: Comparison between the ways in which humans and mantis shrimps see something.

3 TECHNOLOGIES FOR NATURAL

This section provides some examples of technologies that can lead to natural value, and how these technologies should evolve hereafter, particularly for AI, visual media, and ICT infrastructure.

3.1 AI

(1) Natural conversation with robots

The first one is interaction with robots. Even now, there are examples of robots being used in shops to guide customers. But they are not able to function at a particularly high level. This is because that, currently, most robots can only converse within the context of a predetermined scenario, or are capable of asking only simple questions and providing simple answers. However, human conversations frequently involve unscripted small talk and discussions.

Higashinaka et al. [4][5] have developed robots which can enter into a more realistic discussion. This research led to the creation of a discussion structure that allows opinions about certain topics to be expressed, and they developed a mechanism to extract opinions that either support or disagree with a certain proposition depending on what the other party says. Through the evolution of this kind of technology, human activities are supported more naturally by making people and AI understand each other better through authentic conversations.

(2) Crossmodal voice / face conversion

Another example is how AI now has the ability to discern sound in a more human way. Humans can conjure an image of what a person's face looks like from the impression created by his/her voice, or what someone's voice may sound like from the impression created by his/her face. Kameoka et al. [6] showed how AI might be able to do this. They developed a cross-modal voice conversion model using deep generative models, which can convert speech into a voice that matches an input face image and generate a face image that matches the voice of the input speech by leveraging the correlation between faces and voices. Humans can recognize things by using different senses, such as vision and hearing. We believe it is important to create natural AI that is more responsive to people's feelings by providing AI with these unique human abilities.

(3) Seeking more natural AI

The performance of AIs when listening, speaking, and viewing things is improving. The time will come when it is more than adequate. We believe that at some stage in the future, thinking AI that supports human thought processes will become more important than ever.

The future of AI should be one that incorporates various values and helps people to consider complicated problems for which there is no single answer. For example, the best route to travel from one place to another may depend on a person's values, personality, circumstances, and habits, such as wanting to go quickly, have fun, or go safely. We believe it is important for AI to understand these differences and

handle variations in values in order to find the best solution for each individual. We call such AI "generous" AI.

3.2 Ultra-realistic Viewing

(1) Kirari

High image definition technologies such as 4K and 8K will create a greater than ever sense of excitement. However, it is questionable whether it is effective to continue increasing the resolution in order to further raise the level of excitement. People feel a sense of presence through complex perceptual processing, and it is important to utilize multiple types of sensory information beyond the monitor frame. The objective of the "Kirari!" project [7][8] is to provide more natural video services.

The concept of Kirari was announced in 2015 and used a table tennis match as an example (Figure 3). The table tennis tables were real, but the players and the balls were not; they were actually displayed in virtual 3D. This demonstrated that by combining real and virtual, you could experience sports with a very realistic feeling, just as if you were present in the stadium. The most important aspect of the Kirari concept is that it creates a natural and highly realistic space by decomposing a scene into its constituent elements such as video streams, audio, lighting and other sensory information, transmitting these elements separately, and then recomposing them in a way that is best suited to the conditions at the viewing site.

(2) Ultra-wide viewing

Another technical feature of Kirari is ultra-wide viewing. For example, windsurfing competitions are difficult to follow as they are taking place far away from the beach, and spectators cannot understand what is happening in a contest if they can only see a specific part of the course. To understand what is taking place, even a 4K screen alone is not enough. Kirari's ultra-wide viewing technology stitches together multiple 4K screens in real time to create a very wide screen at a remote venue (Figure 4). The spectators will actually feel as if they are present at the venue and watching what is taking place. This can be applied to many different sports including soccer and baseball [9][10]. It also makes it possible for spectators who cannot easily visit a distant venue, such as those confined to a wheelchair, to enjoy sports.

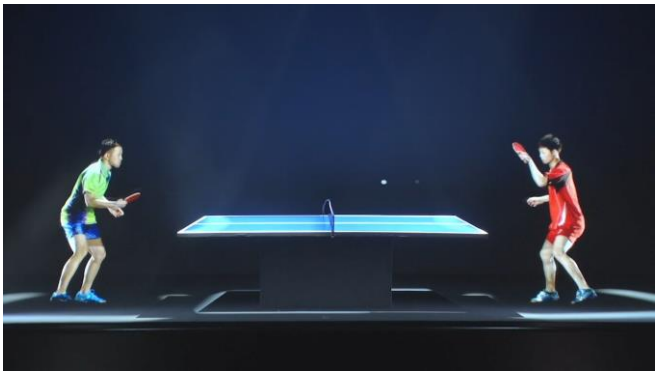

Figure 3: Kirari.

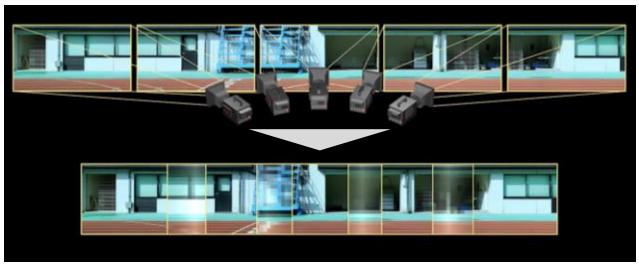

Figure 4: Ultra-wide viewing.

(3) Use case of Kirari

Kirari has also led to innovations in the field of entertainment, for example, new Kabuki productions using ICT. In the show "Cho Kabuki," a virtual idol called Miku Hatsune, and a real Kabuki actor, Shido Nakamura, were able to perform together using ICT [11]. Many people, especially young people who are not familiar with Kabuki, watched Cho Kabuki and discovered how entertaining Kabuki really is. It has really contributed to the creation of new values.

Kirari will continue to evolve. Its aim is not only to convey images and sound as they are, but also to activate people's sensitivity and psychology based on stories, such as those from history, and knowledge. This is truly Natural, as it conveys emotions to the human mind.

3.3 ICT Infrastructure

(1) IOWN

The conventional motivations for development of information and communication processing have been to increase speed, capacity and efficiency using digital signal processing. For example, the Internet has proven useful for providing many services and supporting business activities through adoption of common protocols to make an inexpensive network available based on the "best-effort" principle. Today, the volume of Internet traffic is increasing exponentially. Cisco estimates that global IP traffic is growing at a rate of 26% per year, and will total nearly 400 exabytes of traffic per month in 2022 [12]. However, there are limits. As traffic and data processing volumes grow, the power consumption of IT equipment also continues to increase. To date, integrated circuit performance has continued to increase exponentially, but we are approaching its limits.

If we are to evolve technology to simultaneously capture the diverse values that exist in the world, we need to penetrate new technical domains. Both the umwelt of honeybees and that of mantis shrimps actually exist in this world. But, these worlds are missing from the current world of IP or the digital world. We want to convey sufficient information and process it appropriately based on diverse values, and to provide benefits in a natural way.

To achieve this innovation, NTT, Intel and Sony have announced a new infrastructure concept called IOWN, Innovative Optical and Wireless Network [13][14]. IOWN is aimed at providing an innovative information processing platform that supports processing on a massive, unprecedented scale, and brings about changes that surpass the limitations of conventional technologies, such as power consumption barriers.

Figure 5 shows the three elements that comprise IOWN:

- All-photonics network is designed to dramatically enhance the potential of the information processing base.

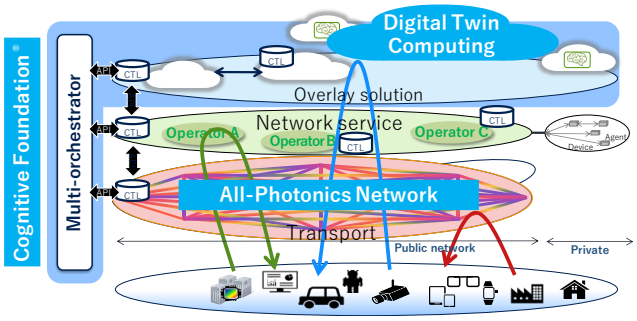

Figure 5: IOWN.

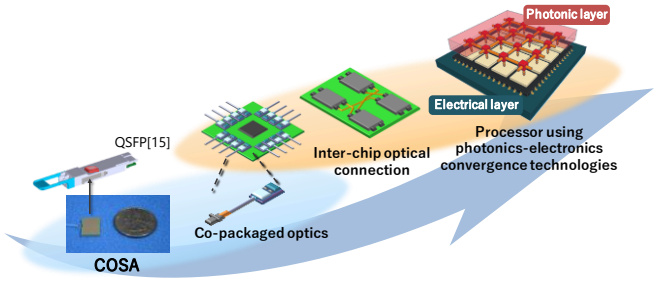

Figure 6: Development of technologies towards Photonics-electronics convergence

- Digital twin computing is designed to create a new environment for services and applications.
- The goal of the Cognitive Foundation is optimal harmonization of all ICT resources.

(2) All-photonics network

Optical technology, which was originally used for long-distance transmission such as intercontinental networks, has come to be used for short-distance transmission like FTTH and intra-data-center networks. IOWN's all-photonics network expands the applications of optical technology, applying it not only to networks but also to inside semiconductors in terminals and servers. The foundation for achieving an all-photonics network is photonics-electronics convergence. This makes it possible to process light and electricity on a single chip (Figure 6). For example, Nozaki et al. [16] developed a femtofarad-scale optical transistor using a photonic-crystal platform, which reduces power consumption by about two orders of magnitude in comparison to conventional devices (Figure 7). All-photonics does not necessarily

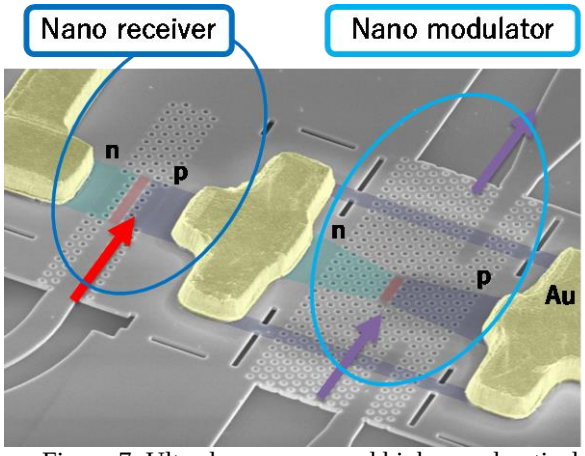

Figure 7: Ultra-low-energy and high-speed optical transistor.

mean that all electrical components will be replaced with optical parts but, rather, to use optical technology everywhere.

The all-photonics network has three technical advantages. The first is low power consumption. We solve the heat problem by incorporating photonics technology into everything from networks to terminals. The second is transmission capacity. Multi-core, multi-wavelength communication technology is increasing the capacity of 1 optical fiber up to 1 peta bps. Yet another advantage is low latency. Some services will be able to greatly reduce processing delay by directly transmitting raw information in a wavelength band, which is currently delayed by such factors as IP packet waiting and data compression.

(3) Digital twin computing

Today, digital twin technology is attracting attention across a wide range of industrial fields. A digital twin is an accurate cyberspace representation of a real-world object such as a production machine in a factory, aircraft engine or automobile (Figure 8(a)). However, most of the current approaches are focused on creating a single umwelt in cyberspace, which is simply a copy of the real world. But, as can be seen in the examples of the umwelts of bees and mantis shrimps, our world is full of various kinds of information that humans cannot perceive.

Digital twin computing [17] is a new computing paradigm

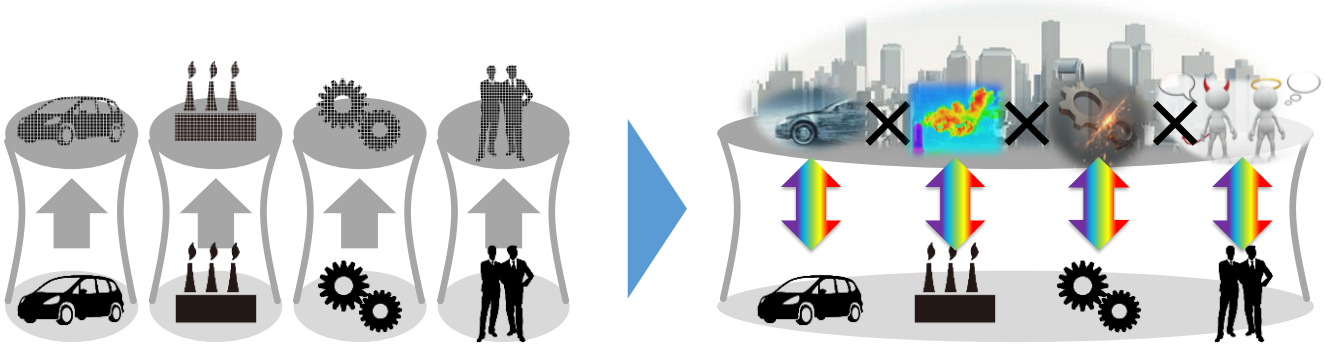

(a) Conventional Digital Twin (b) Digital Twin Computing

Figure 8: Digital Twin Computing.

that will allow us to perform operations and interactions between many digital twins in cyberspace such as cars, robots, and people (Figure 8(b)). For example, digital twin computing can simulate the future of a digitized city in cyberspace. This means the future can be changed by simulating the development and decline of a city and feeding back the results to actual city planning. Thanks to technical innovation, humankind will be able to go beyond its own umwelt and access all types of available information. We believe digital twin computing will capture everything in the real world and by re-presenting it in cyberspace it will enable the creation of new values, previously inconceivable to humans.

Although today's cloud and other computing platforms are underpowered to perform complex calculations between many of the individually focused digital twins, the low-power-consumption, high-capacity information processing enabled by all-photonics network will be the answer.

(4) Cognitive Foundation

The Cognitive Foundation is a concept that flexibly controls and harmonizes all ICT resources. Its key points are self-evolution and optimization. There have been many attempts to detect failures based on logs issued by telecommunications infrastructure devices and to deal with them autonomously using AI. The time has come to move well beyond that approach. The Cognitive Foundation incorporates a wide variety of information that cannot be monitored by the network, such as weather prediction information about the strength and path of an approaching typhoon and information about planned events. It also incorporates information about the various umwelts referred to earlier in this paper. Based on the collected information, the system will optimize the network autonomously. For example, it will plan and execute measures against a disaster before it occurs. It will make predictions and evolve itself accordingly, in other words, self-evolving service lifecycle management.

(5) IOWN Global Forum

Realization of IOWN requires not only telecommunications and computer technologies, but also the insight of researchers and experts from various fields, such as the social sciences and the humanities. The IOWN Global Forum was established in 2020. This is a new industrial forum to facilitate cooperation among global partners with the objective of driving forward research and development for IOWN [18]. The forum accelerates the adoption of a new communication infrastructure to meet our future data and computing requirements through the development of new technologies, frameworks, specifications and reference designs in a number of areas.

4 FUTURE SERVICES CONCEPTS

This section describes the concepts of future services that blend naturally into people's lives as a result of evolving technologies described in the previous section.

Figure 9: Point of Atmosphere.

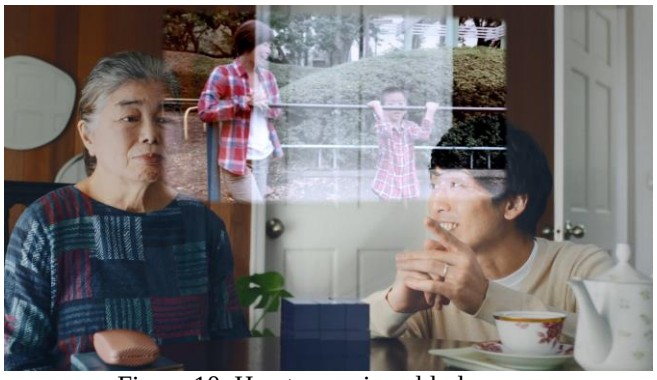
Figure 10: Heart-warming elderly care.

4.1 Point of Atmosphere

"Point of Atmosphere" is a concept for future natural devices (Figure 9). Imagine someone living in a world where there are no terminals anymore. A Point of Atmosphere is a connecting point for all devices to the environment itself. For example, when this person wakes up, various things in the immediate environment can be used to ascertain the person's state of health, traffic and other conditions, and then naturally give this person relevant advice. When this person is about to go out, the bag may appear to be bringing attention to itself by blinking using new projection technology, thereby letting the person know that something has been forgotten. As soon as the closet is opened, the down jacket hanging there advises the person to wear it because it's cold outside. Or when going into a wine bar, the wine bottle itself suggests that this is the wine to be tried. There will be a world where various things around people watch and support their lives. That's natural.

4.2 Heart-warming Elderly Care

The final example of a service concept is one that supports dementia sufferers so that they are able to lead rewarding lives [19]. Imagine a mother who suffers from dementia and she has forgotten the name of her son. To help jog her memory, her digital twin may display videos of the son's childhood (Figure 10). Moreover, the digital twin may sense

her emotions and thoughts and find a piece of music that can help awaken her memories. We believe this helps her to recapture memories of her son, and bring about a future in which everyone can be connected to his or her memories, be connected to other people, and enjoy a contented life supported by mental and physical health.

5 CONCLUSION

This paper described a world where many people from diverse backgrounds and cultures can naturally benefit from technology. Although ICT has evolved as the frontier of "digital," the next step in digital's evolution is towards "natural." Many technologies such as AI, ultra-realistic communication, networks, and information processing are evolving towards creating natural value. We showed how these technologies could continue to evolve in the future and how they will be able to assimilate and respond to various values, how they can convey excitement, and how they can support people's lives in a natural way. This paper also showed the concepts for future services that blend naturally into people's lives as a result of evolving technologies. We hope such a smart world will become a reality in the near future.

REFERENCES

[1] Government of Japan, The 5th Science and Technology Basic Plan, https://www8.cao.go.jp/cstp/english/basic/5thbasicplan.pdf (2016).
[2] H. Thoen, M. How, T. Chiou, and J. Marshall, "A Different Form of Color Vision in Mantis Shrimp", Science, Vol.343, Issue 6169, pp.411-413 (2014).
[3] J. von Uexkül, J. D. O'Neil (trans.), "A Foray into the Worlds of Animals and Humans: with a Theory of Meaning", University of Minnesota Press (2010).
[4] R. Higashinaka, K. Sakai, H. Sugiyama, et al., "Argumentative dialogue system based on argumentation structures", Proc. of the 21st Workshop on the Semantics and Pragmatics of Dialogue (SemDial2017), pp.154-155 (2017).
[5] K. Sakai, R. Higashinaka, Y. Yoshikawa, et al., "Hierarchical Argumentation Structure for Persuasive Argumentative Dialogue Generation", IEICE Trans. on Information and Systems, Vol.E103-D, No.02, pp.424-434 (2020).
[6] H. Kameoka, K. Tanaka, A. Puche, et al., "Crossmodal Voice Conversion", arXiv:1904.04540 [cs.SD] (2019).
[7] H. Nagata, D. Mikami, H. Miyashita, et al., "Virtual Reality Technologies in Telecommunication Services", Journal of Information Processing, Vol.25, pp.142-152 (2017).
[8] A. Akutsu, K. Minami, and K. Hidaka, "Kirari! Ultra-realistic Communication Technology: Beyond 2020", NTT Technical Review, Vol.16, No.12, pp.6-11 (2018).
[9] Press release issued by NTT, NTT Delivers Successful Ultra Reality Viewing of Live MLB Postseason Game, https://www.ntt.co.jp/news2019/1910e/191008a.html (2019).
[10] T. Sato, K. Namba, M. Ono, et al., "Surround Video Stitching and Synchronous Transmission Technology for Immersive Live Broadcasting of Entire Sports Venues", NTT Technical Review, Vol.15, No.12 (2017).
[11] S. Usui, K. Kimura, S. Kinoshita, and K. Minami, "A Kabuki and Information Communication Technology Collaboration: Kabuki × ICT", NTT Technical Review, Vol.17, No.1, pp.20-27 (2019).
[12] Cisco Visual Networking Index: Forecast and Trends, 2017-2022 White Paper, https://www.cisco.com/c/en/us/solutions/collateral/service-provider/visual-networking-index-vni/white-paper-c11-741490.html (2019).
[13] M. Ii and K. Kawazoe, "The IOWN – Innovative Optical and Wireless Network", NTT Publishing (2020).
[14] Press release issued by NTT, NTT, Intel and Sony Establish New Global Forum Dedicated to Realizing the Communications of the Future, https://www.ntt.co.jp/news2019/1910e/191031a.html (2019).
[15] QSFP-DD MSA, QSFP-DD Hardware Specification for QSFP DOUBLE DENSITY 8X PLUGGABLE TRANSCEIVER Rev 5.0, July 9, 2019, http://www.qsfp-dd.com/wp-content/uploads/2019/07/QSFP-DD-Hardware-rev5p0.pdf
[16] K. Nozaki, S. Matsuo, T. Fujii, et al., "Femtofarad optoelectronic integration demonstrating energy-saving signal conversion and nonlinear functions", Nature Photonics, Vol. 13, pp. 454-459 (2019).
[17] NTT, Digital Twin Computing White Paper, Ver. 2.0.0, https://www.ntt.co.jp/svlab/e/DTC/DTC_Whitepaper_en_2_0_0.pdf
[18] IOWN Global Forum, https://iowngf.org/
[19] NTT, Natural ICT supports aging society (concept video), https://youtu.be/rHzgX_kgtHo (2019).

(Received March 16, 2020)

Susumu Yamamoto is a senior research engineer of NTT Media Intelligence Laboratories. He received his B.E. degree in electrical engineering and M.E. degree in computer science from Keio Univ., Kanagawa, in 1997 and 1999, respectively. After his joining NTT in 1999, he has been engaged in image and video processing such as digital watermarking and virtual reality system. He is a member of IPSJ and IIEEJ.

Akira Nakayama is a manager of R&D vision group, Research and Development of NTT holdings. He received his M.E. and Ph.D. degrees in computer science from Nara Institute of Science and Technology in 1999 and 2007, respectively. After his joining NTT in 1999, he has been engaged in robotics, CSCW, recommendation and people flow analysis. He is a member of IPSJ, ACM and RSJ.

Katsuhiko Kawazoe is a senior vice president and the head of Research and Development of NTT holdings. He received his B.E. and M.E. degrees in engineering from Waseda Univ., Tokyo, in 1985 and 1987, respectively. He also received his Ph. D. in Information engineering from Kyoto Univ., Kyoto in 2009. After his joining NTT in 1987, he had been engaged in radio and satellite communication systems, the personal handy-phone system (PHS) and broadcast-broadband convergence services. He became the head of NTT Service Evolution Laboratories in 2014, and head of NTT Service Innovation Laboratory Group in 2016. He assumed his present position in June 2018. He had served as President of ITE from 2018 to 2019.

Industrial Paper

Knowledge Transfer of Project Management Technology Using The PBL Method

Akihiro Hayashi*

*Department of Information Design, Shizuoka Institute of Science and Technology, Japan
pixysbrain@gmail.com

Abstract - Process improvement activities are important in organizations that develop software systems. Using Capability Maturity Model Integration (CMMI), we are working towards achieving maturity level 3. However, if the activity breaks down, the resources of the indirect department become unnecessary, and it often remains a project management office (PMO). However, the PMO's role has not been specifically defined, and in many cases, the original purpose has not been achieved. In this research, we use the case of a company that completed CMMI level-3 activities and have outlined the role played by the PMO. In this case, after pointing out the challenges, we propose the role of process improvement and the method of transferring technology to the project manager as an in-house consultant. When this method is applied to actual development sites, it is expected to effectively improve the reuse rate and implementation of autonomous improvement of Project Manager (PM).
Keywords: CMMI, Project Management Office, Knowledge Transfer

1 INTRODUCTION

According to the Capability Maturity Model Integration (CMMI) Maturity Profile [1] published by the CMMI Institute, CMMI [5] appraisals have been conducted continuously in many countries around the world every year. CMMI is supported worldwide as the most reliable tool in the field of process improvement.

When CMMI was introduced in Japan around the year 2000, the level of competition was that of a temporary boom and focused on not only improving process but also achieving CMMI Maturity level 3. However, it has now been recognized as a perpetual and continuous activity as part of the organizational culture.

When the organization aims to achieve CMMI Level 3, the organization needs a lot of resources to conduct process improvement activities. This resource is named the Engineering Process Group (EPG).

However, once CMMI Level 3 is achieved, the next goal is to maintain this level of surveillance for implementation once every three years. The activity itself is not profitable: From an organizational point of view, EPG is an indirect operation and a cost center. After achieving the preliminary organizational goals, personnel in the indirect department should be transferred to a profit center or assigned a new meaningful role as an indirect department. However, CMMI activities need to be continued and the EPG cannot be abolished.

Therefore, the issue is to define the role and responsibilities of the EPG in the second stage of process improvement. In this context, the study proposes the way in which the project management office (PMO) may be established after achieving a CMMI maturity level and evaluates its validity through application to the actual organization.

As part of a previous study in this field, the authors proposed establishing a methodology for process improvement activities across the entire organization that will continue after achieving CMMI level 3. However, we have cautioned that CMMI's appraisals have rated the achievement of process improvement across the organization based on an evaluation of a few representative projects. We have proposed a methodology for disseminating CMMI activities throughout the organization [2]. However, at this stage, it has not been proposed as a PMO-based activity.

Various consulting firms have proposed that the organization of the EPG be transferred to the PMO after the introduction of CMMI activities. These proposals emphasize the cost improvement through in-house consulting by PMO rather than paying consulting fees to external consulting firms [3], [4].

However, there is no case where experienced PMOs give technology transfer to PMs and propose continuous process improvement using Project Based Learning (PBL).

2 ROLE AND ISSUES OF PMO

After achieving the organizational goals of CMMI activities, the EPG often turns to the PMO to continue to support project management and process improvement. The PMO is defined as a team that supports individual project management in an organization across the board. In general, the role of the PMO is as follows:

- Standardization of the project management system
- Human resource development including training on project management
- Project management support
- Coordination of resources and costs between projects
- Development of a project environment tailored to individual companies
- Other related project management tasks

Because the PMO is an indirect operation, sufficient rationale for the survival of the PMO is required. The long-term role may be CMMI surveillance measures, and the short-term role, support activities such as reducing overload of PMs. If the PMO absorbs the work associated with CMMI activities, it can survive by providing a value-added role.

However, the PMO often does not successfully reduce the burden of the project manager (PM). Here, we will discuss the role of the PMO through a case when a company that achieved CMMI Level 3 established a PMO.

2.1 PMO Failure Case

Company Z started activities of ISO9001 and CMMI about 10 years ago, passed ISO9001 certification registration 3 years later, and achieved CMMI maturity level 3 in 8 years. The management has a strong commitment to CMMI and about 10 EPGs were in operation. Company Z's EPGs were focused on project guidance and included some fixed-term employees who had passed the retirement age of 60.

In the project construction period, development man-hours are set in line with the estimate. About 15% of the entire project term is appropriated for management operations [6], [7]. Furthermore, introducing CMMI increases overhead man-hours by about 10%. Therefore, when CMMI is introduced, about 25% of the total project man-hours would go toward the management, and the delivery date may be delayed due to unnecessary management costs. Therefore, the reduction of management man-hours after achieving CMMI level 3 has become an issue.

The PMO replaced management-related activities with project support. If the delay in delivery date is resolved by this PMO, the PMO activities are considered as value-added activities and it would be a position with merit for both.

PMO was substituted for the following management work as a specific effort to reduce the load on the PM:

- Create weekly reports
- Create progress meeting minutes
- Create the trail necessary for the appraisal

2.1.1 PMO Reporting

The project situation is reported directly to the Executive Committee at a meeting held every Monday. If the project status is not reported in a timely manner by all executives attending the meeting, the management cannot manage the project status.

Until now, the PM has delivered project reports in Company Z. However, in small-scale organizations, the creation of weekly reports tends to be delayed because the PM is involved in both management and development. There have been many cases where reports were lacking in politeness. Since the PMO has EPG knowledge, they have learned to prepare the risk and problem management sheets. They have delivered plausible reports and there have been no delays in reporting. They are also valued by the Executive Committee, and the PMO was recognized as a value-added group.

2.1.2 Create Progress Meeting Minutes

Since the management meeting is held on Mondays, the project progress meetings are held on Thursdays. The project progress meeting reports regular issues that occurred in the week. The PMO attends the progress meeting of the project-in-charge and provides minutes of the meeting. Although the progress meeting had been held until the creation of the PMO, creating the record was the individual responsibility of participants, and no official minutes were captured for the project.

Company Z was a small-scale organization, and was not able to prepare, review, and approve official minutes in weekly progress meetings for small-scale projects.

However, CMMI has processes that require the creation of minutes, such as project progress management, official reviews, and peer reviews, and they tend to be short. The PM therefore took charge of this meaningful activity, but he was not interested in it.

2.1.3 Creation of The Evidence for Appraisal

To pass three-year surveillance, evidence of ongoing practice must be presented. For example, to pass the configuration management process, a configuration management plan must be prepared, and the evidence for carrying out the activities according to the plan must be presented. In addition, when modifying the source code, there is a procedure to check out the source code from the repository, modify the file, hold the configuration management committee, analyze the impact, and check in.

Configuration management was performed at Company Z, but there was no custom of creating forms and recording the contents of changes each time. The PMO substitutes for the difficult task of countermeasures and highlights the added value of the PMO.

In small organizations, the PM is relatively young and the PMO was able to compensate for their lack of skills. A proper weekly report has been submitted to the Executive Committee every week. Surveillance that will be conducted once every three years will also pass with confidence. Since the PM burden has been reduced with the introduction of PMO activities, this method seems to have benefits for both parties.

However, in this method, the PMO is only a substitute for the PM. Furthermore, the PMO sometimes reported the causes of problems and measures to prevent recurrence, to the Executive Committee, without the consent of the PM. The management said, “Every time a problem occurs, we ask for measures to prevent a recurrence, but it is not improved at all.” Measures to prevent recurrence were written by the PMO without confirming the problem with the PM.

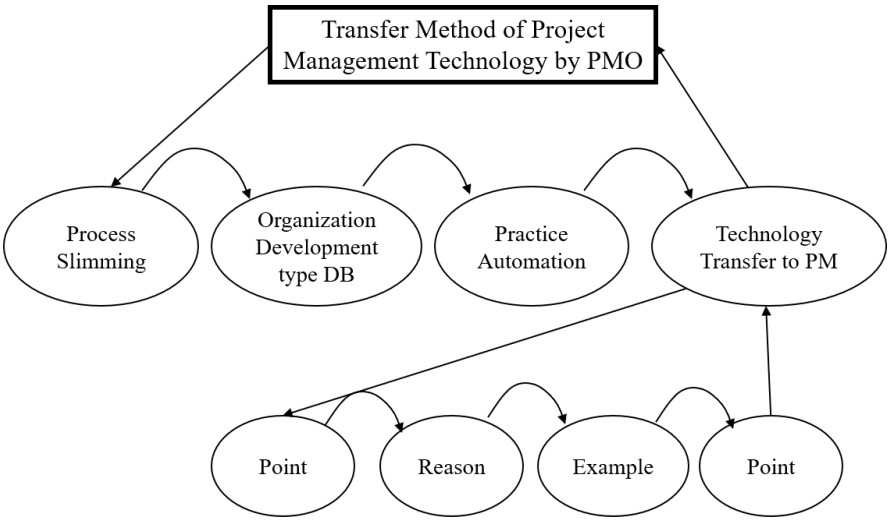

Figure 1 : Framework for the PMO work in this study

The lesson learned from this case is that although the involving the PMO is a value-added activity, the method should be aligned to the process of reducing the burden of the PM. The role of the PMO is to support process improvement and not of a PM substitute.

2.2 Issues to Be Solved

These issues we observed in 2.1 are not specific to Company Z, but are commonly seen in many companies.

The importance of process improvement and project management is recognized widely. Even if one hires an external consulting company and develops an EPG in-house, no methodology has been proposed for how to use the resources after the activity has ended. Defining the PMO's value-added activities remains an issue to be resolved.

3 TRANSFER METHOD OF PROJECT MANAGEMENT TECHNOLOGY BY PMO

In this research, after defining the role and responsibility of the PMO, we propose a method of continuous improvement of the process by PMO.

3.1 Basic policy

In this research, the PMO not only reduces the burden of the PM but also inherits the EPG and is responsible for post-approval in-company process improvement. Unlike the EPG, which is a permanent organization, the PMO has the role of transferring the completed process to the next-generation PM.

3.2 Framework

In this study, we propose a framework for the PMO work that consists of process slimming, organization development-type database creation, practice automation, and technology transfer to PM. The first three are organizational-level activities, and the fourth, a project-level activity. Technology transfer to the PM follows the PREP method. The PREP method first conveys the conclusion, then explains the reason, reinforces the reason with the case, and finally presents the conclusion again. This is then classified based on importance of activities (Point), reasons (Reason), specific examples (Example), and situations where activities are important (Point). This framework is shown in Fig. 1.

3.2.1 Process Slimming

Achieving CMMI's maturity level cannot be avoided through CMMI's "embedding." However, CMMI has been developed as a procurement model for the US Department of Defense, so a large-scale project is assumed. After achieving the CMMI level, the company selects only what is needed and slims the process by removing the excess. However, there are many practices that are not as familiar as domestic practices.

3.2.2 Organization Development Type Database Creation

In a system development organization, projects with the same degree of development and difficulty are repeatedly implemented for similar customers. By classifying the development type of the organization and converting it into a database, standardization for each customer is possible.

Next, the individual information of the classified forms is sanitized, the past information is accumulated in a database for each customer, and the reuse environment is constructed.

3.2.3 Practice Automation

When creating a form for each process area, the form is retrieved from the organization's database and the organization management profile is automatically embedded.

The basis of project management is PDCA (Plan, Do, Check, Act). At the project start stage, make a project plan document and execute the project according to the plan. However, in the upstream process, the load on the PM is large, and there is no time to create a detailed project plan. As a result, project management cannot be planned. Database forms classified by organization type can be used without much change in repeatable projects.

Therefore, we automatically generate forms as much as possible using historical project information accumulated in the organization.

3.2.4 Technology Transfer to PM following The PREP Method

Technology transfer is to transfer management skills to inexperienced PMs through development projects. Generally, the practice is to fill in the form given, even if it was to create a plan for an unknown project. This practice does not outline the intention clearly.

In this study, we use the concept of the PREP method to make the PM learn the management by the PDCA cycle. The PREP method first conveys the conclusion, then explains the reason, reinforces the reason with the case, and finally presents the conclusion again.

First, the purpose of the practice is clarified, and then its necessity is explained through concrete examples. By explaining the purpose of implementing the practice once again, and being convinced by the PM, management skills are passed on.

4 EVALUATION OF APPLICATION

In this chapter, we verify the effectiveness of our proposal through a case of actual application of this framework.

4.1 Case

Company A has approximately 400 employees and is developing control systems for the automotive industry. About half of the employees are in charge of development. The project period is about three months, and many are small projects with less than five project members. One engineer can participate in projects up to four times a year. Usually, about 10 projects of the organization are in operation.

Company A hired a foreign consulting firm to introduce CMMI. In order to implement unified practices in the organization, CMMI is required to create organizational standards, and each project should carry out project management according to the standards.

Company A obliges to execute the project by using CMMI's development work standard and Excel-based format, brought in by the consulting company.

Development work standard corresponds to the process area of CMMI, and refers to “requirement definition standard,” “project plan standard,” “progress control standard,” etc. An Excel-based format refers to work products such as “project plan document” and “Work Breaking Structure (WBS)” created when implementing project management using development standards.

However, this consulting company created consulting materials based on the project management standard originally used by the US headquarters. It is a development standard for large-scale projects. It is hard to say that it is suitable for small-scale companies like Company A.

Company A compared with other companies' proposals at the selection stage of the consulting company. Only this company provided a set of development standards and formats for use in CMMI. Company A adopted this consulting company because there was no effort to create such development standards and formats from scratch.

Company A achieved CMMI Level 3 and is preparing for surveillance after 3 years. Ten employees who worked as EPGs until CMMI Level 3 were considered. Four were transferred to the department, and the remaining six became PMOs who were positioned in the project support team.

4.2 Application of This Framework

4.2.1 Process Slimming

Company A used development standards and formats provided by a consulting company, until CMMI Level 3 was achieved. The CMMI Achievement Appeal is conducted by interviews and document review. The questionnaire is published in advance. If all the forms given by the consulting company were prepared and the questions were answered, CMMI Level 3 could nearly be achieved.

In the first round of CMMI activities, Company A prepared the form of the consulting company on a persuasive basis in preparation for the appraisal. However, after the official appraisal, it was found that several forms were created just for the preparation of the appraisal, and nearly 20 were eliminated.

Therefore, the process was streamlined by eliminating forms that were considered unnecessary. Table 1 presents an example.

4.2.2 Organization Development Type Database Creation

Many customers of Company A are major Japanese automobile manufacturers. Customers are divided into company T, company H, and company N. For customers, projects of the same size and the same degree of difficulty are implemented in a repeating manner. Therefore, the development type was classified for each customer to be delivered and put into a database.

After a certain period of time, the most commonly used format among the three customers was taken out, and customer names and personal information were sanitized, standardized, and stored in the database.

4.2.3 Practice Automation

Company A is doing SAP's ERP (Enterprise Resource Planning), the year after CMMI's level 3 activity has ended. Profile information of the project of the organization is entered into ERP when the contract is established. The ERP information is then downloaded to an MS-Excel file.

When a development project creates a project plan, ERP information is acquired by MS-Excel, and the information is automatically reflected in the standardized project plan.

Next, similar databases were searched based on customer, project schedule, difficulty level, etc. which were classified by T, H, N companies, and those that could be reused at the project planning stage, were also extracted; for example, WBS, risk management ledger, configuration management ledger, etc. If these are similar projects, the same task occurs in almost the same process. As a result, the resulting risk management ledger could be reused.

4.2.4 Technology Transfer to PM following The PREP Method

At Company A, when a project was launched, one PMO was assigned to the project and played the role of a tutor for PM, transferring the technology to the PM by the PREP method.

(1) Project Report (Point)

The role of the PM is project management. However, if young people become PMs without management experience, they would not know what must be done in every phase of the project life cycle. Therefore, the PM was made to participate in the actual project, and the importance of the project management method was highlighted through the PBL method.

Project management is performed in the PDCA cycle. Table 1 shows the relationship between PM and project members throughout the project life cycle.

The project planning and progress management phases are important management skills of the PM. Therefore, Company A taught the progress meeting in the first project to the PM, and in the second cycle, the PM learned to make a project plan. In the third cycle, the PMO became an observer and decided to implement project management through the PM.

(2) Gathering Information for Reporting (Reason)

PM is an intermediate manager. The middle manager refers to the position that reports to the upper management of the organization. In order to report to upper management, the PM correctly understands the current situation of the project and reports the problems in a timely manner.

Table 1 : PDCA Cycle of Project Management

	P	D	C	A
PM	Create a Project Plan		Progress Meeting	
Member		Development		Correction

At Company A, when the project was successful, weekly reports were made by briefly explaining the issues described in the issue management sheet. However, if there is a delay in progress or a technical bottleneck, the upper management will request a detailed report. For this purpose, PMs need to hold weekly progress meetings and collect the information requested by upper management.

In the first cycle, the PMO chaired the progress meeting and held the progress meeting using the CMMI's agenda. Company A is supposed to update WBS before coming to the weekly progress meeting. At the progress meeting, we reviewed the Earned Value Management (EVM) value of the project and interviewed each project member's progress, problems, issues, and risks. This information was collected and reported to the reporting manager.

In the second cycle, I participated in the PMO from the preparation of the project planning documents. Project management is performed by the PDCA, so project plans are prepared first and then managed for progress. However, even if you do not know the purpose, this cannot be understood through merely creating the form. Therefore, the PM had experience in managing the progress meetings and understanding the type of management to be followed with different projects. The project plan was prepared after the meeting.

Company A defines the life cycle process at the project planning stage. Tasks performed in every process are described in the WBS. The output for each process is described in the configuration management register. The first activity is to confirm the output of the process at the actual progress meeting and the second activity is to plan the output of the process at the project planning stage.

(3) Form to be created (Example)

The practices to be implemented as project management are clear. The PM needs to learn all the practices, but as a concrete example of technology transfer, he followed the practice that reversed the PDCA cycle as mentioned above.

- Report content requested by upper management
- Gathering information for accurate and timely reporting
- To manage progress meetings and to collect information weekly
- Enter Gantt chart, WBS, issue management ledger, risk management ledger interviewed at a progress meeting
- List of work products to be created in each process
- Process plan such as configuration management ledger that defined the output for each process
- A project plan document summarizing each process plan

By making a project plan document at the end of the technology transfer, we have made it possible to understand different process for the entire project life cycle.

(4) Report for Clarity (Point)

For organizations achieving CMMI Level 3, the Project Progress Meeting agenda is in the organizational standard. At the progress meeting, interviews with project members will be conducted according to the agenda, and the minutes of the progress meeting will be recorded. A project management trail is kept and used as evidence when conducting an appraisal.

However, the practices required by CMMI are minimal. Even if the information is collected by holding a progress meeting in line with the agenda, it may not be consistent with the reports that the upper management wants to hear. There are times when you call the site many times during closed hours.

The project report is finally reviewed at the management meeting. Even if the project was managed according to CMMI, number of issues were pointed out at the management meeting, and new issues were generated. As a result, management also found that CMMI was not useful.

However, the management complained that extra work would be required in the following process: project plan document → progress meeting → reporting to upper management and implementation. We set the appropriate agenda at the progress meeting and learned how to collect the necessary information.

It was understood that the project plan document would not be prepared by management if it was inaccurate, in order to manage the reality at the progress meeting. The project was planned on more accurate grounds.

4.3 Application Results

4.3.1 PM Recognized Autonomous Management

The PMO is a role set up for a fixed period, and not permanently. The number of indirect personnel should be reduced if the PM manages the project autonomously. This activity was started, and technology transfer activities were conducted for the PM. After three rounds of short-term projects were evaluated using the PREP method, the PM, who could perform autonomous project management by himself, finished with the PMO's support. This situation is shown in Fig. 2.

4.3.2 Format Reuse Rate

At first, the project plan was prepared from the beginning using the format which closely followed the given blank sheet. In the third year of introducing this activity, about 60% of the preparation of the project plan had been automated. It became better for the PM to manually input the remaining 40%. This is because project planning documents and other forms used for each client is collected, converted to DB, sanitized, and reused.

Necessary information for clients is almost the same, so it can be reused. Information required for each project automatically inputs from the Excel file output from ERP. Nearly 48% of these improvements have been automated. This situation is shown in Fig. 3.

4.3.3 The Contradiction Between Measures Against Appraisal and Slimming

Company A's form was brought in by an external consulting firm for appraisal. At Company A, the form was streamlined and made easy to read.

CMMI passes if a practice called REQUIRED is implemented. There is no problem in slimming the “nice to have” part. This caused the metamorphosis. It is inevitable that this activity “fits in the mold.” It was decided that the unnecessary aspects of the organization would not be included in the form.

We repeated the procedure of slimming down a part that was not actually used even though it was introduced as a full set. Moreover, only the passing of the appraisal was maintained. As a result, a lean development standard was completed, conforming to the spirit of CMMI.

4.3.4 Inconsistency of Form Creation Automation and PDCA

Project management is to create a project plan document and manage it according to the plan. If more than 60% of the project plan document is generated automatically by automating the form, the perspective of planning the project is missing. There is a meaning in labor saving. However, if you do not plan the project carefully in the upstream process of the project, it will be overturned.

About 60% of the format automatically generated in this study was client information or the project profile output from ERP. The individual information on the project is about 40% of the rest. This part was created manually by the PM.

There is an idea called Pareto's law. If 40% of the project plan is hand-crafted by the PM, it will be sufficient as a project plan. Specifically, information on project schedule and process, allocation of resources and assignment of personnel have completed.

The project plan of Company A is created with an MS-Excel of about 12 sheets in one book. In terms of the number of sheets, eight sheets were automated. The remaining 4 sheets were created by the PM. This part implements the project plan firmly and is in line with the spirit of PDCA.

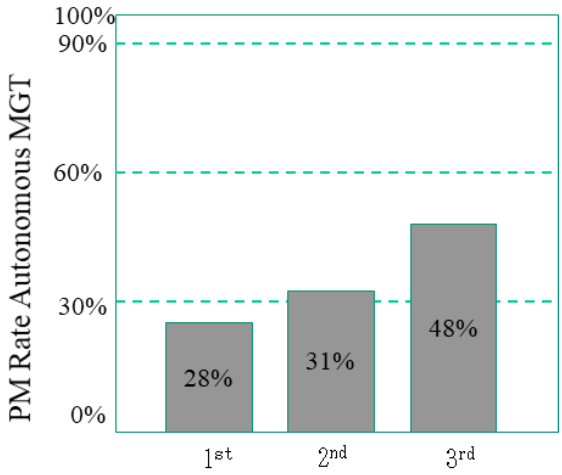

Figure 2 : PM Rate recognized autonomous MGT

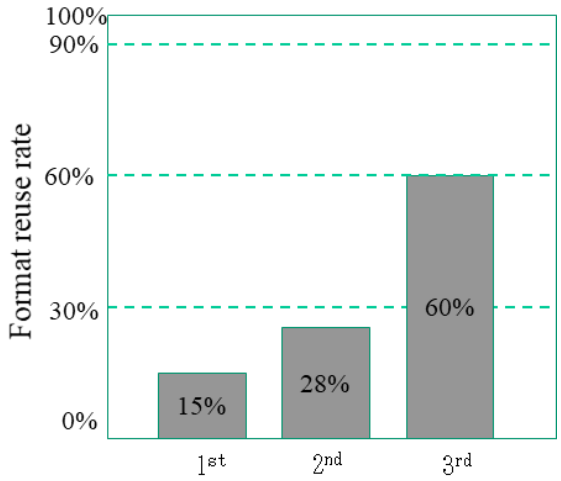

Figure 3 : Format Reuse Rate

5 DISCUSSION

5.1 Background of Process Improvement

Process improvement focuses on the idea that it is necessary to improve the underlying process to improve product quality, as suggested by the saying that "good quality comes from good processes." Even if it is difficult to improve the quality directly, it would become possible if the manufacturing process is improved. Therefore, process improvement methodologies are widely discussed globally.

However, the challenge is to improve the "current situation" to "the way it should be," which would vary greatly across organizations. The model approach is commonly used to improve processes. Under this method, a methodology generally called a best practice model, such as the CMMI, is introduced, and the level is improved according to the rank of the maturity model.

However, it is not easy to implement the CMMI, as the first steps for its introduction into an organization are often unclear. In many cases, a consulting company must be hired for guidance. Contrastingly, from the standpoint of a consulting company, improving the process means achieving the CMMI level, and for example, a contract of "achieving CMMI level 3 in 3 years" might be signed with a client. To this end, development standards and forms are prepared in advance and provided by consulting companies and are used by development projects to achieve the CMMI level.

5.2 Process Improvement and Project Management

The basis of project management is PDCA. In this procedure, a project plan is created in the upstream process of the project, according to which the project operates, and the project is managed through proactive management. When creating a project plan, the project scope is defined in a meeting with the customer, the target requirements during the project period are agreed upon, the scale and man-hours are estimated, the budget is determined, and the planning procedure is undertaken.

However, as noted in Section 5.1, when project management is included in the large flow of process improvement activities, in reality it becomes a project plan in name only rather than an actual project plan. The focus is reduced to merely filling in the blanks in the form.

Even if a relatively young PM, who has not yet gained sufficient experience, creates a project plan for this purpose, this can only be seen as a countermeasure against the CMMI appraisal.

5.3 Purpose Consciousness by PREP Method

In the research, a PREP method was proposed. First, it explains the practice (Point) to be implemented in the project management and the reason (Reason) for its implementation. Next, it shows a specific example (Example), and helps the PM understand the significance of the practice (Point) to be implemented.

In this study, I explained to the PM that project management is incorporated in the workflow of a company. The company must report the progress of the project at the management meeting. Therefore, a project report must be prepared every week.

To make the weekly report, a progress meeting must be held weekly to understand the plan's goal. A project plan is required for the management. To create a project plan, it is necessary to estimate the scale and man-hours that will serve as its basis.

To provide an accurate estimate, the project scope and requirements must be defined. We decided to carry out project management in this way, after understanding the each of the company's practices and the reason for its implementation.

However, when adopting a process improvement such as CMMI, achieving CMMI level 3 becomes a goal, and even if the PM does not recognize its necessity, it leaves a trail in the form of appraisal measures. Often, it is necessary to achieve this goal. If such a thing is continued for many years, it will

become perfunctory with the result that the essential project management is not carried out. This seems to be the reason that CMMI, which was very popular between 2000 and 2010, is now almost unheard of.

5.4 Role of PMO after CMMI Activities

In this study, we proposed a method in which the resources that had been active in the EPG were left in the organization as PMO after the CMMI activities were completed. The EPG has most extensive knowledge about process improvement in the organization and is suitable for to mentor young PMs. The PMO joined the project and demonstrated a real example of the practice to be implemented by the PREP method, and the need for it, through a model.

In this study, the PBL method was chosen for PMOs joining the project and to train young PMs in project management. The PMO is an indirect department and a cost center and the company would like to reduce the number of staff to the extent possible. In such a case, even after the completion of CMMI activities, we can show that maintaining the CMMI level achieved by the PMO is important. The PM can also learn project management based on CMMI under the guidance of a PMO. This will allow for a mutually beneficial relationship.

6 CONCLUSION

This study proposes that, after the CMMI's activity is completed, the resources that were active in an EPG continue to function in the PMO.

As it is difficult to achieve CMMI Level 3 alone, we hire an outside consulting company. However, it is not desirable to keep paying high external consulting fees. It is therefore desirable for knowledge-rich EPGs to be in charge of process improvement as in-house consultants and to transfer technology to young PMs.

Many organizations set up PMOs after CMMI activities. However, they prepare weekly reports and minutes and collect CMMI appraisal trails, which does not fulfill the roles and responsibilities of effective in-house consulting.

In this study, we focused on the role of process improvement in PMO. The activities required for the organization were identified and narrowed down. Next, by classifying the forms for each customer, we added it to the database and made it reusable. The knowledge was transferred to young PMs using the PREP method in which the PMO played a significant role.

In a company that adopted the proposed method, the process reuse rate increased, and the PM began to carry out project management after acquiring knowledge of process improvement, which was considered to be an effective method.

REFERENCES

[1] CMMI Institute, ”Process Maturity Profile”, CMMI Institute (2013).

[2] A.Hayashi, Nobuhiro Kataoka, “A method to Stabilize Process Improvement Activities—Proceeding to Conduct Process Improvement Activities after Achieving CMMI Level 3—”, IEICE, D, vol. J98-D, no. 9, pp. 1237-1246 (2015).

[3] K.Watanabe, “Process Improvement to lead Project Success”, CSK (2005).

[4] Hitachi Solutions, “Software Quality Assurance” (2011).

[5] CMMI Product Team, “CMMI for Development, ver.1.3, Improving processes for developing better products and services”, CMU/SEI-2010-033. Software Engineering Institute (2010).

[6] S. Okamura, “Progress Management in Project, Master Schedule, Earned Value Management, and Project Management System”, Nikkei BP (2010).

[7] Ten Step Japan, ”Project Management Process (Ten step process)”, http://www.tenstep.jp/cms/.

(Received October 31, 2019)
(Revised July 28, 2020)

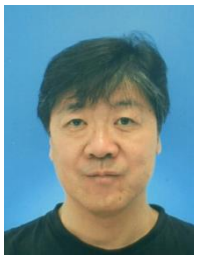

Akihiro Hayashi received an MBA and a Ph.D from the University of Tsukuba, Tokyo Japan and Dr.Eng from Nanzan University, Nagoya, Japan. His professional career includes International excellent companies: Motorola, NTT, and IBM. In 2018 he became a Professor of Shizuoka Institute of Science and Technology. His research interests include Total Quality Management, Process Improvement, and Quantitative Project Management.

Regular Paper

A Frame Rates Stabilization Mechanism for Trust-oriented Internet Live Video Distribution Systems

Tomoki Yoshihisa[*], Satoru Matsumoto[*], Tomoya Kawakami[**], and Yuuichi Teranishi[***,*]

[*]Cybermedia Center, Osaka University, Japan
[**]Nara Institute of Science and Technology, Japan
[***]National Institute of Information and Communications Technology, Japan
yoshihisa@cmc.osaka-u.ac.jp

Abstract - Due to the recent popularization of Internet live video distributions, Internet live video distributors such as YouTubers have attracted great attention. Some of them hide the image regions related to personal information, e.g., their faces or current locations, so as not to encounter public concerns such as threats or attacks to them. In the cases that the video processing time to hide these image regions is long, the frame rate fluctuates and unstable frame rates annoy the viewers. Hence, in this paper, we propose a frame rates stabilization mechanism for trust-oriented Internet live video distribution Systems[1]. Our proposed mechanism adopts two approaches. One is changing the image region for video processes. The other is changing the video process when the video processing time is going to exceed the interval of the video frame. Our evaluation results revealed that our developed system with the proposed mechanism can stabilize the frame rate for trust-oriented Internet live video distributions.
Keywords: Broadcasting, YouTubers, Continuous Media, Data Streaming, Video-on-Demand

1 INTRODUCTION

Due to the recent popularization of Internet live video distributions, Internet live video distributors have attracted great attention. Most of Internet live distributors distribute the videos shooting themselves by cameras. For example, video distributors on YouTube are called YouTuber and 1 million of YouTubers distribute the videos shooting themselves. They often distribute live videos. Some of them hide image regions related to personal information, e.g., their faces or current locations, so as not to encounter public concerns such as threats or attacks by the viewers. It has a large possibility that public concerns do not occur if there is a trust between Internet live video distributors and the viewers because the trust construct their social relations. Therefore, trust-oriented Internet live video distributions proposed in [1] have a large possibility to realize safer and wider used Internet live video distributions.

In the cases that the distributors shoot themselves, the most sensitive personal information is their faces. To avoid public concerns, some of them change or hide their faces by adding video effects [2]. Such video effects include some processes for detecting their faces, creating mask images, and drawing the mask images to their faces, and have a higher computational load compared with a simple process. In the cases that the video processing time is longer than the interval of the video frames, the time to draw the processed image for a video frame delays and the frame rate decreases. The video processing times depend on the complexity of the processes and the images, and the delays cause unstable frame rates. Unstable frame rates annoy the viewers. Therefore, stable frame rates are required for Internet live video distributions.

Various techniques to reduce video processing time have been proposed. Some of them give an upper limit on the video processing time and cancel the process when the processing time reaches to the upper limit. In the cases that the video process is changing or hiding the distributor's face, the face appears in the video when the processing time reaches to the upper limit because the process is cancelled. This is not a trust-oriented Internet live video distribution since the video exposes the distributor's personal information even when there is no trust between the distributor and the viewers. In trust-oriented Internet live video distributions, distributors' personal information should be hidden when there is no trust. However, existing video processing time reduction techniques do not consider trust and cannot realize trust-oriented Internet live video distributions.

In this paper, we propose a frame rates stabilization mechanism for trust-oriented Internet live video distribution systems. In trust-oriented Internet live video distributions, the distribution situation is classified into two situations. One is the situation that there is no trust between the distributor and the viewers (un-trusty). The other one is the situation that there is trust (trusty). In Figure 1, the left image shows the left image shows the case of an un-trusty situation and the distributor's face is blurred to hide his personal information. The right image shows the case of a trusty situation and no areas are blurred. In the un-trusty situations, our proposed system always hide the distributor's personal information. To achieve this, our proposed mechanism changes the video processes when the video processing time is going to exceed the interval of the video frame to a simple process. For example, in the cases that the time is close to draw the image for the next frame while the processing computer executes the process to detect the distributor's face in the video, the computer cancels the face detection process and starts executing the

[1] The work was supported by a Grants-in-Aid for Scientific Research (C) numbered JP18K11316, and by I-O DATA Found.

Figure 1: Live video images for an un-trusty situation (left) and a trusty situation (right).

process to blur the whole region of the image. In addition, we develop a system with our proposed mechanism and evaluate its performance. The main novelty of the paper is the stabilization of the frame rates considering trust on Internet live video distribution. Although some previous researches try to stabilize frame rates, they do not consider trust and wholly give up to execute video processing when the processing time reaches to the upper limit. Our proposed system change the process considering to manage the trust. The contributions of this research are; 1) the proposition of a frame rates stabilization mechanism for trust-oriented Internet live video distribution systems, 2) the design and the development of a system with the mechanism, 3) the evaluation of the system.

The result of the paper is organized as follows. We introduce related work in Section 2. We explain the trust-oriented Internet live video distributions in Section 3 and our proposed video processing system to stabilize frame rates in Section 4. We show some evaluation results and discuss about them in Section 5. Finally, we will conclude the paper in Section 6.

2 RELATED WORK

Many systems have been proposed for distributed stream processing (DSP) in a peer-to-peer (P2P), cloud, edge, or fog computing model [3]-[13]. Some of the proposed systems assume or are implemented by open-source stream processing platforms such as Apache Hadoop [14], Storm [15], Flink [16], and Spark Streaming [17]. Lopez et al. carried out two experiments concerning threats detection on network traffic to evaluate the throughput efficiency and the resilience to node failures for Storm, Flink, and Spark Streaming [18]. The results show that the performance of native stream processing systems, Storm and Flink, is up to 15 times higher than the micro-batch processing system, Spark Streaming. On the other hand, Spark Streaming was robust to node failures and provided recovery without losses.

Some of the DSP systems are designed for real-time processing and can be applied for live video streaming. In [5], the proposed scheme determines the evaluation order for the conditional expressions in continuous queries to reduce the processing time. Its evaluation shows that the proposed scheme can reduce the maximum number of communication hops and the average amount of communication traffic in IoT environments. Ning et al. proposed Mobile Storm as a distributed real-time stream processing system for mobile cloud [7]. Without offloading computation to remote servers, Mobile Storm processes real-time streaming data using a cluster of mobile devices in a local network. Mobile Storm was implemented on Android phones, and a video stream processing application was developed to evaluate its performance. The

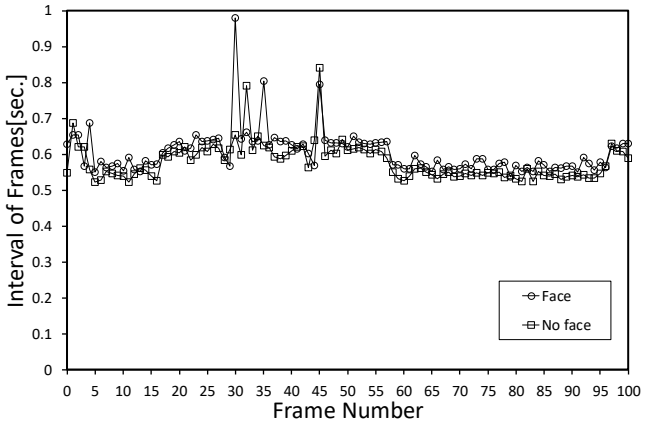

Figure 2: Example intervals of frames

results show that Mobile Storm is capable of handling video streams of various frame rates and resolutions in real-time. Choi et al. proposed DART as a fast and lightweight stream processing framework for the IoT [9]. In DART, a logical group of data sources, namely, a Cloud of Things (CoT) is composed to process the data streams more efficiently in a fully distributed fashion. DART aims to overcome both server-based and edge-only-based methods by grouping IoT devices as a CoT. RIDE was proposed to process real-time massive image stream on distributed environment efficiently [10]. RIDE consists of four layers: application, master, buffer, and worker layers. To minimize the communication overhead between the tasks on distributed nodes, coarse-grained parallelism is achieved by allocating partitions of streams to worker nodes in RIDE. In addition, fine-grained parallelism is achieved by parallel processing of task on each worker node. Yang et al. focused on distributed fault-tolerant processing (DFP) method and proposed a distributed image-retrieval method designed for cloud-computing based multi-camera system in smart city [11]. Through the combination of the cloud storage technology, data encryption, and data retrieval technology, efficient integration and management of multi-camera resources are achieved. In [12], processing and bandwidth issues for a typical video analytics application were investigated to help understand placement decision of methods between edge and cloud. The authors in [12] also say that there are further considerations than made in [12], such as privacy, central sharing, edge device maintenance, and processing and bandwidth costs.

Related to security or privacy of real-time video data, Liu et al. proposed an infrastructure for secure sharing and searching for real-time video data [19]. The proposed infrastructure is particularly suitable for mobile users by deploying 5G technology and a cloud computing platform. Its security is guaranteed even if the cloud server is hacked since data confidentiality is protected by cryptographic encryption algorithms. In addition, the proposed infrastructure also provides secure searching functionality within a user's own video data. Wang et al. proposed OpenFace, an open-source face recognizer whose accuracy approaches that of the best available proprietary recognizers [20]. Integrating OpenFace with interframe tracking, they also built RTFace, a mechanism for denaturing video streams that selectively blurs faces according to speci-

fied policies at full frame rates. In [20], privacy-aware architecture for large camera networks using RTFace were presented.

The existing techniques mentioned above can reduce the stream processing time by efficiently distributing the computational and communication loads to the processing nodes. However, those techniques do not give an upper limit for the processing time and there is a large possibility that the frame rate fluctuates. This paper is positioned to the consideration of the situations such as allowed processing time and adaptive task modification on the trust-oriented Internet live video distribution.

3 TRUST-ORIENTED INTERNET LIVE VIDEO DISTRIBUTIONS

In this section, we briefly explain trust-oriented Internet live video distributions proposed in [1].

In trust-oriented Internet live video distributions, the distribution situation is classified into two situations. One is the situation that there is no trust between the distributor and the viewers and is called the *un-trusty* situations. The other one is the situation that there is trust and is called the *trusty* situation. The situation that an Internet live video distribution belongs to depends on various factors. For example, in the cases that the viewers of an Internet live video distribution is limited to only the friends of the distributor, the situation is a trusty situation. In the cases that the viewers are the stranger of the distributor, the situation is an un-trusty situation. In a simple system, the un-trusty/trusty situation that the current situation belongs to is selected by the distributor manually. Automatic selection is also possible by using the information about the viewers, the locations, and so on. Figure 1 shows example images of live video in an un-trusty situation and a trusty situation.

The trust-oriented Internet live video distributions have three policies, “close-information”, “limit-information”, and “expose-information” policies. In the un-trusty situation, the distributors may use the close-information policy. In this policy, the processing computer executes the processes so as to close personal information. The distributor can safety distribute the shot live video since the distributor’s personal information is closed. However, the possibility to be able to construct trust decreases since the viewers cannot get the personal information about the distributor so any more. In the limit-information policy, the processing computer executes the processes accepted by the distributor. The distributors select this policy aiming to keep the trust. In the trust situation, the distributors may use the expose-information policy. In this policy, the processing computer executes the processes so as to expose personal information. The possibility to be able to construct trust increases since the viewers can get the personal information about the distributor. However, the live video distribution is unsafe.

In the trust-oriented Internet live video distribution, the processing computer executes video processes based on the policy selected by the distributor (un-trusty or trusty). However, conventional trust-oriented Internet live video distribution systems do not consider the processing time and the frame rate usually fluctuate.

4 PROPOSED MECHANISM

We explain our proposed frame rates stabilization mechanism in this section. We explain our target problem first and our approach to solve the problem after that.

4.1 Target Problem

As described in Section 1, long video processing times cause unstable frame rates and this annoy the viewers. For example, we show the intervals of the frames in Fig. 2. The horizontal axis is the frame number. In this example, the processing computer executes the processes to detect faces and to blur the detected region. “Face” indicates the interval of the frames when there is a distributor’s face in the live video. “No face” indicates that when there is no distributor’s face. As shown in this example, the interval of the frames fluctuate and have a range of approximately 200 [msec.] in this case. Such a large change of the interval has a large possibility to annoy the viewers. Therefore, in this paper, we propose a frame rates stabilization mechanism.

In the cases that the processing time is shorter than the interval of the frames, the system can control the time to draw the image for the next frame by waiting for some time. Otherwise, the time to draw the image for the next frame delays and the frame rate changes. We propose a frame rates stabilization mechanism even when the processing time is long.

4.2 Our Approach

To stabilize frame rates for trust-oriented Internet live video distributions, we adopt two approaches.

The first one is the reduction of the video processing time. As explained in the previous subsection, the system can stabilize the frame rate if the processing time is shorter than the interval of the frames. Therefore, shorter video processing times than the interval of the frames enables stable frame rates. Various techniques to reduce video processing time has been proposed. However, they do not focus on the trust-oriented Internet live distributions and some public concerns can occur even when the system adopts these techniques. The most sensitive personal information is their faces. Therefore, we focus on hiding the distributor’s faces and propose a video processing time reduction method for hiding the face in the trust-oriented Internet live video distributions.

The other one is the change of the video process to a simple video process. As explained in Section 1, most of video effects require a higher computational load compared with a simple process. Therefore, our proposed method changes the video process when the video processing time is going to exceed the interval of the video frames to a video effect that the processing computer can execute the process with a shorter processing time. An example of a simple video process is blurring the whole region of the image. Since the processing time of a simple video process is relatively short compared with complicated video processes, the system can finish the process before the time to draw the image for the next frame and thus can stabilize the frame rate.

We will explain the detail of each approach in Subsections 4.4 and 4.5.

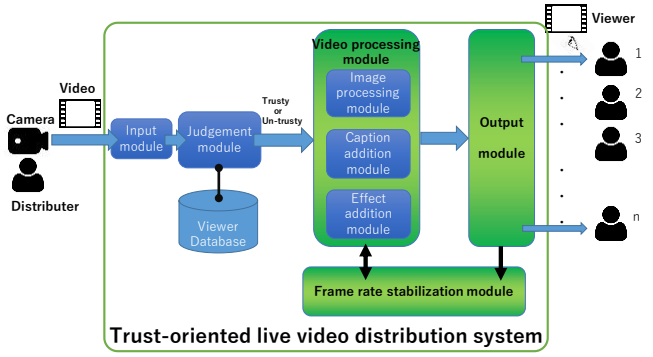

Figure 3: Our assumed system for our proposed mechanism

4.3 Assumed System

Figure 3 shows our assumed system for our proposed mechanism. In the system, the distributors distribute their shot live videos to the viewers using the trust-oriented live video distribution system. The situation judgement module judges whether the current situation is an un-trusty or a trusty situation using the viewer database and other information. The video processing module executes the designated video processes. A part of the viewers login to the system before watching the live videos. The details of these modules are inscribed in [1].

The frame rate stabilization module is newly added to the system. The frame rate stabilization module manages the video processing module and checks the frame rates of the output module. The output module is the system module to distribute the live videos to the viewers. When the frame rate is going to fluctuate, the frame rate stabilization module changes the video process executed in the video processing module to a simple process and try to reduce the processing time. The processed video data are transferred to the output module and are distributed to the viewers.

4.4 A Method to Hide Faces Faster

In this subsection, we explain our proposed method to hide the distributor's face faster. Our proposed method does not fix the face detection algorithm. Various algorithms that were already proposed can be adopted to our proposed method.

4.4.1 Position of Face

Most of live video distributors shoot themselves and the position of the face does not change largely. We do not assume that the position of the face does not change. For example, the distributor fixes the camera to his room by a tripod and shoots himself sitting on the front of the camera. In this case, the position of his face in the video image does not change largely although the position waves when he moves his upper body. For another example, the distributor uses her smartphone to distribute the live video. She grasps her smartphone forwarding the camera to herself and shoots herself while walking. The distributors generally allocate their faces to the center of the video image and the position does not change largely and frequently.

In the cases that the position of the face does not change largely, the position of the face in the next frame image is close to that in the current frame image. By shrinking the range to detect the faces using this feature, we can reduce the video processing time since a smaller image gives a shorter processing time. However, a smaller range to detect the faces has a large possibility to fail to detect the faces since the possibility that the shrunk image does not include the face increases. Therefore, our proposed method takes a margin from the position of the face in the current frame image and detects the face in the range.

The appropriate margin length is the length that the position of the face changes within the interval of frames. If the position changes to the out of the detection area even taking the margins, the face detection fails.

4.4.2 Region to Detect Face

Let X_c, Y_c denote the upper left corner of the region for the detected face in the current video frame image and W_c, H_c denote the width and the height of the region. We set the same margin to the right and the left sides of the region (M_X) and to the top and the bottom sides of the region (M_Y). Then, the region to detect the faces in the next video frame image X_d, Y_d, W_d, H_d are given by:

$$\begin{aligned} X_d &= X_c - M_X \\ Y_d &= Y_c - M_Y \\ W_d &= W_c + 2M_X \\ H_d &= H_c + 2M_Y \end{aligned} \quad (1)$$

In our proposed method, the region to detect the face is determined by the above equations. In the evaluation section, we will confirm the effectiveness of shrinking the region to detect the face.

4.5 A Method to Change Video Process

In this subsection, we will explain our proposed method to change video process to stabilize the frame rates.

4.5.1 Timing to Change Video Process

In our proposed mechanism, the frame rate stabilization module changes the video process when the processing time is going to exceed the interval of the frame to a simple process that the video processing module can execute the process with a shorter processing time. Even when the video process is changed to the simple one, the video processing time arises and it takes some time. Therefore, our proposed method gives a margin time for the simple video process. Let T_m denote the margin time. When the current time satisfies the following inequality, the frame rate stabilization module changes the video process to the simple one.

$$T_c > T_{nf} - T_m \quad (2)$$

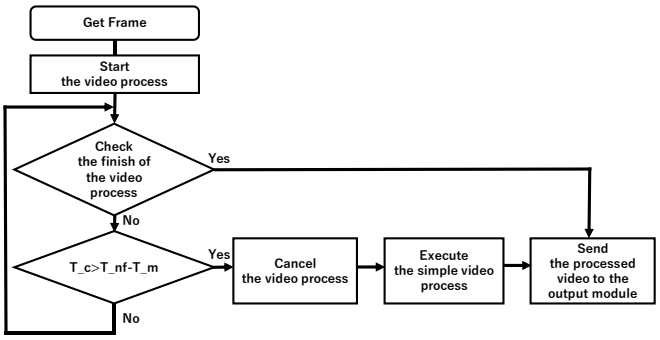

Figure 4: The flowchart for the frame rate stabilization module

Here, T_c is the current time and T_{nf} is the time to draw the next frame image. That is, the value of $T_{nf} - T_m$ is the *deadline* of the original video process. Our proposed method decides T_m enough to finish the simple video process within the margin time. For example, in our brief experiment, the maximum processing time to blur the whole region in a video processing system is 129 [msec.]. In this case, we can predict the sufficient time to finish the simple video process although the time fluctuates. In this case, the value of T_m larger than 129 [msec.] is sufficient.

In the cases that the right formula of Equation (2) is very close to the left, the video process can frequently change. This can cause the annoyance of the views. To determine T_m, it is better to consider such an influence of the viewers.

4.5.2 Video Process to Hide Face

Figure 4 shows the flowchart for the frame rate stabilization module. When the module gets a video frame image from the camera, it starts the video processing to the image in other thread. To manage the processes, the video processes are executed in parallel and in other thread from the frame rate stabilization module. After that, the module continuously checks whether the process finishes and whether the above inequality is satisfied or not. When the process finishes, the module transfers the processed image for the video frame to the output module. When the above inequality is satisfied, the module cancels the video process and start executing the simple video process. When the simple video process finishes, it transfers the processes image for the video frame to the output module.

5 EVALUATION

In this section, we investigate the influence of changing the video processes and show the results in Subsection 5.1. After that, to evaluate the performance of our developed system with the proposed mechanism, we show some evaluation results about the intervals of the frames and the video processing.

5.1 Influence of Changing Video Process

The objective of the evaluation is to check which video gives a higher QoE, i.e., the viewers can watch the video without a more annoyance, in un-trusty situations. For this objective, the videos shown to the subjects are not necessarily live videos. To show the same video to all subjects, therefore, we shoot a video and create three videos from it although our research target is live videos. In this section, to evaluate the performance of our developed system with the proposed mechanism, we show some evaluation results about the intervals of the frames and the video processing.

Table 1: The videos created for the subjective evaluation

Video name	Description
Original	Human faces are hidden.
Blurred	The whole region is blurred after 10 [sec.] from the beginning.
Paused	The video is paused after 10 [sec.] from the beginning.

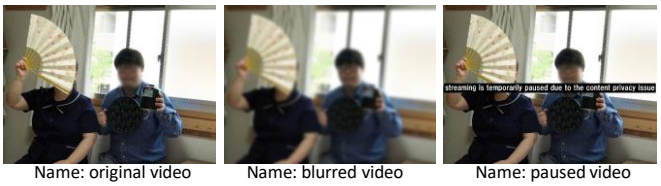

Name: original video Name: blurred video Name: paused video

Figure 5: The videos for the subjective evaluation

Table 2: The subjective evaluation result

Video name	1st	2nd	3rd
Original	11	0	0
Blurred (proposed)	0	9	2
Paused	0	2	9

5.1.1 Subjective Evaluation Setting

A realistic scenario to which our proposed trust oriented live video distribution is applied is the situation that the distributor fixes the camera to his room by a tripod and shoots himself siting on the front of the camera as explained in Subsection 4.4.1. Moreover, to avoid the exposure of the distributor's personal information in un-trusty situations, we blur the human faces and hid them. We call this the *original* video. The duration is 30 [sec.] Table 1 shows the explanations of our created three videos. The *blurred* video is the video created from the original video to simulate our proposed mechanism. To investigate the influence of changing the video processes, we blur the whole region of the video after 10 [sec.] from the beginning to the end. Only the human face is blurred by 10 [sec.] from the beginning and thus the beginning part of the video is the same as the original video. The *paused* video is the video created from the original video to simulate pausing the video when the load for the video processes is high. During the pausing, the text message "streaming is temporarily paused due to the content privacy issue" is shown in the center of the video. In the video, we pause the video after 10 [sec.] from the beginning to the end. Similar to the blurred video, the beginning part of the video is the same as the original video. The audios for all the videos were not interrupted and kept playing. Figure 5 shows a screen shot of the videos.

We show these videos to 11 subjects and ask the subjects to rank the videos in the order that he/she can watch the video

without a more annoyance. Also, we get the reason for their ranking.

5.1.2 Subjective Evaluation Result

Table 2 shows the result. From the result, we can see that the rank of our proposed mechanism is higher than the paused video. The summary of the reason was that the blurred video kept playing although the whole region is blurred, and thus the subjects could somehow grasp the contents of the video compared with the cases of the paused video. However, two subjects gave a higher rank to the paused video than the blurred video. The summary of the reason was that the text message that explained the reason why the video was paused was shown in the paused video. Thus, the subjects could understand why the video was paused and they did not get annoyance further than the blurred video. We think that this can be improved by adding a text message that explains the reason why the whole region is blurred to the blurred video. All subjets gave the highest rank to the original video because the case of the original video did not encounter any troubles.

5.2 Performance Evaluation Setting

From this subsection, we evaluate the performance of our developed system. We developed a video processing system that detects the faces in the shot video images and blurs the detected region. In the cases that the time to finish the video process is longer than the deadline (Equation (2)), the system cancels the processing and changes it to the simple process that blurs the whole region of the image. The system has a function to distribute the live video, but the function is not directly related to this research and we do not focus on this function.

To show the effectiveness of our proposed method, we show the intervals of the frames. We set the frame rate of the video to f [fps] in this evaluation. In our proposed method, when the current time exceeds the deadline, the processing computer changes the video process to the simple one. Therefore, in the cases that the interval of the frame is shorter than the $1/f$ [msec.], our proposed method can achieve a constant frame rate by waiting for drawing the next frame image.

We use the ratio of changing process in this evaluation. The ratio means the ratio that the video process is changed to the simple one and is the number of the simple video process divided by the number of the all video process. A larger value means that a more number of the video frames is wholly blurred (the whole region is blurred). A smaller value is better for the trust-oriented Internet live distributions since just for the region related to the personal information is blurred.

5.3 Evaluation Environment

For the evaluation, we use our developed video processing system. We developed the system using the Visual Studio 2017 and the system uses OpenCV 4.1.0 to get the images from the camera and to detect the faces in the images. The processing computer is a laptop computer (CPU: Core i7@2.4GHz, Memory: 8GB). We use the camera equipped on the laptop and get 640x480 RGB (32bits) images. For the face detection, we use the detectMultiScale function implemented in the OpenCV.

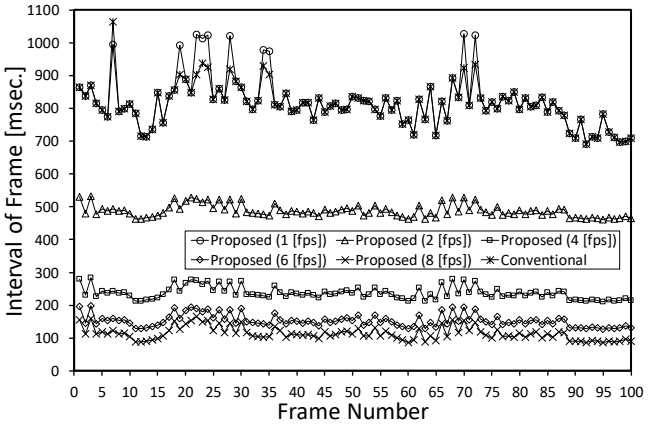

Figure 6: The frame number and the intervals of the frames

5.4 Evaluation Results

In this subsection, we show some evaluation results. First, we show the intervals of the frames and evaluate the effectiveness of our two approaches. After that, we show the performances changing the region sizes for the processes to evaluate our approach to change the region size to hide the face faster. Then, we show the performances changing some parameters for the face detection. We evaluate our developed system under the situations that the video records just one faces although the system can detect multiple faces to make the evaluation results easily understandable. In the situations that the video records multiple faces, their positions also influence the results.

5.3.1 Interval of Frame

The target problem of this research is the stabilization of the frame rate. This means that the intervals of the frames are more constant. Therefore, we measured the intervals of the frames.

Figure 6 shows the intervals of the frames. The horizontal axis is the frame number and the vertical axis is the intervals of the frames. In the figure, "Proposed (f [fps])" indicates the intervals of the frames under our proposed method when the frame rate is set to f. "Conventional" indicates the intervals of the frames under conventional methods, i.e., without our proposed method. The result under the conventional method does not depend on the frame rate since the method does not consider the frame rate. The margin time is 100 [msec.]

From this result, we can see that our proposed method achieves a shorter interval than the inverse value of the frame rate in many cases. This means that our proposed method gives stable frame rates. However, the intervals of the frames are sometimes longer in the cases that the video processing time is longer than the predicted margin time. The conventional method can achieve almost 1 [fps]. In the cases that the frame rate is 1 [fps], some intervals of the frames under our proposed method is the same as that under the conventional method because the video process finishes before the deadline. However, in the cases that the video process before changing it finishes earlier than the simple video process, the

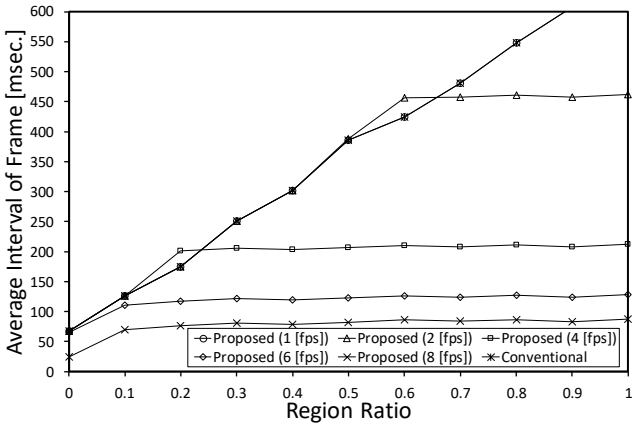

Figure 7: The average interval of the frames under the different region sizes for the processes

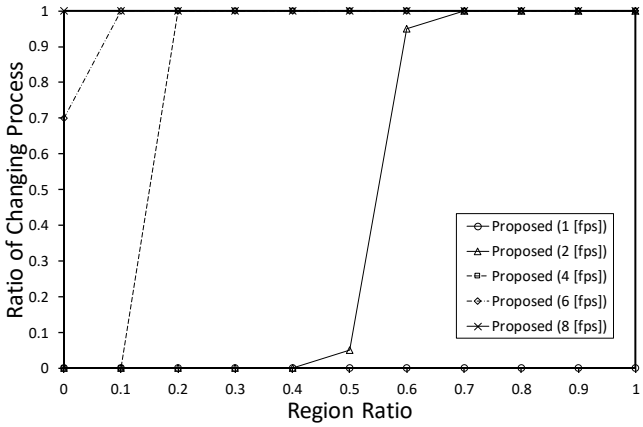

Figure 8: The ratio of changing the processes under the different region sizes for the processes

intervals of the frames under our proposed method is longer than that under the conventional method. For example, in the case of 1 [fps], the video processing times of 6 frames in 100 frames exceed the time to draw the image for the next frame. In the case of 4 [fps], the video processing times of 19 frames in 100 frames exceed the time to draw the image for the next frame. We can reduce the number of the frames in that the processing time exceeds the time to draw the image for the next frame by increasing the margin time.

The ratio of changing the process increases in proportional to the frame rate since a larger frame rate gives an earlier deadline. For example, in the cases of 1 [fps], 10 video processes are changed to the simple video processes in 100 frames and this means the ratio of changing the process is 10/100=0.1. In the cases of 4 [fps], all video processes are changed to the simple video processes and the ratio is 1.0. Therefore, Our proposed method gives stable frame rates but the ratio of changing process increases.

In the following evaluation results, we use the average interval of frame.

5.3.2 Region Size for Process

A smaller region size for the process gives a shorter video processing time because the data amount for executing the video process decreases. Hence, changing the region size for the process, we measured the average interval of the frames and the ratio of changing the processes.

Figure 7 shows the average intervals of the frames under the different region sizes for the processes. The horizontal axis is the region ratio. The region ratio is the ratio of the region for the process in the whole region and given by the number of the pixels in the region for the process divided by that in the whole region. The vertical axis is the average intervals of the frames. The margin time is 100 [msec.]. The legends are similar to the previous results.

In our proposed method, when the region ratio is small, the average interval of the frames increases as the region ratio increases since the data amount for executing the video process increases. When the region ratio is large, our proposed method gives almost constant average interval of the frames since the video process is changed to the simple video process when the video processing time reaches to the deadline. The video processing time earlier reaches to the deadline as the frame rate increases. The average interval of the frames under the conventional method increases in proportional to the region ratio, since the method does not consider the deadline. For example, the average interval of the frames in the cases of 4 [fps] is approximately 200 [msec.] This is smaller than 250 [msec.] (the interval of the frames under 4 [fps]) and our proposed method can give a stable frame rate. On the other hand, in the conventional method, the region ratio should be less than 0.23 to achieve the frame rate of 4 [fps].

Figure 8 shows the ratio of changing the processes under the different region sizes for the processes. The horizontal axis is the region ratio and the vertical axis is the average interval of the frames. In the conventional method, the processing computer does not change the video process and always execute the process to detect the faces. Therefore, the ratio of changing the process is always zero and we do not show it in the figure.

In the case of 2 [fps], the ratio of changing the processes increases sharply when the region ratio is 0.6. This is because the video processing time for detecting the face in the frame image is almost constant and most of all video processing time exceeds the deadline when the region ratio is larger than 0.5. A similar situation occurs in the case of 4 [fps] and the ratio of changing the processes sharply increases when the region ratio is 0.2. In the cases of 8 [fps] and larger frame rates, the ratio of changing processes are always 1.0 because the video processing time exceeds the time to draw the image for the next frame even if the video process changes to the simple video process.

5.3.3 Number of Neighbors

One of the main parameters for the face detection techniques is the number of the neighbors. General face detection techniques moves the target region to detect the face in the original image with changing the size of the target region and compares the image in each target region with a template image for faces. Therefore, one face in the original image is detected several times as shown in Fig. 9. To reduce the error for the face detections, the region in that some faces are detected within the close range is finally defined as the region of the face. This is called the neighbors and the number of the

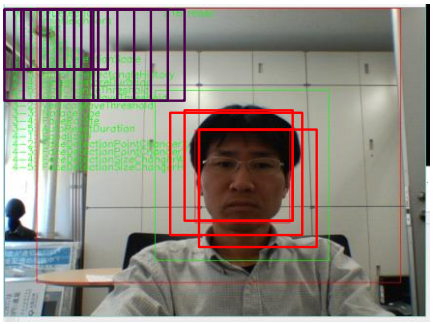

Figure 9: The image of detecting faces

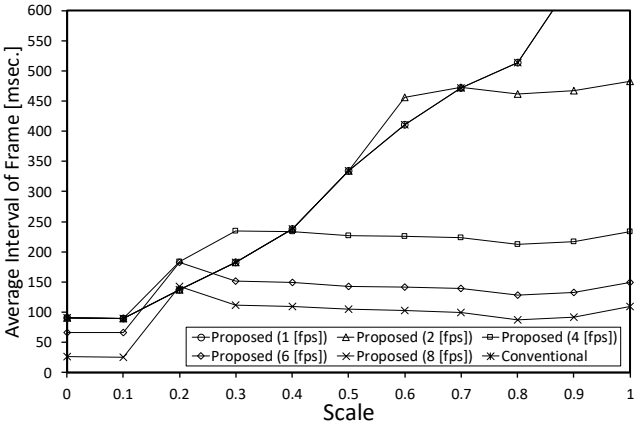

Figure 11: The average intervals of the frames under the different sizes of the images

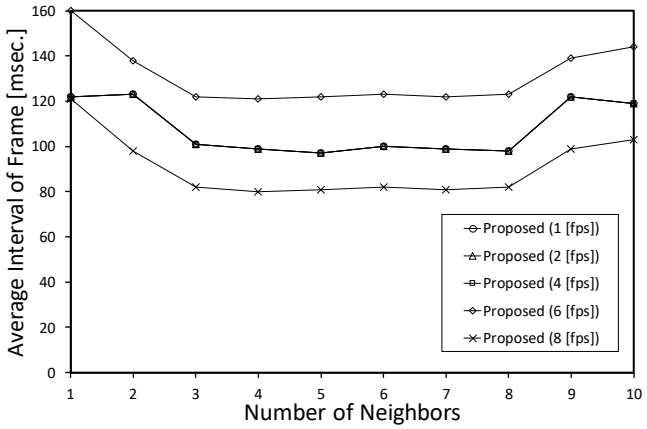

Figure 10: The average intervals of the frames under the different number of the neighbors

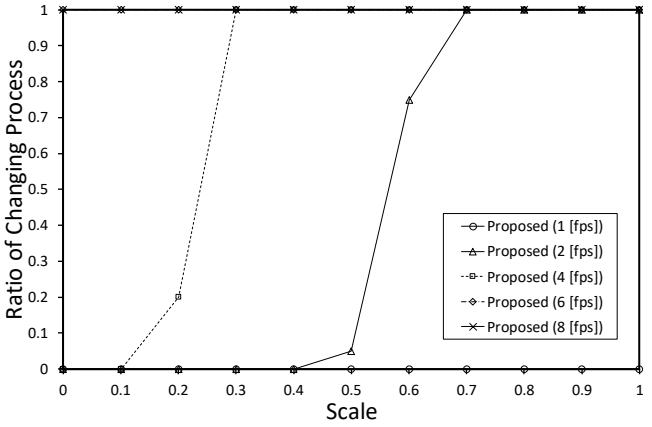

Figure 12: The ratios of changing the processes under the different sizes of the images

neighbors has a possibility to influence the video processing time. Hence, we calculated the average interval of the frames changing the number of the neighbors.

Figure 10 shows the average interval of the frames under the different number of the neighbors. The margin time is 100 [msec]. The region size for the video process is 320x240. From this figure, we can see that the average interval of the frames does not change largely even when the number of the neibhbors changes. This is because the algorithm we used detects all regions of the faces in the whole image and counts up the number of the neighbors after that. Thereore, the number of the neighbors has not so large influence on the average interval of the frames. The ratio of changing processes is 0.0 when the frame rate is 1, 2, 4 [fps] and is 1.0 when the frame rate is 6, 8 [fps]. The result is very simple and we do not show it here.

5.3.4 Scale of Image

As we explained in the previous section, a smaller size of the region for the process gives a shorter video processing time because the data amount for executing the video process decreases. In this section, changing the size of the image for the video process, we measured the average interval of the frames and the ratio of changing the processes.

Figure 11 shows the average intervals of the frames under the different sizes of the images. The horizontal axis is the scale. The scale is the ratio of the size of the image for the video process compared with the original image size. For example, when the scale is 0.5, the image downsizes to 320x240 in the cases that the original image size is 640x480. The vertical axis is the average intervals of the frames. The margin time is 100 [msec]. The region size for the process is 640x480. Similar to the results changing the region size for the process, when the scale is small, the average interval of the frames increases as the scale increases.

Figure 12 shows the ratio of changing the processes under the different sizes of the images. This is also similar to the result changing the region size for the process. The ratio sharply increases since almost video processing time exceeds the deadline under a large value of the scale.

6 CONCLUSION

In this paper, we proposed a frame rates stabilization mechanism for trust-oriented Internet live video distribution systems. Our proposed mechanism changes the image region for video process and also changes the video process when the video processing time is going to exceed the interval of the video frame. We developed a system with our proposed mechanism. Our evaluation results revealed that our developed system can stabilize the frame rate for trust-oriented Internet live video distributions. In the future, we will further

reduce the video processing time and investigate the frame rates in practical Internet live video distributions.

REFERENCES

[1] T. Yoshihisa, S. Matsumoto, T. Kawakami, and Y. Teranishi, "Trust-oriented Live Video Distribution Architecture", in Proc. IEEE Int'l Conf. on Computers, Software and Applications, to appear (2019).

[2] S. Matsumoto, T. Yoshihisa, T. Kawakami, and Y. Teranishi, "A Distributed Multi-Viewpoint Internet Live Broadcasting System with Video Effects", in Proc. International Workshop on Informatics (IWIN'18), pp. 83-88 (2018).

[3] X. Zhao, H. Ma, H. Zhang, Y. Tang, and Y. Kou, "HVPI: Extending Hadoop to Support Video Analytic Applications", in Proceedings of the 8th IEEE International Conference on Cloud Computing (CLOUD 2015), pp. 789-796 (2015).

[4] W. Kou, H. Li, and K. Zhou, "Turning Video Resource Management into Cloud Computing", Future Internet 8(3), 35, 10 pages (2016).

[5] T. Yoshihisa, T. Hara, "A Low-Load Stream Processing Scheme for IoT Environments", in Proceedings of the 2016 IEEE International Conference on Big Data (Big Data 2016), pp. 263-272 (2016).

[6] N. Chen, Y. Chen, Y. You, H. Ling, P. Liang, and R. Zimmermann,"Dynamic Urban Surveillance Video Stream Processing Using Fog Computing", in Proceedings of the 2016 IEEE Second International Conference on Multimedia Big Data (BigMM 2016), pp. 105-112 (2016).

[7] Q. Ning, C.-A. Chen, R. Stoleru, and C. Chen, "Mobile Storm: Distributed Real-Time Stream Processing for Mobile Clouds", in Proceedings of the 4th IEEE International Conference on Cloud Networking (CloudNet 2015) (2015).

[8] T. Li, J. Tang, and J. Xu, "A Predictive Scheduling Framework for Fast and Distributed Stream Data Processing", in Proceedings of the 2015 IEEE International Conference on Big Data (Big Data 2015), pp. 333-338 (2015).

[9] J.-H. Choi, J. Park, H. D. Park, and O.-G. Min, "DART: Fast and Efficient Distributed Stream Processing Framework for Internet of Things", ETRI Journal, Vol. 39, No. 2, pp. 202-212 (2017).

[10] Y.-K. Kim, Y. Kim, and C.-S. Jeong," RIDE: Real-Time Massive Image Processing Platform on Distributed Environment", EURASIP Journal on Image and Video Processing, 13 pages (2018).

[11] J. Yang, B. Jiang, and H. Song," A Distributed Image-Retrieval Method in Multi-Camera System of Smart City Based on Cloud Computing", Future Generation Computer Systems, Vol. 81, pp. 244-251 (2018).

[12] L. O'Gorman and X. Wang, "Balancing Video Analytics Processing and Bandwidth for Edge-Cloud Networks", in Proceedings of the 24th International Conference on Pattern Recognition (ICPR 2018), pp. 2618-2623 (2018).

[13] K. Kato, A. Takefusa, H. Nakada, and M. Oguchi, "Construction Scheme of a Scalable Distributed Stream Processing Infrastructure Using Ray and Apache Kafka", in Proceedings of the 34th International Conference on Computers and Their Applications (CATA 2019), pp. 368-377 (2019).

[14] Apache Hadoop, available at https://hadoop.apache.org/ (accessed June 1, 2019).

[15] Apache Storm, available at http://storm.apache.org (accessed June 1, 2019).

[16] Apache Flink, available at http://flink.apache.org (accessed June 1, 2019).

[17] Apache Spark Streaming, available at http://spark.apache.org/streaming/ (accessed June 1, 2019).

[18] M. A. Lopez, A. G. P. Lobato, and O. C. M. B. Duarte, "A Performance Comparison of Open-Source Stream Processing Platforms", in Proceedings of 2016 IEEE Global Communications Conference (GLOBECOM 2016), 6 pages (2016).

[19] J. K. Liu, M. H. Au, W. Susilo, K. Liang, R. Lu, and B. Srinivasan,"Secure Sharing and Searching for Real-Time Video Data in Mobile Cloud", IEEE Network, Vol. 29, No. 2, pp. 46-50 (2015).

[20] J. Wang, B. Amos, A. Das, P. Pillai, N. Sadeh, and M. Satyanarayanan, "Enabling Live Video Analytics with a Scalable and Privacy-Aware Framework", ACM Transactions on Multimedia Computing, Communications, and Applications, Vol. 14, No. 3s, Article No. 64 (2018).

(Received November 29, 2019)
(Revised May 7, 2020)

Tomoki Yoshihisa received the Bachelor's, Master's, and Doctor's degrees from Osaka University, Osaka, Japan, in 2002, 2003, 2005, respectively. Since 2005 to 2007, he was a research associate at Kyoto University. In January 2008, he joined the Cybermedia Center, Osaka University as an assistant professor and in March 2009, he became an associate professor. From April 2008 to August 2008, he was a visiting researcher at University of California, Irvine. His research interests include video-ondemand, broadcasting systems, and webcasts. He is a member of the IPSJ, IEICE, and IEEE.

Satoru Matsumoto received his Diploma's degrees from Kyoto School of Computer Science, Japan, in 1990. He received his Master's degrees from Shinshu University, Japan, in 2004. From 1990 to 2004, he was a teacher in Kyoto School of Computer Science. From 2004 to 2007, he was Assistant Professor of The Kyoto College of Graduate Studies for informatics. From 2007 to 2010, he was Assistant Professor of Office of Society Academia Collabo-ration, Kyoto University. From 2010 to 2013, he was Assistant Professor of Research Institute for Economics & Business Administration, Kobe University. From 2015 to 2016, he was a specially appointed assistant professor of Cybermedia Center, Osaka University. From April 2016 to September 2016, he became a specially appointed researcher. Since November 2016, he became an assistant professor. His research interests include distributed processing systems, rule-based systems, and stream data processing. He is a member of IPSJ, IEICE, and IEEE

Tomoya Kawakami received his B.E. degree from Kinki University in 2005 and his M.I. and Ph.D. degrees from Osaka University in 2007 and 2013, respectively. From 2007 to March 2013 and from July 2014 to March 2015, he was a specially appointed researcher at Osaka University. From April 2013 to June 2014, he was a Ph.D. researcher at Kobe University. From April 2015 to February 2020, he was an assistant professor at Nara Institute of Science and Technology. Since March 2020, he has been a senior assistant professor at University of Fukui. His research interests include distributed computing, rule-based systems, and stream data processing. He is a member of the Information Processing Society of Japan (IPSJ) and IEEE.

Yuuichi Teranishi received his M.E. and Ph.D. degrees from Osaka University, Japan, in 1995 and 2004, respectively. From 1995 to 2004, he was engaged Nippon Telegraph and Tele-phone Corporation (NTT). From 2005 to 2007, he was a Lecturer of Cybermedia Center, Osaka University. From 2007 to 2011, He was an associate professor of Graduate School of Information Science and Technology, Osaka University. Since August 2011, He has been a research man-ager and project manager of National Institute of Information and Communications Technology (NICT). He received IPSJ Best Paper Award in 2011. His research interests include technologies for distributed network systems and applications. He is a member of IPSJ, IEICE, and IEEE.

Regular Paper

How to Theorem-Prove Trace-Based Safety Properties

Toshinori Fukunaga[1], Hideki Goromaru[1], Tadanori Mizuno[2], Kazuhiko Ohkubo[1], and Yoshinobu Kawabe[2]

[1]NTT Secure Platform Laboratories, NTT Corporation
3-9-11 Midori-cho, Musashino-shi, Tokyo 180-0012, Japan
E-mail : { toshinori.fukunaga.vf, hideki.goroumaru.mx }@hco.ntt.co.jp,
ohkubo.kazuhiko@lab.ntt.co.jp
[2]Department of Information Science, Aichi Institute of Technology
Yachigusa 1247, Yakusa-cho, Toyota, Aichi 470-0392, Japan
E-mail : { tmizuno, kawabe }@aitech.ac.jp

Abstract - Recently, it is getting more important to analyze the trust of information and the trust of information sources. This is because information exchanged in social media may not be trustable; for example, even though you receive a message which is consistent with other messages, you might be skeptical if the message is sent from an unknown sender. Thus, we need to analyze trust values and their transitions. In this paper, we discuss how to analyze the transitions of two-dimensional trust values. Specifically, after formalizing a time-related trust safety property, this paper introduces an efficient verification method for the property. By conducting a case study with a theorem-proving tool, we show the applicability of our proof method.

Keywords: On-Line Trust, I/O-automaton, Safety Properties, Theorem-Proving

1 INTRODUCTION

In recent years, social media is actively used in large-scale disasters such as earthquakes and typhoons, and safety information and relief information are actively exchanged in social media. However, such information is not always trustable. Some information may be incorrect, and the incorrect information may be deliberately distributed in the wake of disasters. Moreover, the correctness of information may change as time passes. Even if the information "A person is seriously injured but currently alive," is true in a disaster site, it may become false one hour later. When dealing with such information in social networks, it is important to evaluate the trust of messages and the trust of information sources.

Marsh and Dibben introduced an evaluation on trust [1], which is a value between -1 and 1. In addition, the trust values are classified with the notions of trust, distrust and untrust; also, another notion called mistrust is introduced. As for these properties, there are studies [2] (on distrust and mistrust) and [3] (on trust and mistrust) by Primiero et al. This classification is based on the one-dimensional definition of trust values, where the point of total trust and the point of total distrust are at the extremities. However, Lewicki has indicated that trust and distrust should be treated as independent dimensions [4]. Trust is a concept closely related to human's impressions; hence, in evaluating the trust values "contradictions/confusions" and "ignorance" should be considered. From this point of view, we introduced a two-dimensional trust representation with a pair of trust value and distrust value [5]-[6]. Specifically, we employed Oda's Fuzzy-set Concurrent Rating method [7] (hereinafter referred to as FCR method), which is a fuzzy-logic-based psychological theory for impression formation, as a basis for the trust representation, and by applying [8]-[9] we explored the correspondence between our trust representation and Marsh and Dibben's representation.

The two-dimensional trust value of [5]-[6] represents a trust state at a certain moment. However, to analyze trust-related properties, it is necessary to handle the changing nature of trust values. Thus, in this paper, we model the property of ever-changing trust value, and we conduct a computer-assisted verification. Specifically, we define a safety property with the transition sequences of trust values. Furthermore, based on the results in I/O-automaton theory [10]-[11], we conduct an efficient computer-assisted proof for the trust safety property.

This paper is organized as follows. Section 2 shows an overview of [5]'s FCR-based two-dimensional trust representation. Then, in Section 3 we describe how to deal with ever-changing trust values. Finally, Section 4 shows a case study, and we describe how to theorem-prove a trust safety property.

2 TWO-DIMENSIONAL TRUST REPRESENTATION

The trust classification by Marsh and Dibben is as follows, where a trust value ranges over $[-1, 1)$:

- *Trust*: is a state where a trust value of a trustee is more than a threshold value. We can see that this is a state enough to cooperate, and this is a measure of how much an agent believes a trustee;
- *Distrust*: is a state where the trustee's trust value is negative. This is a measure of how much an agent believes that the trustee will actively work against the agent in a given situation;
- *Untrust*: is a state where the trustee's trust value is positive but not enough to cooperate. This is a measure of

The second and fourth authors are currently at Chiba Institute of Technology and KYOWA EXEO Corporation, respectively.

how little the trustee is actually trusted; and

- *Mistrust*: is a state in which the initial trust has been betrayed; more precisely, the notion of mistrust can be considered as "Either a former trust destroyed, or former distrust healed," since the trustee may not have had bad intentions and it is not always "betrayed".

Suppose that you received a message, and you calculated its trust value. If the trust value is 0.9 and the cooperation threshold is 0.85, then from the definition of the trust notion, the message should be trusted. However, can we say that there is no distrust on this message? The maximum of the trust value is 1, hence we can see that there is a deficit of 0.1 points on the trust value. In this sense, the message might not be trusted enough. In [5]-[6], we considered that this was due to the limitation on the expressive power of one-dimensional trust representation, and we introduced a two-dimensional trust value to be an element of $Trust \times DisTrust$, where $Trust$ and $DisTrust$ are respectively degrees of trust and distrust, and we have $Trust = DisTrust = \{\, v \,|\, 0 \leq v \leq 1\}$. Following the manner in the FCR method, a two-dimensional trust value is also called an observation.

We focus on some observations to consider the meaning of the two-dimensional trust values. We can see that an observation around $(1, 0)$ has a high trust value and a low distrust value. Thus, we can see that the observation represents a state of "trust". Similarly, observations around $(0, 1)$ are the states of "distrust" since they have a low trust value and a high distrust value. For any observation (t, d) on the line between $(1, 0)$ and $(0, 1)$, we can see that (t, d) is ideal in the sense that the trust value and the distrust value satisfy the consistency condition $t + d = 1$. We consider that Marsh and Dibben's trust values are on this line. That is, the conventional trust value is defined with a limitation with regard to the consistency condition. Finally, the observation which corresponds to the conventional trust value of 0 is $(0.5, 0.5)$.

We introduced a classification of trust for two-dimensional trust values for observations with the consistency condition $t + d = 1$. Let CT be a cooperation threshold. The observations of the *trust* region should satisfy $t - d \geq CT$; that is, they are between $(\frac{1+CT}{2}, \frac{1-CT}{2})$ and $(1, 0)$. The observations between $(0.5, 0.5)$ and $(0, 1)$ correspond to a negative trust value; that is, they are in the *distrust* region. Actually, for any observation (t, d) in the distrust region we have $t < d$ where the degree of distrust is greater than the degree of trust. We can see that the other observations are in the *untrust* region.

For any observations (t, d) which may not satisfy $t+d = 1$, the above definition for trust notions is generalized as follows. To explain this, we employ a transformation:

$$\left[\begin{pmatrix} \cos\frac{\pi}{4} & -\sin\frac{\pi}{4} \\ \sin\frac{\pi}{4} & \cos\frac{\pi}{4} \end{pmatrix} \left\{ \begin{pmatrix} t \\ d \end{pmatrix} - \begin{pmatrix} 1 \\ 0 \end{pmatrix} \right\} + \begin{pmatrix} \frac{\sqrt{2}}{2} \\ 0 \end{pmatrix}\right] \times \frac{1}{\frac{\sqrt{2}}{2}} = \begin{pmatrix} t-d \\ t+d-1 \end{pmatrix}$$

and the resulting point $(t - d,\ t + d - 1)$ is called (i, c).

First, we consider the first element $i = t - d$ of (i, c). This is a value with $-1 \leq i \leq 1$, and the value corresponds to the conventional trust value of Marsh and Dibben. In fact, the value i indicates that the result of subtracting the degree of trust by the degree of distrust is actually the net trust value, and we see that this matches the intuition.

The value of i is calculated graphically. Actually, we first draw a perpendicular line from (t, d) to the diagonal line between $(1, 0)$ and $(0, 1)$, and let (p, q) be the resulting point. The value of p is in $[0, 1]$, and the value of i is calculated as the result of normalizing p to be in $[-1, 1]$. We can see that this is a calculation of an integration value $I_2(t, d) = \dfrac{t + (1 - d)}{2}$ by the reverse-item averaging method; actually, the integration value should be normalized with $i = 2(I_2(t, d) - 0.5)$ to be a value in $[-1, 1]$.

We find that two observations in the same perpendicular line have the same integration value. For example, observation $A = (t, d)$ and its nearest point on the diagonal line

$$A' = (\frac{t + (1 - d)}{2},\ 1 - \frac{t + (1 - d)}{2})$$

have the same integration value. However, for observations A and A', the distance from the diagonal line is different. The distance between the observation (t, d) and the diagonal line is given by $|t + d - 1|$, which is the absolute value of the second element $c = t + d - 1$ of (i, c). We can easily see that the formula of c is equivalent to the degree of contradiction-irrelevance $C(t, d)$ of the FCR method. The degree of contradiction represents how much it deviates from the consistent condition ($t + d = 1$), and its value is between -1 and 1. The degree of contradiction is close to 1 if we deal with a trustee of a contradictory evaluation; for example, "I trust him but at the same time I feel some distrust on his behaviour". Also, if the degree is around -1, then a truster is ignorant on a trustee; that is, this is a situation like "I do not care for him at all." If we have $t + d = 1$, then the degree of contradiction is 0.

With the notion of the degree of contradiction, we can introduce two types of new untrust notions:

- *Untrust confusional*: This is a case where a trustee is both trusted and distrusted. Formally, this is a case with $0 < i < CT$ and $c \geq 0$; and
- *Untrust ignorant*: This is a case where the trustee is ignored; in other words, the trustee is both little trusted and little distrusted. Formally, this is a case with $0 < i < CT$ and $c < 0$.

The original untrust notion in [1] is considered as the notion of untrust ignorant.

3 TRANSITION OF OBSERVATIONS

Mistrust is a trust property with regard to a misplaced trust, and this is related to a change of trust values over time. In order to build a trust relationship among victims and volunteers in a large-scale disaster [12]-[14], it is important to analyze a chronological change of trust values. Also, a trust concept called *swift trust* [15]-[16] attracts an attention, which is a

trust property for building trust relations in a short period of time. In this section, we deal with the observations in the previous section as states, and we formalize time-related trust properties with state machines.

I/O-automaton [10]-[11] by Lynch et al. is a well-known mathematical model for distributed algorithms. In the theory of I/O-automata, a system is regarded as a collection of state machines which interacts with each other; the interactions are formalized with events. Some of events are observable from the outside of the system; for example, keyboard input, screen output, communication through the Internet are typical observable events. Some events cannot be observed; computer's internal processing and communications using a private line are such examples. A sequence of observable events from the initial state is called a trace, and a set of traces represents the behavior of the system. In general, systems have multiple (possibly infinite) traces, and the properties of automata are characterized with the set of traces.

Safety and liveness properties are well-known properties of distributed algorithms and they are defined with traces. A safety property guarantees that there is no occurrence of (specified) bad event. For example, if a computer program has no "division by 0" errors, then we regard that the program satisfies a safety property. On the other hand, a liveness property represents that finally some good behaviour will happen. For example, if a computer program always terminates, we can see that the program has a liveness property. If a communication system can reach an initial state from any state of the system, then we can see that the communication system satisfies another liveness property.

If we regard observations as states, the property "The trustee never goes to the region of distrust," is regarded as a safety property on trust transitions. Also, "A trustee will finally reach the region of trust," can be considered an liveness property on trust. In the following, let CT be a cooperation threshold with $0 < CT \leq 1$. We define the trust region $T(CT)$, the distrust region D, and the untrust region $U(CT)$ with:

$$\begin{cases} T(CT) &= \{\,(t,d)\,|\,t \in Trust \wedge d \in DisTrust \\ & \quad \wedge t - d \geq CT\,\}, \\ D &= \{\,(t,d)\,|\,t \in Trust \wedge d \in DisTrust \\ & \quad \wedge t < d\,\}, \text{ and} \\ U(CT) &= Trust \times DisTrust \setminus (T(CT) \cup D) \end{cases}$$

and we formalize trust safety properties. Note that operator "$\setminus$" is for the set subtraction.

Formally, automaton X has a set of actions $sig(X)$, a set of states $states(X)$, a set of initial states $start(X) \subset states(X)$ and a set of transitions $trans(X) \subset states(X) \times sig(X) \times states(X)$. Transition $(s, a, s') \in trans(X)$ is written as $s \xrightarrow{a}_X s'$. In this paper, a state is a tuple of values. Each element of the tuple has a corresponding distinct variable name. The name of a variable is used as an access function to the value. This kind of modeling is standard in I/O-automaton theory and its extensions such as [17]. In this paper, we use variables tr and dis for trust value and distrust value, respectively. The degrees of trust and distrust in state $s \in states(X)$ are referred as $s.tr$ and $s.dis$, respectively.

For any state $s \in states(X)$, a property "If s is not in the distrust region then the next state of s is not in the distrust region," is defined with:

$$\begin{array}{l} stepTrustSafe(s) \\ \quad \Longleftrightarrow \\ \quad\quad (s.tr,\, s.dis) \notin D \\ \quad\quad\quad \Longrightarrow\ \forall a \in sig(X)\, \forall s' \in states(X) \\ \quad\quad\quad\quad\quad [\, s \xrightarrow{a}_X s' \ \Longrightarrow\ (s'.tr,\, s'.dis) \notin D\,]. \end{array}$$

Hence, if we prove

$$\begin{array}{rl} & \forall s \in start(X)[\,(s.tr, s'.tr) \notin D\,] \\ \wedge & \forall s \in state(X)[\,stepTrustSafe(s)\,] \end{array} \quad (1)$$

then we have "The system X never reaches the distrust region." This formula consists of two conditions. The first condition represents that an initial state is not in the distrust region. The second condition means that every state s should satisfy $stepTrustSafe(s)$; that is, for any transition from s the system X never goes to the distrust region. If we use the predicate $reachable(s, s')$ for the reachability from state s to state s', the second condition can be:

$$\begin{array}{l} \forall s_{init} \in start(X),\, \forall s \in state(X) \\ \quad\quad [\,reachable(s_{init}, s) \ \Longrightarrow\ stepTrustSafe(s)\,] \end{array}$$

In this case, we consider the safety property only for reachable states. In any cases, this is to prove a trust safety property by induction on the length of execution sequences.

With the predicate $reachable$, another safety property "If a user exits the region of distrust, then the user never goes back to the distrust region," is formalized with:

$$\begin{array}{l} \forall s, s' \in states(X) \\ \quad [(reachable(s, s') \wedge (s'.tr, s'.dis) \notin D) \\ \quad\quad \Longrightarrow\ \forall s'' \in states(X) \\ \quad\quad\quad\quad [reachable(s', s'') \\ \quad\quad\quad\quad\quad \Longrightarrow\ (s''.tr, s''.dis) \notin D]\,]. \end{array}$$

We believe trust liveness properties can be formalized similarly.

4 PROVING TRUST SAFETY PROPERTY — A CASE STUDY

Let X be an automaton which specifies a communication system. In order to prove a trust safety property of X, it suffices to prove the condition (1) in the previous section with a theorem-proving tool directly. However, this proof approach is not efficient.

In this section, we apply an efficient proof method for trace inclusion of I/O-automaton to the verification of trust safety properties. Specifically, we describe two automata. The first automaton is what we can easily check that the automaton satisfies a trust safety property. The second automaton is a specification of the target communication system. If we can prove the trace inclusion between the two automata, the trust safety property of the first automaton leads to the trust safety property of the second automaton.

4.1 Preliminary Definition

First, we introduce the definition for sort `VL` with the Larch language. Specifically, the definition is:

```
VL: trait

  introduces
    vl0, vl1, otherValues: -> VL
    -__, abs: VL           -> VL
    __+__, __-__: VL, VL   -> VL
    __<__, __<=__,
    __>__, __>=__: VL, VL  -> Bool
    CT:                    -> VL
    D: VL, VL              -> Bool
    T: VL, VL, VL          -> Bool
    U: VL, VL, VL          -> Bool

  asserts with x, y, z, t, d, ct: VL
    x + vl0 = x;
    vl0 + x = x;
    x - vl0 = x;
    vl0 - x = -x;
    -(-x) = x;
    (x >= vl0) => abs(x)  = x;
    (x < vl0) => abs(x)  = -x;
    abs(-x) = abs(x);
    (-vl1) <= x;
    x <= vl1;
    (x >= y) <=> ((x = y) \/ (x > y));
    (x <= y) <=> ((x = y) \/ (x < y));
    (x > y) <=> ~(x <= y);
    (x < y) <=> ~(x >= y);
    CT > vl0;
    CT < vl1;
    D(t, d) <=> ((t-d) < vl0);
    T(t, d, ct) <=> ((t-d) >= ct);
    U(t, d, ct)
        <=> (~D(t, d) /\ ~(T(t, d, ct)))
```

and this kind of description is called a trait. The trait `VL` is for the set of real numbers whose domain is $[-1, 1]$. In this trait, several constants and operators are introduced; for example, constants `vl0` and `vl1` are respectively for 0 and 1 in sort `VL`. `CT` is a term for the cooperation threshold. Addition `+`, subtraction `-`, an unary operator for negative numbers `-`, comparison operators `<`, `>`, `<=` and `>=`, and the function for absolute value `abs` are defined as usual.

Predicates `D(t, d)`, `T(t, d, ct)` and `U(t, d, ct)` are true if observation `(t, d)` is in the distrust region, the trust region and the untrust region, respectively; note that `ct` is a parameter for the cooperation threshold.

4.2 Specifying and Proving Trust Safety Property

We introduce Fig. 1's I/O-automaton `testerSafety` to define a trust safety property. The automaton has three actions:

- `move(ev, pt, pd, dt, dd)`: enabled if event `ev` occurs and the two-dimensional trust value changes from `(pt, pd)` to `(pt+dt, pd+dd)`;
- `inDistr(t, d)`: enabled if trust value `(t, d)` is in the distrust region; and
- `notInDistr(t, d)`: enabled if trust value `(t, d)` is not in the distrust region.

```
uses testerSafetyDT

automaton testerSafety
  signature
    internal move(ev:Event, pt: VL,
                  pd: VL, dt: VL, dd: VL)
    output inDistr(t:VL, d:VL)
    output notInDistr(t:VL, d:VL)

  states
    tr: VL := vl0,
    dis: VL := vl0,
    stateOfAgent: agtState := InitState

  transitions
    internal move(ev, pt, pd, dt, dd)
      pre    pt = tr
          /\ pd = dis
          /\ (   vl0 <= (pt + dt)
              /\ (pt + dt) <= vl1)
          /\ (   vl0 <= (pd + dd)
              /\ (pd + dd) <= vl1)
          /\ condition(stateOfAgent, ev,
                       pt, pd, dt, dd)
      eff tr  := tr + dt;
          dis := dis + dd;
          stateOfAgent
              := change(stateOfAgent, ev)

    output inDistr(t, d)
      pre tr < dis /\ t = tr /\ d = dis
      eff tr := tr

    output notInDistr(t, d)
      pre ~(tr < dis) /\ t = tr /\ d = dis
      eff tr := tr
```

Figure 1: `testerSafety`: An Abstract System

Note that actions `inDistr` and `notInDistr` are special actions for analyzing trust transitions. If action `inDistr` does not appear on any trace, the automaton will not go to the distrusted region.

The transition of trust values is determined only by action `move`, and the action is enabled if predicate `condition` in the `pre`-part is true. The predication `condition` is introduced in Fig. 2's `testerSafetyDT`, and it is defined as

```
condition(st, ev, pt, pd, dt, dd)
    <=> ~D(pt, pd) /\ ~D(pt+dt, pd+dd)
```

in this study. This condition means that "The observation `(pt, pd)` of the current state and the observation `(pt + dt, pd + dd)` of the next state are neither in the distrust region." It is important for verifiers that the correctness of automaton `testerSafety` can be checked easily. Actually, `testerSafety` is small and simple. Moreover, with the `condition` predicate above, we can easily see that there is no occurrence of `inDistr` in `testerSafety`'s traces; this leads to the correctness of `testerSafety`. The correctness may look straightforward, but we should formally verify the correctness. This is because the result with regard to `testerSafety` is required when we conduct a simulation-based proof for trace inclusion in Sec. 4.3.2. The correctness for `testerSafety` is shown in the end of this section.

An example of event sequence from `testerSafety` is:

```
testerSafetyDT: trait

includes VL

introduces
  condition: agtState, Event,
             VL, VL, VL, VL -> Bool,
  InitState: -> agtState,
  AnotherState: -> agtState,
  change: agtState, Event -> agtState

asserts with st: agtState, ev: Event,
             pt, pd, dt, dd: VL
  condition(st, ev, pt, pd, dt, dd)
       <=> ~D(pt, pd) /\ ~D(pt+dt, pd+dd)
```

Figure 2: Datatype for `testerSafety`

```
notInDistr(vl0, vl0).
  move(get_mes(usrA, "hello"),
               vl0, vl0, vl0.3, vl0.2).
    notInDistr(vl0.3, vl0.2).
```

In the initial state, both of the trust and distrust degrees are 0; that is, we have `(tr, dis) = (vl0, vl0)`. In this case, `tr < dis` holds, and this allows an occurrence of event `notInDistr(vl0, vl0)`. Then, after the occurrence of event `get_mes`, the pair of trust and distrust degrees becomes `(vl0.3, vl0.2)`, where constants `vl0.3` and `vl0.2` in sort `VL` represent 0.3 and 0.2 respectively. In the resulting state, the distrust degree still does not exceed the trust degree, thus event `notInDistr(vl0.3, vl0.2)` can occur.

In the above example, it looks that "random" real numbers 0.2 and 0.3 are used in the event sequence. However, "arbitrary" numbers are actually assumed for the parameters. That is, at a level of abstraction, theorem-proving is exhaustive with regard to the event sequences, and all the event sequences are logically checked in a verification.

In the specification of Fig. 1, we have variables `dt` and `dd` in action `move`. They are variables of sort `VL`, and the definitions in trait `VL` restrict their values to be in $[-1, 1]$. Additionally, `dt` and `dd` should be the values which satisfy both of values `pt + dt` and `pd + dd` are in $[0, 1]$. This condition is written in the precondition part of `move`.

The I/O-automaton `testerSafety` can be translated into first-order predicate logic formulae, and a trust safety property can be proven with Larch Prover (LP) [18]. In the following we prove the trust safety property that "For any state `s` of automaton `testerSafety`, if `s` is reachable then the two-dimensional trust value at `s` is not in the distrust region." This is formally described as:

```
(\A st:States[testerSafety]
    (reachableAbst(st)
     => ~D(st.tr, st.dis))).
```

Proving this formula is equivalent to proving two conditions

```
   (\A st:States[testerSafety]
       (start(st)
        => ~D(st.tr, st.dis)))
```

and

```
(\A st:States[testerSafety]
(\A at:Actions[testerSafety]
    (reachableAbst(st)
     => ((   enabled(st, at)
          /\ ~D(st.tr, st.dis))
         => ~D(effect(st, at).tr,
               effect(st, at).dis))))).
```

We can see that this is to prove a trust safety property by induction on the length of execution sequences starting from initial states; the first condition represents a base case, and the second condition is an induction step.

Below, we show a proof script for a trust safety property.

```
prove
 (\A st:States[testerSafety]
     (reachableAbst(st)
      => ~D(st.tr, st.dis)))
..
%
 prove
  (\A st:States[testerSafety]
      (start(st) => ~D(st.tr, st.dis)))
 ..
 res by =>
 %
 prove
  (\A st:States[testerSafety]
      (\A at:Actions[testerSafety]
          (reachableAbst(st)
           => ((enabled(st, at)
                /\ ~D(st.tr, st.dis))
               => ~D(effect(st, at).tr,
                     effect(st, at).dis)))))
 ..
 res by =>
 %
 res by ind on at
 res by =>
 res by =>
 res by =>
qed
```

From this, `~D(st.tr, st.dis)` holds for any reachable state `st` of `testerSafety`. This means action `inDistr` is not enabled at `st`. Therefore, we obtain the following lemma; a screenshot of computer-assisted theorem-proving for this lemma is shown in Fig. 3.

Lemma 1 *Every trace of I/O-automaton* `testerSafety` *does not have any occurrence of action* `inDistr`. □

In this sense, we can see that `testerSafety` never goes to the region of distrust; this leads to a trust safety property.

We have shown that `testerSafety` satisfies a trust safety property. We can see that the property is, informally, "The transition of trust value does not reach the region of distrust." Note that this is a trust safety property but is not the only trust safety property. In general, and more formally, if the following conditions are satisfied for the set $traces(P)$ of all traces of automaton P, we say P is called a safety property [10]:

(i) $traces(P)$ is non-empty;

(ii) $traces(P)$ is prefix-closed, that is, if $\beta \in traces(P)$ and β' is a finite prefix of β, then $\beta' \in traces(P)$; and

(iii) $traces(P)$ is limit-closed, that is, if $\beta_1, \beta_2, \ldots$ is an infinite sequence of finite sequences of $traces(P)$, and

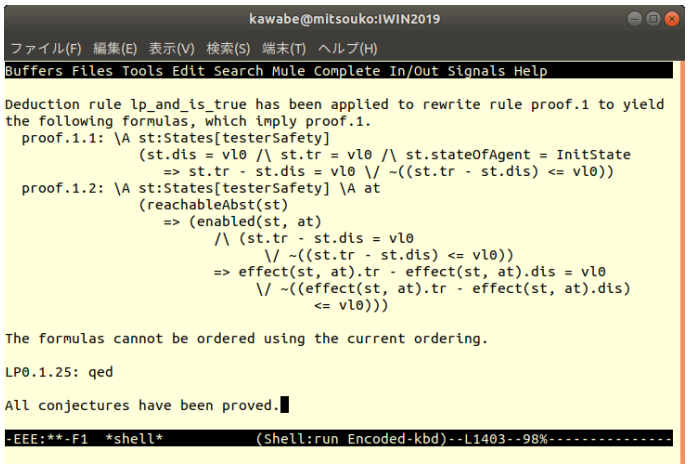

Figure 3: Theorem-Proving Trust Safety of `testerSafety`

> for each i, β_i is a prefix of β_{i+1}, then the unique sequence β that is the limit of the β_i under the successive extension ordering is also in $traces(P)$.

Automaton `testerSafety` is not general in this sense, however, from a practical viewpoint, it is too strong to require a general automaton satisfying the above conditions. We consider `testerSafety` is powerful enough for analysis.

4.3 Specifying Communication System and Safety Proof by Trace Inclusion

4.3.1 Specification of Communication System

We consider a specification `bbdSystem` of a communication system; see Fig. 4. This communication system sends a message to an online bulletin board after evaluating the user's trust value. The system receives a message from a user by action `get_mes` and evaluates the trust value of the message with actions `discard_mes` and `approve_mes`. If the trust value in the next state reaches the distrust region when writing the message to the bulletin board, the message is not sent and discarded by `discard_mes`. Otherwise, the message is written to the bulletin board by actions `approve_mes` and `say`. Actions `inDistrC` and `notInDistrC` are special actions to discuss the trust values, and they correspond to actions `inDistr` and `notInDistr` of `testerSafety`.

Automaton `bbdSystem` uses a datatype defined in the trait `bbdSystemDT` shown in Fig. 5. This trait employs `Sequence(MES)`, which defines a message queue.

We introduce functions `evalTr` and `evalDis` for calculating the degree of trust and the degree of distrust, respectively, though the concrete definitions of these functions are not given in this paper; giving a definition for these functions is a future work. In this paper, only the constraints on these functions are defined as follows. For function `evalTr`, we employ a constraint

```
(\A tr:VL
      ((vl0 <= tr /\ tr <= vl1)
       => (\A m:MES
              (   vl0 <=
                  (tr + evalTr(tr, m))
               /\ (tr + evalTr(tr, m))
                  <= vl1))))
```

```
uses bbdSystemDT

automaton bbdSystem
  signature
    input get_mes(i:ID, m:MES)
    internal discard_mes(i:ID, m:MES)
    internal approve_mes(i:ID, m:MES)
    output say(i:ID, m:MES)
    output inDistrC(t:VL, d:VL)
    output notInDistrC(t:VL, d:VL)

  states
    tr: VL := vl0,
    dis: VL := vl0,
    flg: Bool := false,
    mesQ: Seq[MES] := empty

  transitions
    input get_mes(i, m)
      eff mesQ := mesQ ||
                  (packet(i, m) -| empty)

    internal discard_mes(i, m)
      pre    ~flg
          /\ mesQ ~= empty
          /\ packet(i, m) = head(mesQ)
          /\ ((tr + evalTr(tr, m))
              -(dis + evalDis(dis, m)))
             < vl0
      eff mesQ := tail(mesQ)

    internal approve_mes(i, m)
      pre    ~flg
          /\ mesQ ~= empty
          /\ packet(i, m) = head(mesQ)
          /\ ((tr + evalTr(tr, m))
              -(dis + evalDis(dis, m)))
             >= vl0
      eff flg := true

    output say(i, m)
      pre flg /\ mesQ ~= empty
              /\ packet(i, m) = head(mesQ)
      eff tr := tr + evalTr(tr, m);
          dis := dis + evalDis(dis, m);
          mesQ := tail(mesQ);
          flg := false

    output inDistrC(t, d)
      pre tr < dis /\ t = tr /\ d = dis
      eff tr := tr

    output notInDistrC(t, d)
      pre ~(tr < dis) /\ t = tr /\ d = dis
      eff tr := tr
```

Figure 4: `bbdSystem`: A Concrete System

for the degree of trust to be in $[0, 1]$. For `evalDis`, a similar condition is introduced.

We do not introduce the definition of `change`, which is a function in the effect part of action `move`. This is because in our case study the value of `stateOfAgent` is not required in evaluating the precondition part of `move`. However, if we modify the definition of predicate `condition`, a concrete definition might be required.

4.3.2 Safety Proof by Trace Inclusion

We replace `bbdSystem`'s observable actions `get_mes` and `say` with internal actions of the same name; the resulting automaton is called `bbdSystem`$\backslash\{$`get_mes, say`$\}$. If we prove the existence of a binary relation called a forward simulation from automaton `bbdSystem`$\backslash\{$`get_mes, say`$\}$ to

```
bbdSystemDT: trait

includes VL, Sequence(MES)

introduces
  packet:  ID, MES -> MES
  evalTr:  VL, MES -> VL
  evalDis: VL, MES -> VL
  getMesFromPacket:  MES -> MES

asserts with tr, dis: VL, i:ID, m: MES
  (\A tr:VL
      ((vl0 <= tr /\ tr <= vl1)
       => (\A m:MES
              (   vl0 <=
                  (tr + evalTr(tr, m))
               /\ (tr + evalTr(tr, m))
                  <= vl1))));
  (\A dis:VL
      ((vl0 <= dis /\ dis <= vl1)
       => (\A m:MES
              (   vl0 <=
                  (dis + evalDis(dis, m))
               /\ (dis + evalDis(tr, m))
                  <= vl1))));
  getMesFromPacket(packet(i, m)) = m;
```

Figure 5: Datatype for bbdSystem

automaton testerSafety, then we have a trace inclusion

$$traces(\texttt{bbdSystem}\backslash\{\texttt{get\_mes}, \texttt{say}\}) \subseteq traces(\texttt{testerSafety})$$

from Theorem 3.10 of [11]. From Lemma 1, every trace in $traces(\texttt{testerSafety})$ does not have any occurrence of action inDistr. Hence, if we prove a trace inclusion, every trace in $traces(\texttt{bbdSystem}\backslash\{\texttt{get\_mes}, \texttt{say}\})$ does not contain inDistr; this leads to the absence of inDistr in $traces(\texttt{bbdSystem})$.

A candidate binary relation for a forward simulation is defined as follows:

```
fs(sb, st) <=> (   (sb.tr = st.tr)
                /\ (sb.dis = st.dis)
                /\ (sb.flg => X) )

where X =
 ( ((sb.tr
     + evalTr(sb.tr,
         getMesFromPacket(head(sb.mesQ))))
   - (sb.dis
      + evalDis(sb.dis,
         getMesFromPacket(head(sb.mesQ)))))
   >= vl0)
```

To prove that binary relation fs is a forward simulation, we should prove the initial state condition

```
(\A sb:States[bbdSystem]
    (start(sb)
     => (\E st:States[testerSafety]
            (start(st) /\ fs(sb, st)))))
```

and step correspondence condition

```
(\A sb:States[bbdSystem]
(\A sb':States[bbdSystem]
(\A st:States[testerSafety]
(\A ab:Actions[bbdSystem]
    (reachableAbst(st)
     => ((fs(sb, st) /\ step(sb, ab, sb'))
         => (\E st':States[testerSafety]
                (   steps(st, ab, st')
                 /\ fs(sb', st')))))))))
```

with a theorem proving tool. We show a proof script as follows.

```
% ------------------------------
% Initial states' correspondence
% ------------------------------
prove
 (\A sb:States[bbdSystem]
     (start(sb)
      => (\E st:States[testerSafety]
             (start(st) /\ fs(sb, st)))))
..
res by =>
res by spec st to [InitState, vl0, vl0]
qed

% ------------------------------
% Step's correspondence
% ------------------------------
prove
 (\A sb:States[bbdSystem]
 (\A sb':States[bbdSystem]
 (\A st:States[testerSafety]
 (\A ab:Actions[bbdSystem]
     (reachableAbst(st)
      => ((fs(sb, st) /\ step(sb, ab, sb'))
          => (\E st':States[testerSafety]
                 (   steps(st, ab, st')
                  /\ fs(sb', st')))))))))
..
res by =>
%
make passive c-o(steps)
res by ind on ab
%
res by =>
res by spec st' to stc
%
res by =>
res by spec st' to stc
%
res by =>
res by spec st' to stc
prove getMesFromPacket(head(sbc.mesQ)) = mc
crit c-o(mc) / c-o(packet) with *
%
res by =>
res by spec st' to
  effect(stc, move(ev, stc.tr, stc.dis,
  evalTr(sbc.tr, mc), evalDis(sbc.dis, mc)))
..
make passive c-o(intTrans)
rewrite con with reversed
  (c-o(intTrans) / c-o(enabled)) ~ c-o(steps)
..
res by spec at to
  move(ev, stc.tr, stc.dis,
       evalTr(stc.tr, mc),
       evalDis(stc.dis, mc))
..
make active c-o(intTrans)
prove getMesFromPacket(head(sbc.mesQ)) = mc
crit c-o(mc) / c-o(packet) with *
%
crit c-o(stc) with *
crit c-o(stc) with *
%
res by =>
res by spec st' to stc
res by spec st1 to stc
prove effect(stc, inDistr(t, d)) = stc
crit c-o(inDistr) with *
%
res by =>
res by spec st' to stc
res by spec st1 to stc
prove effect(stc, notInDistr(t, d)) = stc
crit c-o(notInDistr) with *
%
qed
```

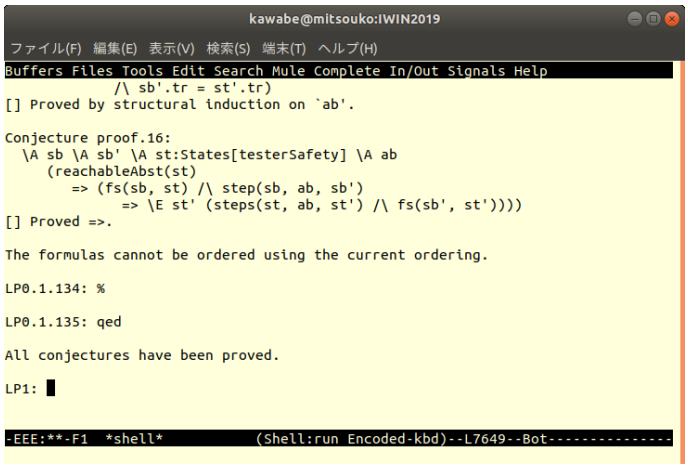

Figure 6: Theorem-Proving Trace Inclusion

This leads to the following lemma.

Lemma 2 *Binary relation* `fs(sb, st)` *is a forward simulation from automaton* `bbdSystem`$\backslash\{$`get_mes, say`$\}$ *to automaton* `testerSafety`. □

Summarizing, we have the following result.

Theorem 1 *Every trace of I/O-automaton* `bbdSystem` *does not have an occurrence of action* `inDistr`.

Proof: Proven by Lemmata 1 and 2. □

Consequently, a trust safety property has been shown for automaton `bbdSystem`; see Fig. 6 for a snapshot of proving with LP.

We can see that the specification of `bbdSystem` is small. Thus, it may look straightforward that automaton `bbdSystem` satisfies some safety-related trust property. This observation is correct in some sense. However, it is not easy to rigorously state what kind of safety property is satisfied by `bbdSystem`. Based on the correctness of `testerSafety`, we can define the correctness of `bbdSystem` formally. Moreover, the correctness can be proven with a semi-automatic theorem-proving approach.

Suppose that we write automaton `distSystem`, which is a specification of distributed or more concrete version of `bbdSystem`. If we can prove a trace inclusion

$$traces(\texttt{distSystem}) \subseteq traces(\texttt{bbdSystem})$$

at a level of abstraction, this paper's result with regard to the safety property of `bbdSystem` leads to the safety property of `distSystem`. In this sense, a stepwise verification for trust safety properties is possible when we deal with larger specifications. This is an advantage of this paper's verification method.

5 DISCUSSION AND CONCLUSION

In this paper, we discussed how to analyze transitions of two-dimensional trust values. Specifically, we employed a theory of distributed algorithms to formalize trust safety properties such as "Any transition does not lead to the distrust region," or "After reaching some region other than the distrust region, the system never goes to the distrust region."

We cannot say that it efficient to theorem-prove the condition for trust safety property of each automaton. In this paper, we employed I/O-automata to represent a trust safety property, and applied a proof method for trace inclusion. This enables us to verify trust safety properties efficiently. Furthermore, with simple examples, we empirically demonstrated that it is possible to verify trust safety properties with automatic theorem provers. In this study, we employed the Larch Prover (LP), which is theorem proving tool based on first-order predicate logic and equational theory. LP proves formulae with the techniques of term rewriting systems [19]-[21]. Although we need to translate IOA specifications into each theorem prover's formulae as in [18][22], we believe that a similar proof with another theorem proving tool (such as Coq [23], Isabelle [24], and Maude [25]) is possible. With regard to the functions `evalTr` and `evalDis`, we introduced the constraint on the range of the trust value only, and we did not discuss the concrete evaluation method of the trust value. In other words, this paper gives an analysis method for the transition of the evaluated trust value at each moment. It is an interesting future work to define the trust value of each moment.

The trust, distrust, and untrust notions were defined for two-dimensional trust values in [5]-[6]. This is defined with the value of $i = t - d$, and we do not use the value of c. We can see that this is formalized as a linear case; for example, the trust notion and the distrust notion are defined with linear restrictions $d \leq -t + CT$ and $d > t$, respectively. This is just for simplicity, and we believe it is possible to provide a finer definition for trust notions with both of i and c. Introducing such a non-linear definition is an interesting future work. In order to deal with the non-linear settings, it would be required to change the definitions for the regions of trust, distrust and untrust. However, we believe that the verification method in this paper is also applicable for the non-linear case.

Finally, conducting larger verification examples is an important work. Specifically, we are planning a trust verification for communication systems [26]-[27] based on social media.

REFERENCES

[1] S. Marsh and M. R. Dibben, "Trust, untrust, distrust and mistrust – an exploration of the dark(er) side," in *Proceedings of the Third International Conference on Trust Management*, iTrust'05, (Berlin, Heidelberg), pp. 17–33, Springer-Verlag (2005).

[2] G. Primiero, "A calculus for distrust and mistrust," in *Trust Management X* (S. M. Habib, J. Vassileva, S. Mauw, and M. Mühlhäuser, eds.), (Cham), pp. 183–190, Springer International Publishing (2016).

[3] G. Primiero, F. Raimondi, M. Bottone, and J. Tagliabue, "Trust and distrust in contradictory information transmission," *Applied Network Science*, vol. 2, p. 12 (2017).

[4] R. J. Lewicki, D. J. B. McAllister, and R. J. Bies, "Trust and distrust: New relationships and realities," *Academy of Management Review*, vol. 23, pp. 438–458 (1998).

[5] K. Ohkubo, T. Oda, Y. Koizumi, T. Ohki, M. Nishigaki, T. Hasegawa, and Y. Kawabe, "Trust representation under confusion and ignorance," in *Proceedings of International Workshop on Informatics (IWIN 2018)*, pp. 191–198 (2018).
[6] Y. Kawabe, Y. Koizumi, T. Ohki, M. Nishigaki, T. Hasegawa, and T. Oda, "On trust confusional, trust ignorant, and trust transitions," in *Proceedings of IFIPTM 2019* (2019).
[7] T. Oda, "Fundamental characterestics of fuzzy-set concurrent rating method," *Journal of Japan Association for Management Systems*, vol. 12, no. 1, pp. 23–32 (1995). In Japanese.
[8] T. Oda, "Fuzzy set theoretical approach for improving the rating scale method : Proposing and introducing the FCR-method and the IR-method as novel rating methods," *Japanese Psychological Review*, vol. 56, no. 1, pp. 67–83 (2013). In Japanese.
[9] T. Oda, "Measurement technique for ergonomics, section 3: Psychological measurements and analyses (3) measurements and analyses by kansei evaluation," *The Japanese Journal of Ergonomics*, vol. 51, no. 5, pp. 293–303 (2015). In Japanese.
[10] N. A. Lynch, *Distributed Algorithms*. Morgan Kaufmann Publishers (1996).
[11] N. Lynch and F. Vaandrager, "Forward and backward simulations — part I: Untimed systems," *Information and Computation*, vol. 121, pp. 214–233, (1995).
[12] Y. Murayama, "Issues in disaster communications," *Journal of Information Processing*, vol. 22, no. 4, pp. 558–565 (2014).
[13] M. G. Busa, M. T. Musacchio, S. Finan, and C. Fennell, "Trust-building through social media communications in disaster management," in *Proceedings of the 24th International Conference on World Wide Web*, WWW '15 Companion, (New York, NY, USA), pp. 1179–1184, ACM (2015).
[14] F. Lemieux, "The impact of a natural disaster on altruistic behaviour and crime," *Disasters*, vol. 38, pp. 483–499 (2014).
[15] D. Meyerson, K. E. Weick, and R. M. Kramer, *Swift Trust and Temporary Groups in Trust in Organizations: Frontiers of Theory and Research*. SAGE (1995).
[16] J. Wildman, M. Shuffler, E. Lazzara, S. Fiore, and S. Burke, "Trust development in swift starting action teams: A multilevel framework," *Group & organization management*, vol. 37, no. 2, pp. 137–170 (2012).
[17] D. Kaynar, N. Lynch, R. Segala, and F. Vaandrager, *The Theory of Timed I/O Automata, Second Edition*. Morgan & Claypool Publishers, 2nd ed. (2010).
[18] J. F. Soegaard-Andersen, S. J. Garland, J. V. Guttag, N. A. Lynch, and A. Pogosyants, "Computer-assisted simulation proofs," in *CAV '93*, vol. 697 of *Lecture Notes in Computer Science*, pp. 305–319, Springer-Verlag (1993).
[19] F. Baader and T. Nipkow, *Term Rewriting And All That*. Cambridge University Press (1998).
[20] J. W. Klop, "Term rewriting systems," in *Handbook of Logic in Computer Science* (D. G. S. Abramsky and T. S. E. Maibaum, eds.), vol. 2, pp. 1–112, Oxford University Press (1992).
[21] E. Ohlebusch, *Advanced topics in term rewriting*. Springer-Verlag (2002).
[22] A. Bogdanov, "Formal verification of simulations between I/O-automata," Master's thesis, Massachusetts Institute of Technology (2000).
[23] "The Coq Proof Assistant." `https://coq.inria.fr/`, (June 13, 2020).
[24] L. C. Paulson, "Isabelle: The next seven hundred theorem provers," in *Proceedings of the 9th Conference on Automated Deduction*, vol. 310 of *Lecture Notes in Computer Science*, pp. 772–773, Springer-Verlag (1989).
[25] N. Martí-Oliet and J. Meseguer, "Rewriting logic: Roadmap and bibliography," Theoretical Computer Science, Vol. 285, pp. 121–154 (2002).
[26] J. Chen, M. Arumaithurai, X. Fu, and K. K. Ramakrishnan, "CNS: Content-oriented notification service for managing disasters," in *Proceedings of ACM Conference on Information-Centric Networking*, pp. 122–131, ACM (2016).
[27] M. Jahanian, Y. Xing, J. Chen, K. K. Ramakrishnan, H. Seferoglu, and M. Yuksel, "The evolving nature of disaster management in the internet and social media era," in *2018 IEEE International Symposium on Local and Metropolitan Area Networks, LANMAN 2018, Washington, DC, USA, June 25-27, 2018*, pp. 79–84 (2018).

(Received October 30, 2019)
(Revised April 9, 2020)

Toshinori Fukunaga received the B.E., and M.E. degrees in electrical engineering from Chiba University in 1996 and 1998. He joined Nippon Telegraph and Telephone Corporation in 1998. His main research area is cryptography and its implementation. He is also involved in information security management system work and is currently engaged in human resource development for researchers.

Hideki Goromaru received the M.E. degree in Graduate School of Engineering from the Kagoshima University in 1995 and received the Ph.D. degree in Graduate School of System Engineering from the Wakayama University, Japan, in 2015. In 1995, he joined NTT Corp. and he had been a research and development engineer at NTT Laboratories until 2020. In 2020, he is an Associate professor at the Chiba Institute of Technology, Japan. His research interests include groupware, security and risk management. He is a member of Information Processing Society of Japan, the Institute of Electronics, Information and Communication Engineer, Japan Creativity Society and the Japan Psychological Association.

Tadanori Mizuno received the B.E. degree in Industrial Engineering from the Nagoya Institute of Technology in 1968 and received the Ph.D. degree in Engineering from Kyushu University, Japan, in 1987. In 1968, he joined Mitsubishi Electric Corp. From 1993 to 2011, he had been a Professor at Shizuoka University, Japan. From 2011 to 2016, he had been a Professor at the Aichi Institute of Technology, Japan. Since 2016, he is an Affiliate Professor at the Aichi Institute of Technology, Japan. His research interests include mobile computing, distributed computing, computer networks, broadcast communication and computing, and protocol engineering. He is a member of Information Processing Society of Japan, the Institute of Electronics, Information and Communication Engineers, the IEEE Computer Society and Consumer Electronics, and Informatics Society.

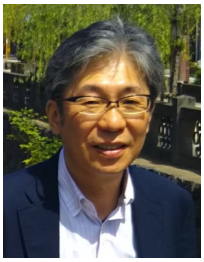

Kazuhiko Ohkubo received his B.E. degree in Informatics from the University of Tsukuba in 1987 and his M.E. in Electrical Engineering from the University of Tokyo in 1989. In 1989, he joined NTT (Nippon Telegraph and Telephone Corporation) Telecommunication Laboratories and earned his M.S. degree in Management of Technology from the MIT Sloan School of Management, USA in 2000. From 2016 to 2019, he had been the head of NTT Secure Platform Laboratories and also been a director of NTT Security Corporation, the specialized security company of NTT Group. In 2019, he received his Ph.D. in Business Administration and Computer Science from the Aichi Institute of Technology. Since 2019, he is the CISO of Kyowa Exeo Corporation. He is a member of IEEE.

Yoshinobu Kawabe received his B.E., M.E., and D.E. degrees in information engineering from Nagoya Institute of Technology in 1995, 1997, and 2003. He joined NTT Communication Science Laboratories, Nippon Telegraph and Telephone Corporation in 1997. In 2002, he was a visiting research scientist at MIT Laboratory for Computer Science. Since 2008, he has been at Aichi Institute of Technology, where he is a professor at the Department of Information Science. His research interests include term rewriting systems, process algebras, network programming languages, formal methods, security/privacy verification, and computational trust. He is a member of ACM, JSSST, IPSJ, and IEICE.

Industrial Paper

Failure Prediction of Factory Automation Equipment using the Interaction between Parallel Links

Masanori Haga†, Kazuhiko Tsutsui‡, Katsuhiko Kaji*,
Katsuhiro Naito*, Tadanori Mizuno*, and Naoya Chujo*

†Graduate School of Informatics, Aichi Institute of Technology, Japan
‡Mitsubishi Electric Co., Ltd., Japan
* Aichi Institute of Technology, Japan
{Tsutsui. Kazuhiko}@ay.MitsubishiElectric.co.jp
{b19723bb, kaji, tmizuno, ny-chujo}@aitech.ac.jp
{naito}@pluslab.org

Abstract - Maintenance of factory automation (FA) equipment is important for quality assurance in the manufacture of industrial products. In the present paper, we develop a failure prediction method for FA equipment with parallel links.

Recently, predictive maintenance has been considered as a maintenance system for FA equipment. In predictive maintenance, sensors are attached to the equipment. The failure time is estimated based on the sensor data, and maintenance is carried out in advance. Unsupervised learning is the recommended method, because FA equipment is not prone to failures and may not accumulate much failure data. The principal component analysis used in the present study can be used unsupervised, and related studies have shown that principal component analysis is more accurate than other unsupervised learning methods.

The considered method has a simple structure in which links of the same type are arranged in parallel. The considered method is shown to have great potential for enhancing predictive maintenance.

Since each link is connected to one mechanism, when the operation of a particular link is abnormal, the operations of other links are affected. By monitoring these interactions between links, failure prediction for the entire link mechanism can be performed using the measurement data from the sensor of a single link.

Experimental equipment with two links was produced. Time series data were obtained from measurements using the sensor of the servomotor when a load was applied to one link. Using principal component analysis, changes in link classes were observed based on the measurement data of not only the loaded link but also the unloaded link. In the present paper, we confirm the existence of the interaction between the links using an experimental apparatus of the parallel linkage mechanism. These interactions are used to predict failures with a small number of sensors.

Keywords: Predictive Maintenance, Factory Automation, Parallel Link, Principal Component Analysis

1 INTRODUCTION

Recent factory automation (FA) systems support a wide range of industrial products, from electronic devices, such as mobile phones, to transportation equipment such as automobiles. Proper maintenance of FA systems is required in order to ensure the quality of these products. In general, the maintenance cost of an FA system has been reported to be 15 to 60% of the manufacturing cost of the product, and thus is not insignificant [1].

There are two types of maintenance methods for FA equipment. The first is preventive maintenance which involves regularly performing maintenance, regardless of the state of the equipment. Therefore, unnecessary maintenance is performed on the FA equipment, which increases maintenance costs. The second type of maintenance is predictive maintenance, in which maintenance is performed according to the predicted state of the FA equipment. The state of the FA equipment is measured by sensors, and future failure times are predicted. The maintenance cost can be reduced by conducting maintenance based on failure prediction. The International Air Transport Association (IATA) has estimated that the cost of maintenance would be reduced by 15 to 20% if aircraft were to be subjected to predictive maintenance [2]. Failure prediction is required in order to perform predictive maintenance. The installation cost and physical space in a system, including wiring, for the sensor must also be considered [3]. In addition, a communication channel must be secured in order to upload real-time measurement data to the cloud. The purpose of the present paper is to predict the failure of FA equipment. FA equipment consists of a combination of several servo motors, links, and other mechanical components. By attaching sensors to the components in a system, it is possible to accurately measure mutations that lead to component failure. We herein examine a failure prediction method that is suitable for edge computing.

In the present paper, we predict failure for predictive maintenance using the interaction between mechanical parts. Defective components in FA equipment are detected based on changes in the sensor data. We examine the accuracy of the failure prediction using an experimental apparatus while increasing the load on the equipment until failure. We use prin-

cipal component analysis (PCA) for feature extraction in the failure prediction.

The remainder of the present paper is organized as follows. Section 2 introduces related research. Section 3 presents the considered method for failure prediction. Sections 4 and 5 describe the experimental system, the experimental method, and the obtained results. Section 6 discusses the evaluation results, and a summary is presented in Section 7.

2 RELATED RESEARCH

System diagnostics can be separated into model-based diagnostics and signal-based diagnostics [4]. Model-based diagnosis is used when the theoretical modeling of a target system is straightforward. A deterministic model is created using equations to represent the actual system, and the diagnosis is performed by comparing the output of the system with the output of the model.

Signal-based diagnosis is used when theoretical modeling of a target system is difficult. In this case, we use a model derived from measurements. We extract the characteristics for normal and abnormal operating conditions of the equipment from the measurements and use these characteristics to diagnose faults.

In recent years, a method for signal-based diagnosis using machine learning techniques has been introduced. With the increasing accuracy of sensors and developments in the field of AI, the accuracy of failure prediction is improving. There are also techniques to perform signal-based diagnosis under dynamic conditions, as compared to static conditions alone [5].

FA equipment is generally reliable and resistant to failure. However, in real environments, it is difficult to apply supervised learning because of the small accumulation of failure data. Therefore, it is common to use unsupervised machine learning for FA equipment. According to a review paper on FA equipment diagnosis by unsupervised machine learning, methods using PCA provide the best results [6]. The considered method uses unsupervised learning because it is not possible to know the parameters at failure from the beginning. Maintenance is carried out and monitoring the parameters and actually operating the FA equipment and is optimized by adjusting the operation period little by little.

In addition, there is a problem in signal-based diagnosis in that signal-based diagnostics require high computational power for recording and processing large amounts of measurement data. Therefore, it is necessary to apply these methods using cloud computing [7]. In the case of FA equipment, it is necessary to secure a large capacity communication line.

For this reason, it is desirable that the computer on the edge side be able to diagnose faults in the FA equipment. In addition, it is desirable that sensor count be reduced when edge computing is used. There are interactions between components such as the resonance between the components in the FA equipment, and the status of the entire FA system can be diagnosed using a small sensor count with appropriate signal processing. However, as far as we know, methods for predicting failure using the interaction between parallel links in FA equipment have not been studied.

3 FAILURE PREDICTION OF FACTORY AUTOMATION EQUIPMENT WITH PARALLEL LINKS

In the present paper, we examine a method for predicting failure by signal-based diagnosis for FA equipment with parallel links. Parallel link robots [8] are multiple link mechanisms of the same type that are arranged in parallel and operate synchronously. Robots using parallel links use many more shared control components compared to a single-arm robot. Therefore, the manufacturing cost is low, and the mechanism is simple and easy to maintain. For this reason, parallel links have been widely used. Fault prediction is performed by the parallel link mechanism with the installed sensor. Since each link is combined to form a single mechanism, the movement of a link is affected by other links. Therefore, if there is an abnormality in the operation of a certain link, the behavior of other links is expected to be affected. In the present paper, by considering the interaction between parallel links, using only measured data of sensors from a single link, we considered a method to detect an abnormal sign of an FA apparatus with parallel links to carry out its fault prediction. Generally, FA equipment does not change suddenly from the normal state to an abnormal state, and there may be a sign of abnormality due to wear of parts between the normal state and the abnormal state. The considered method measures the time series data of FA devices with parallel links. PCA is performed for these data. Based on the change in the PCA result, a sign of the abnormality is obtained, and the failure time is predicted. The procedure of the considered method is shown below.

- Measurement of time series data during operation of FA equipment
- PCA for measured time series data
- Classification of the data using the plane with the first and second principal components as axes
- Representation of each class by elliptic approximation and extraction of elliptic parameters
- Prediction of failure time from time series variation of elliptic parameters

The concept of fault prediction based on the considered method is shown in Fig. 1. The two axes represent the first and second components of the PCA. An ellipse approximating the measured data is shown. A normal ellipse indicates normal operation. This ellipse gradually changes with various factors to an abnormal state which is indicated by an abnormal ellipse. This change is obtained as an ”abnormal sign” ellipse in the middle, which indicates a sign of the abnormality. A class is a collection of data measured at the same timing in an operation of an apparatus. Therefore, classification is possible by collecting data in the order of measurement. In addition, we use curve approximation to predict elliptic parameters. In the next section, we discuss how to verify the degree of abnormal behavior from other links that can be detected.

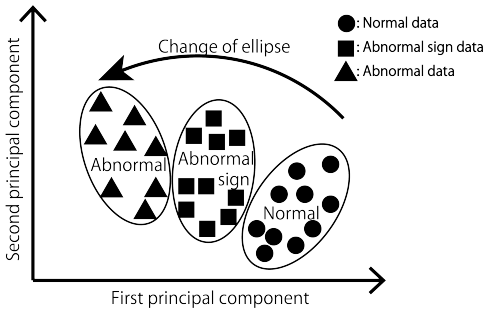

Figure 1: Concept of failure prediction

4 EXPERIMENTAL METHOD

In this section, we describe the experimental apparatus with a parallel link as well as the procedure for using the experimental apparatus. The experiment was carried out in a room in which an air conditioner was set at a constant temperature in order to suppress the change of motor data due to the change in temperature between day and night. An outline of the experiment is as follows. In this experiment, the abnormality of the bearing due to seizure and rusting due to a lack of grease is shown by mounting the weight. This is a fatal failure as a parallel link robot because the movement of the joint is impeded.

- Applying a load, which assumes an increase in the friction load at a specific link, and measuring the data.
- Analysis of changes due to increased load.
- Comparison of data between loaded and non-loaded links to evaluate the possibility of failure prediction.

4.1 Experimental Apparatuses

The experimental apparatuses are shown in Fig. 2. These apparatuses are systems that predict failure times from data obtained from the servo motors and can cover anomalies in joints such as bearing wear and seizure due to a lack of grease. In this experiment, the method was first examined on an apparatus (Type 1) that imitates FA equipment. By applying the method to an apparatus similar to actual FA equipment (Type 2), we obtain the results reported herein, and the generality to the parallel link mechanisms is confirmed. The Type 1 system is shown in Fig. 3. The Type 1 system consists of a personal computer and parallel link mechanisms using two servo motors. The personal computer transfers control to the servo motors, and the servo motors transmit the data to the personal computer. Six kinds of data can be obtained from the servo motors. The Type 1 sensor data consist of temperature, current, voltage, rotation angle, rotation speed, and rotation time, which can be obtained from the servo motor. The data acquisition frequency is 10 Hz. The temperature data measurements of the servo motor are affected by the temperature of the room. Therefore, this temperature is stabilized in the range of ± 1°c using air conditioning. This method prevents temperature change due to factors other than the heat generated by the operation of the servo motor.

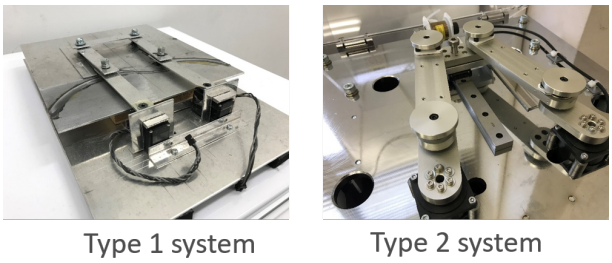

Figure 2: Experimental apparatuses

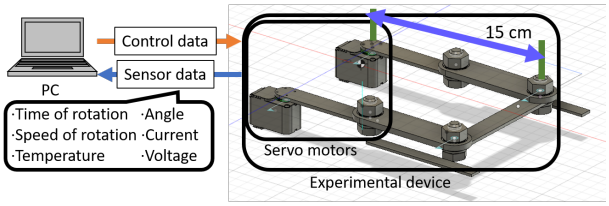

Figure 3: Type 1 experimental system

The Type 1 system is approximately 15 cm and is smaller than actual FA equipment. The specifications of the servo motor are listed in Table 1. The Type 2 system consists of an external hard disk drive (HDD) and parallel link mechanisms, as well as a controller using two servo motors. The controller operates the servo motors and transmits the data to the external HDD. Three kinds of data can be obtained from the servo motors. The Type 2 sensor data consist of current, rotation speed, and overshoot, which can be obtained from the servo motor. The data acquisition frequency is approximately 2252 Hz.

The specifications of the servo motor are listed in Table 2.

In the experiment, by operating the experimental apparatus which is similar to FA equipment, we obtain the sensor data necessary for failure prediction by increasing the load on the servo motor. In particular, we increase the load on the link component in order to create abnormal operating conditions. The experimental apparatus is shown in Fig. 4. The joints connect the links of the link components. The guide rails limit the movement of the drive unit. The drive unit is perpendicular to the guide rail.

Table 1: Specifications of the Type 1 servo motor (RS302CD)

Torque (during operation 7.4 V)	5.0 kgf·cm
Current consumption (when stopped)	40 mA
Current consumption (when moving)	125 mA
Working voltage	7.2–7.4 V
Movable angle	150°
Temperature limit	0–40 °C
Communication speed	max 460.8 kbps

Table 2: Specifications of the Type 2 servo motor (MDH-4012-324KE)

Torque	6.1182 kgf·cm
Temperature limit	0–40 °C

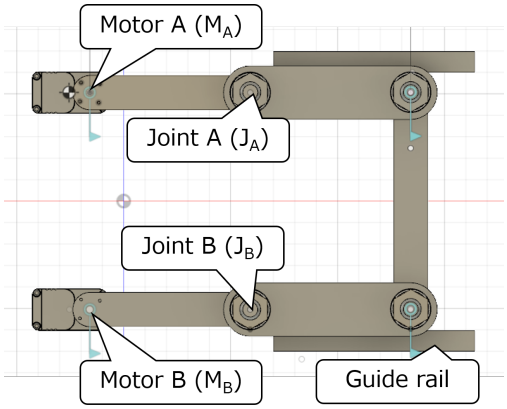

Figure 4: Parallel links

The drive unit moves backward and forward by rotating servo motors A (M_A) and B (M_B) outward. The weights are placed either at Joint A (J_A) or Joint B (J_B).

4.2 Experimental Procedure of Type 1 System

Experiments are conducted to increase the friction between the links. First, we record the sensor output for 20 minutes without placing a load on the system. Second, weights are fixed to J_A for a 30-second interval. Next, we record the sensor output for another 20 minutes under a 70 g load. Weights are fixed to J_A, again. Finally, we record the sensor output for 20 minutes under a 130 g load.

4.3 Experimental Procedure of Type 2 System

Experiments are conducted to increase the friction between the links.The weight on joint A is the same as in the Type 1 experiment. The change is that the motor of the Type 2 system has a stronger force than that of the Type 1 system. We performed measurements from 0 g to 2500 g at 100 g intervals.

This experiment is carried out in order to verify whether the load increase can be observed by only the measurements from M_B when placing a weight on J_A.

5 EXPERIMENTAL RESULTS

We first describe the observed interactions. Next, we describe the results of PCA using 12-dimensional data. Finally, we describe the results of PCA using six-dimensional data. The data obtained from the servo motors are shown separately in Figs. 5 through 12.

5.1 Changes in Rotational Angle

Figures. 5 and 6 show the rotational angles of the servo motors.In the rotational angle data, M_A indicates that the movement of the horn is faster than usual due to the loading. Figure. 7 shows an enlarged view of the angle data for M_B. The region of the rotational angle data containing abnormal readings are enclosed by a black circle. Figure. 7 shows an enlarged view of the black circle. In M_B, there was an interaction in which the timing of the action was shifted by M_A.

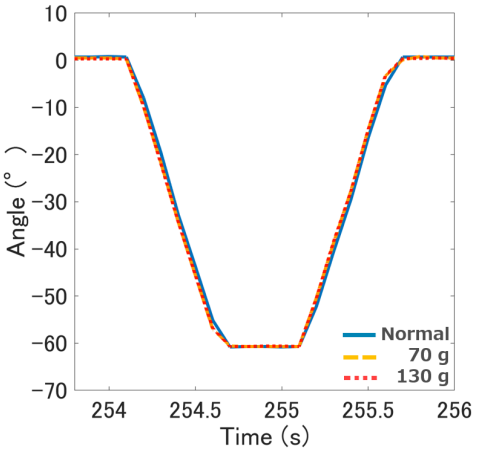

Figure 5: Angle data for Motor A

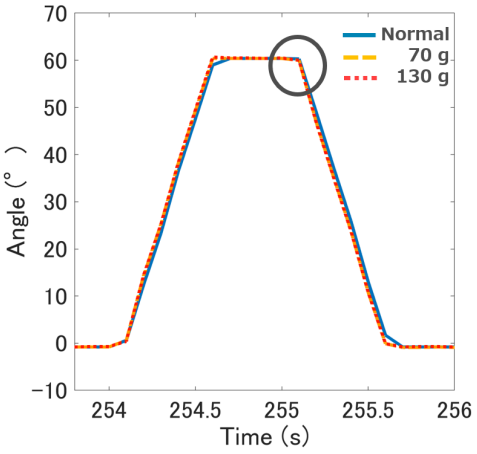

Figure 6: Angle data for Motor B

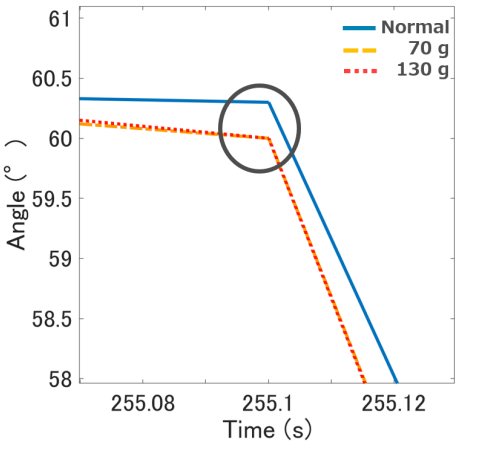

Figure 7: Enlarged view of angle data for Motor B

5.2 Changes in Rotation Time

Figures. 8 and 9 show the rotation times of the servo motors. Rotation time indicates the elapsed time from the start of the movement of the servo horn, and the value is retained until the next movement after arrival at the target angle. The abnormal measurements in the rotation time data are enclosed by a black circle. Figure. 10 shows an enlarged view of the area indicated by the black circle. Here, M_A indicates that the time of movement is clearly earlier than that for the case without a load. Figure. 10 shows an enlarged view of the M_B rotation time data. In addition, M_B is also moving slightly faster than before the load was added.

5.3 Changes in Voltage

Figures. 11 and 12 show the voltages of the servo motors. The three sets of measurements for M_A show that the tendencies in the voltage change do not agree. The M_A voltage under the 130 g load is more stable than that under the 70 g load, probably because the play in the experimental apparatus was suppressed by the weight. The abnormal voltage data are enclosed by a black ellipse. The voltage data for M_B show a small variation, but an abnormal voltage drop was observed due to the interaction.

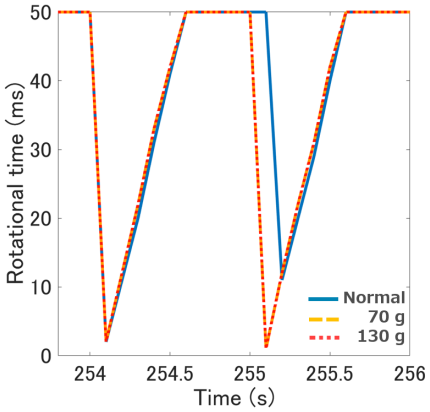

Figure 8: Rotation time data for Motor A

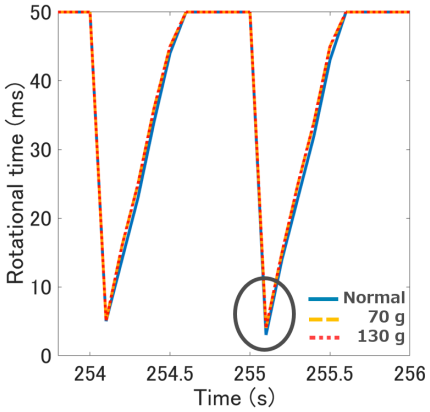

Figure 9: Rotation time data for Motor B

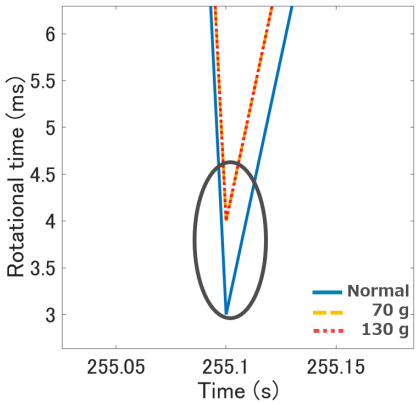

Figure 10: Enlarged view of rotation time data for Motor B

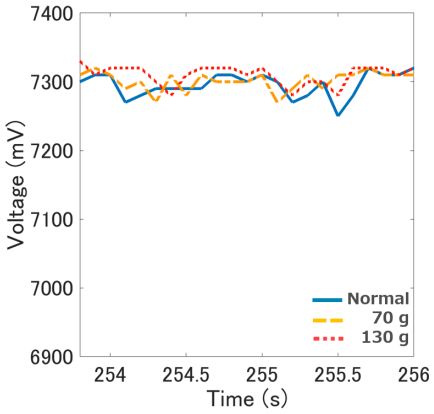

Figure 11: Voltage data for Motor A

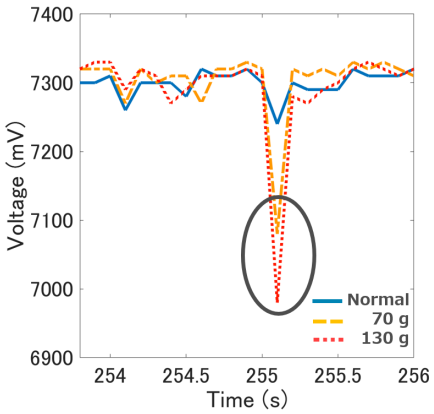

Figure 12: Voltage data for Motor B

5.4 Results of Principal Component Analysis

PCA was performed using 12-dimensional data from both motors. Figure. 13 shows the contribution of the principal components (PCs) of the normal time data. The contributions of the PCs of the loaded data were approximately the same. We can explain less than 50% of the variance in the data in two dimensions.

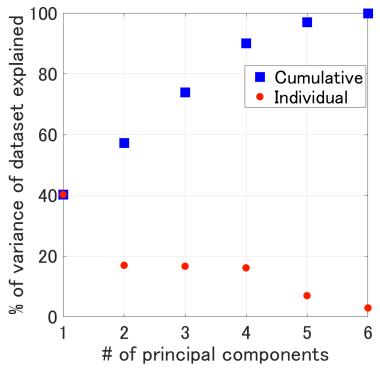

Figure 13: Cumulative explained variance for the principal components

Figures. 14 and 15 show the 12-dimensional data distribution without and with load, respectively. The solid and dashed ellipses indicate the 70 g data and the 130 g data, respectively, in Fig. 15. The class count could be observed to change as the load increased. Classes are formed by grouping points for each operation of the experimental equipment. A given point moves between multiple classes after one movement of the experimental equipment, before returning to the initial class. Classes P_1 through P_4 are highlighted in Fig. 14. Other classes are moving between assigned numbers. The classes are changing as the load increases. In particular, the change of the P_3 class is remarkable.

From the PCA result for the 12-dimensional data, only P_3 was individually analyzed, and the change of P_3 in each state was confirmed. Table 3 shows the change of P_3. We applied a normal distribution to the data and analyzed the average value and the angle of the distribution on the x-and y-axes and the length of the main axis of the distribution. The major and minor axes are the standard deviations for each axis multiplied by a constant. Ellipses represent equal probabilities of 95%. In the 12-dimensional data, the change of P_3 was observed in the x mean value, the angle of distribution, and the principal axis. This is because some of the data for P_3 are located at P_2 in the operation.

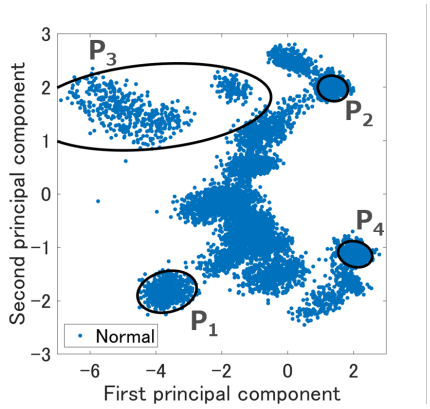

Figure 14: Twelve-dimensional data distribution: without load

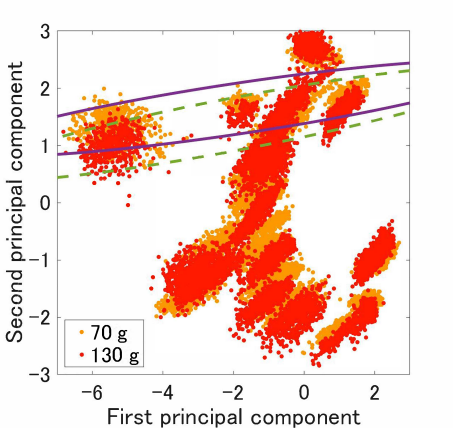

Figure 15: Twelve-dimensional data distribution: with load

Table 3: Twelve-dimensional data change for P_3

	P_3 Center (x, y)	P_3 (Angle)	P_3 (Major, Minor)
Normal	(-4.16, 1.63)	3.02°	(2.99, 0.65)
70 g	(-1.84, 1.65)	5.24°	(6.34, 0.36)
130 g	(-1.90, 1.38)	6.66°	(6.28, 0.38)

5.5 Failure Prediction of Type 1 System

PCA was performed using six dimensional data for each servo motor. Figsure. 16 and 17 show the results of PCA of M_A for the data distributions without and with load, respectively. Since M_A was directly loaded, the transition in the entire class from right to left was remarkable. Figures. 18 and 19 show the results of PCA of M_B for the data distributions without and with load, respectively. A transition was observed in the class. From this result, it is considered that abnormality in the equipment operation can be detected based only on PCA of the data of M_B without applying the load directly.

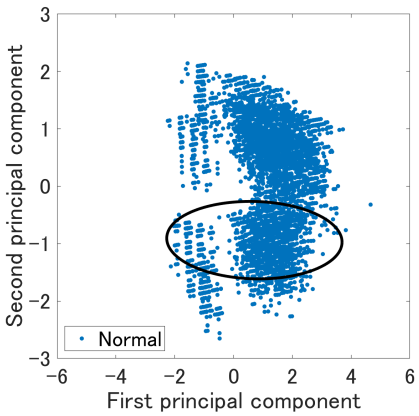

Figure 16: Six-dimensional data distribution for Motor A without load

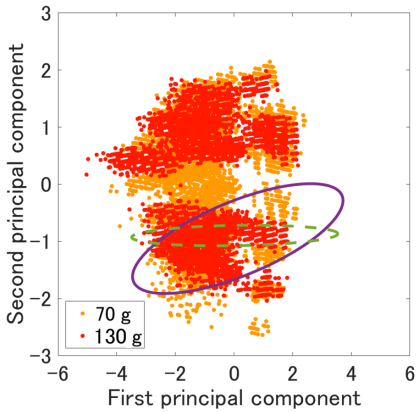

Figure 17: Six-dimensional data distribution for Motor A with load

Based on the PCA result for the six-dimensional data of M_A, only P_3 was individually analyzed, and the change of P_3 in each state was confirmed. Table 4 shows the change of P_3. In the M_A data, the change of P_3 was observed in the x mean value and the angle of distribution. In this case, as in the case of the 12-dimensional data, the data are arranged from P_3 to P_2 by the operation.

Based on the result of PCA for the six-dimensional data of M_B, only P_3 was individually analyzed, and the change of P_3 in each state was confirmed. Table 5 shows the change of P_3.

Table 4: Six-dimensional data (M_A) change of P_3

	P_3 Center (x, y)	P_3 (Angle)	P_3 (Major, Minor)
Normal	(0.71, -0.94)	-0.68°	(8.45, 1.80)
70 g	(0.13, -0.95)	10.9°	(7.41, 1.73)
130 g	(0.02, -0.90)	0.49°	(7.47, 1.62)

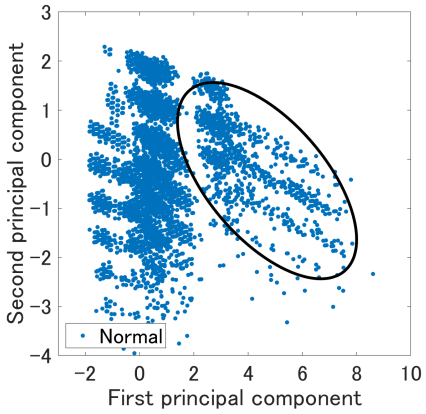

Figure 18: Six-dimensional data distribution for Motor B without load

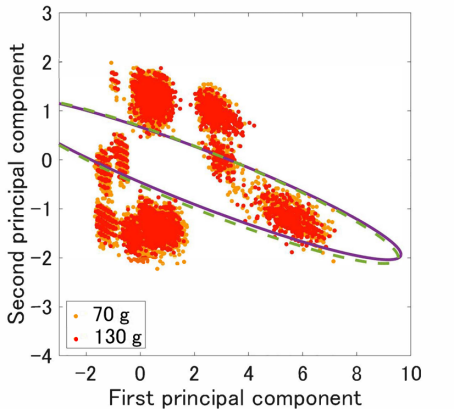

Figure 19: Six-dimensional data distribution for Motor B with load

Table 5: Six-dimensional data (M_B) change of P_3

	P_3 Center (x, y)	P_3 (Angle)	P_3 (Major, Minor)
Normal	(4.70, -0.44)	-24.5°	(2.91, 1.21)
70 g	(2.30, -0.38)	-12.0°	(6.12, 0.47)
130 g	(2.31, -0.42)	-12.4°	(6.04, 0.51)

In the M_B data, the change of P_3 was observed in the x mean value, angle of distribution, and principal axis.In this case, as in the case of the 12-dimensional data, the data are arranged from P_3 to P_2 by the operation.By looking at the long axis of the distribution, it is possible to observe the abnormality even from the motor under no load.

5.6 Failure Prediction of Type 2 System

In order to confirm the validity of the method, we designed the Type 2 system using high-power motors used in actual FA equipment. Figure. 20 shows that the results of the same data processing for the Motor B data of the Type 2 system. The results of the PCA were categorized on the axis of the plane with the first and second PCs and were approximated as an ellipse. In order to observe the change, 4.5% of the data from the beginning were extracted and defined as class 1.

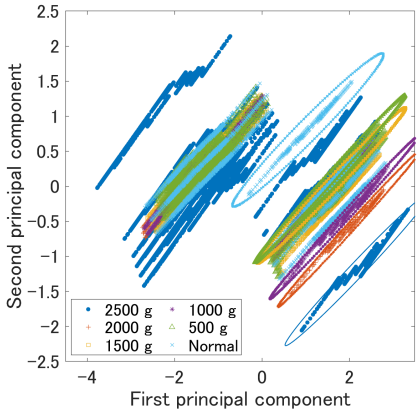

Figure 20: Three-dimensional data distribution for Motor B

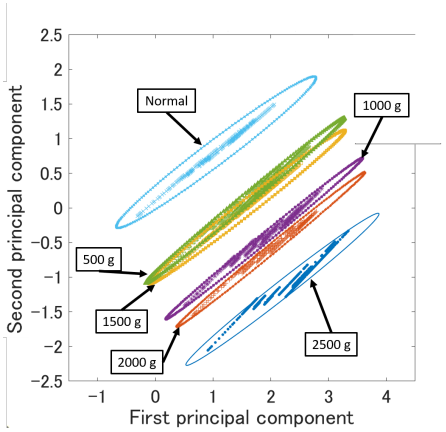

Figure 21: Three-dimensional data distribution for Motor B (class 1)

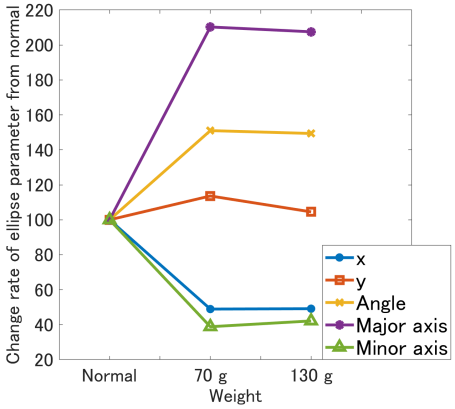

Figure 22: Change of M_B ellipse parameter (Type 1)

Table 6: Type 1 data (M_B) for change of class

	(x, y)	(Angle)	(Major, Minor)
Normal	(1.01, 0.80)	32.1°	(4.08, 0.38)
500 g	(1.55, 0.10)	34.7°	(4.20, 0.18)
1000 g	(1.89, -0.44)	34.3°	(4.14, 0.14)
1500 g	(1.59, 0.01)	33.1°	(4.06, 0.24)
2000 g	(2.00, -0.60)	34.4°	(3.94, 0.14)
2500 g	(2.20, -1.18)	33.2°	(4.00, 0.26)

The results for class 1 are shown in Fig. 21. As shown in the figure, the class 1 data change as the weight is increased. In addition, the parameters of the ellipse are shown in Table 6. In the present verification, it was confirmed that the x and y coordinates of the center of gravity changed with increasing weight, except for 1000 g.

6 DISCUSSION

In the present paper, we considered a fault prediction method for FA equipment with parallel links using the interaction between links. An experimental apparatus for monitoring parallel links using two servo motors was developed. An experiment in which a load was placed on one link was carried out in order to determine whether an increase in friction could be detected from the other link. Based on the results of PCA of 12-dimensional data from the servo motors, it was confirmed that multiple data classes changed when the load was increased. Based on the results of the PCA for six-dimensional data obtained from one servo motor, it was possible to observe changes in the data classes when increasing the load not only in the servo motor with the load but also in the servo motor without the load. This indicates that failure prediction for the robot joint based on the interaction between parallel links of FA equipment is possible.

Changes in the Type 1 M_B ellipse parameter are shown in Fig. 22. The figure shows that the change from 70 g to 130 g is small. It is considered that the equipment has already entered the failure condition from the usual condition, because it has been confirmed that the operation of the equipment stops during the experiment, when the experiment is carried out when the weight exceeds 130 g. In addition, if the data count is low, the evaluation of the parameter prediction will be insufficient.

Therefore, evaluation of the prediction is possible by acquiring more data for the 70 g load from the usual time.

Changes in the Type 2 M_B ellipse parameter are shown in Fig. 23. In this verification, it is confirmed that the process applied to the Type 1 parameter can be applied to Type 2 parameter. Therefore, it is conceivable that this method can be applied in the same manner to other parallel link mechanisms to predict anomalies. The considered method does not look for learned patterns, but rather predicts gradual changes in the data. This method is applicable to anomalies other than bearing seizure. For example, it is possible to predict failures due to aging and wear. For these anomalies, we need to conduct verification experiments.

On the other hand, there is a limitation in the considered method in that it cannot predict failures in which gradual changes in the data cannot be observed. Such failures include chipping of bearings due to sudden overloads.

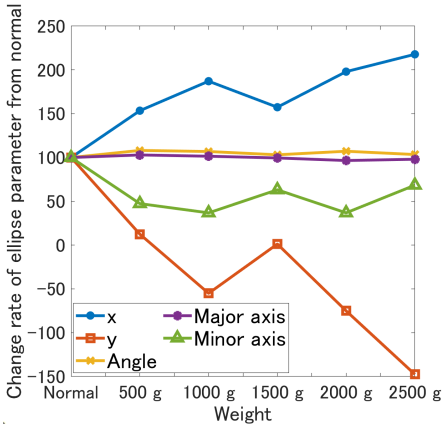

Figure 23: Change of M_B ellipse parameter (Type 2)

7 CONCLUSION

In the present paper, we considered a failure prediction method for FA equipment assuming there exists an interaction between parallel links. The experimental apparatus of the parallel link was developed, and the abnormality of the bearing used for the joint was expressed in the load quantity. The sensor output data were then measured. PCA of the time series data confirmed that multiple data classes changed as the load increased. In the analysis of the measurements for each servo motor, it was possible to observe the change in the data classes under increasing loads, i.e., not only in the servo motor with a load but also in the servo motor without a load. This indicates the possibility of fault prediction based on observation of the interaction between links.

Two experimental systems, Type 1 and Type 2, were designed in order to simulate actual parallel links of FA equipment. As a result, it was confirmed that the considered method applied to both systems can predict failures in which gradual changes in the data were observed. Future issues include verification experiments of the considered method for other kinds of anomalies, such as ageing and wear.

REFERENCES

[1] R. K. Mobley, “An Introduction to Predictive Maintenance,” c. 1, Butterworth-Heinemann, (2002).

[2] “IATA’S Maintenance Cost Task Force”, AirLine Maintenance Cost Executive Commentary, (2016).

[3] A. Yamashita, H. Mineno, and T. Mizuno, Distributed Remote Input/Output Control Method in Real Time Processing for CNC, International Journal of Informatics Society, Vol. 8, No. 2, (2016).

[4] Z. Gao, C. Cecati, and S. X. Ding, “A Survey of Fault Diagnosis and Fault-Tolerant Techniques—Part I: Fault Diagnosis With Model-Based and Signal-Based Approaches,” IEEE Transactions on Industrial Electronics, Vol. 62, No. 6, (2015).

[5] B. Luo, H. Wang, B. Li, F. Peng, “Early Fault Detection of Machine Tools Based on Deep Learning and Dynamic Identification,” IEEE Transactions on Industrial Electronics, Vol. 66, No. 1, (2019).

[6] N. Amruthnath, and T. Gupta, “A Research Study on Unsupervised Machine Learning Algorithms for Early Fault Detection in Predictive Maintenance,” 5th International Conference on Industrial Engineering and Applications, (2018).

[7] S. Singh, “Optimize cloud computations using edge computing,” 2017 International Conference on Big Data, IoT and Data Science (BID), (2017).

[8] J. Merlet, “Parallel Robots (Solid Mechanics and Its Applications),” pp. 12-17, Springer Netherlands, (2000).

(Received November 12, 2019)
(Revised April 6, 2020)

Masanori Haga received his B.E. degree in information science from the Aichi Institute of Technology, Japan in 2019. His research interests include analyzation of machine information. He is a member of Information Processing Society of Japan.

Kazuhiko Tsutsui received the B.E. and M.E. degrees in Mechanical Engineering from Kumamoto University, Japan in 1990 and 1992 respectively. In 1992, he joined Mitsubishi Electric Corp. Since when he joined Mitsubishi Electric Corp, he has been engaged in development of Servo and Spindle drive system.

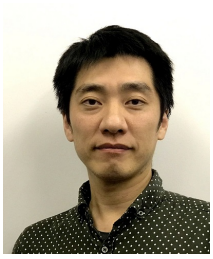

Katsuhiko Kaji received a Ph. D. in information science from Nagoya University in 2007. He became a RA at the NTT Communication Science Laboratories in 2007 and an assistant professor at Nagoya University in 2010. He has been an associate professor of the Faculty of Information Science, Aichi Institute of Technology since 2015. His research interests include indoor positioning and remote interaction. He is a member of IPSJ and JSSST.

Katsuhiro Naito received the B.S. degree in Electronics Engineering from Keio University, Japan in 1999, and received the M.S. and Ph.D. degrees in Information Engineering from Nagoya University, Japan in 2001 and 2004, respectively. From 2004 to 2014, Dr. Naito was an assistant professor in the electrical and electronic engineering department of Mie university. He was a visiting scholar in the computer science department of University of California, Los Angeles (UCLA) in 2011. Since 2014, he has been an associate professor in the information science department of Aichi Institute of Technology. His research interests include 5G technologies, vehicular communication systems, Internet of Things (IoT) and Machine to Machine (M2M) systems, overlay networks, and network protocols and architectures.

Tadanori Mizuno received the B.E. degree in Industrial Engineering from the Nagoya Institute of Technology in 1968 and received the Ph.D. degree in Engineering from Kyushu University, Japan, in 1987. In 1968, he joined Mitsubishi Electric Corp. From 1993 to 2011, he had been a Professor at Shizuoka University, Japan. From 2011 to 2016, he had been a Professor at the Aichi Institute of Technology, Japan. Since 2016, he is an Affiliate Professor at the Aichi Institute of Technology, Japan. His research interests include mobile computing, distributed computing, computer networks, broadcast communication and computing, and protocol engineering. He is a member of Information Processing Society of Japan, the Institute of Electronics, Information and Communication Engineers, the IEEE Computer Society and Consumer Electronics, and Informatics Society.

Naoya Chujo received his B.E. degree in applied physics and M.S. degree in information science, and Ph.D. degree in electrical engineering from Nagoya University in 1980, 1982, and 2004, respectively. He joined Toyota Central R&D Labs. in 1982. He has been a professor at the Aichi Institute of Technology since 2010. His research interests are in the area of embedded systems and automotive electronics. He is a member of IEEE, IPSJ, IEICE, IEEJ, and Informatics Society.

Submission Guidance

About IJIS

International Journal of Informatics Society (ISSN 1883-4566) is published in one volume of three issues a year. One should be a member of Informatics Society for the submission of the article at least. A submission article is reviewed at least two reviewer. The online version of the journal is available at the following site: http://www.infsoc.org.

Aims and Scope of Informatics Society

The evolution of informatics heralds a new information society. It provides more convenience to our life. Informatics and technologies have been integrated by various fields. For example, mathematics, linguistics, logics, engineering, and new fields will join it. Especially, we are continuing to maintain an awareness of informatics and communication convergence. Informatics Society is the organization that tries to develop informatics and technologies with this convergence. International Journal of Informatics Society (IJIS) is the journal of Informatics Society.

Areas of interest include, but are not limited to:

- Internet of Things (IoT)
- Smart Cities, Communities, and Spaces
- Big Data, Artificial Intelligence, and Data Science
- Network Systems and Protocols
- Computer Supported Cooperative Work and Groupware
- Security and Privacy in Information Systems
- Intelligent Transportation System
- Distributed Computing
- Multi-media communication
- Information systems
- Mobile computing
- Ubiquitous computing

Instruction to Authors

For detailed instructions please refer to the Authors Corner on our Web site, http://www.infsoc.org/.

Submission of manuscripts: There is no limitation of page count as full papers, each of which will be subject to a full review process. An electronic, PDF-based submission of papers is mandatory. Download and use the LaTeX2e or Microsoft Word sample IJIS formats.

http://www.infsoc.org/IJIS-Format.pdf

LaTeX2e

LaTeX2e files (ZIP) http://www.infsoc.org/template_IJIS.zip

Microsoft Word™

Sample document http://www.infsoc.org/sample_IJIS.doc

Please send the PDF file of your paper to secretariat@infsoc.org with the following information:

Title, Author: Name (Affiliation), Name (Affiliation), Corresponding Author. Address, Tel, Fax, E-mail:

Copyright

Publisher

Address: Informatics Laboratory, 3-41 Tsujimachi, Kitaku, Nagoya 462-0032, Japan

E-mail: secretariat@infsoc.org

CONTENTS